Design and construction of permanent magnetic gears

Jørgensen, Frank Thorleif

Publication date:
2010

Design and construction of permanent magnetic gears

By

Frank T. Jørgensen

Dissertation submitted to the Faculty of Engineering Science at Aalborg University in partial fulfilment of the of the requirements for the degree of Doctor of Philosophy in Electrical Engineering

Aalborg University, Denmark
Institute of Energy Technology
May, 2010

Aalborg University
Institute of Energy Technology
Pontoppidanstræde 101
DK-9220 Aalborg East

Printed in Denmark by: UNI.PRINT. Aalborg University

Second print, May 2010.

ISBN 978-8789179-86-5

Preface

This thesis is submitted to the Faculty of Engineering and Science at Aalborg University in partial fulfilment of the requirements for the Ph.D. degree in Electrical Engineering. Research is conducted at the section of Electrical Machines, which is part of the Institute of Energy Technology (IET), Aalborg University.

I would like to thank the sponsors of the project. The sponsor contributions are from PSO funds controled by ELFOR, Aalborg University and 3 companies. The following companies have supported the project: Sauer-Danfoss ApS, Danfoss A/S and Grundfos A/S. Representatives from these companies are: M.Sc.E.E. P. Sandholdt, Imagineering R&D, Sauer-Danfoss ApS, adjunct professor, P.B. Thøgersen, Danfoss A/S, ELFOR and K.F. Rasmussen, Grundfos A/S.

The project has been followed by my supervisors, associate professor P.O. Rasmussen and professor T.O. Andersen. I would like to thank them for their help and supervision throughout the project.

Aalborg, May 2010.
Frank T. Jørgensen

franktjoergensen@gmail.com

Abstract

This thesis deals with design and development of permanent magnetic gears. The goal of this thesis is to develop knowledge and calculation software for magnetic gears. They use strong NdFeB permanent magnets and a new magnetic gear technology, which will be a serious alternative to classical mechanical gears. The new magnetic gear will have a high torque density[1] relationship –high efficiency and are maintenance free. In this project was manufactured two test gears which is tested and verified with models developed in this project.

Present technological status for magnetic gears is introduced in a state of the art analysis. Furthermore made an analysis for mechanical gears in order to estimate performance characteristic compared to traditional mechanical gears was created.

Some of the gear types found at the state of the art analysis are chosen for further investigation. Analytical and numerical calculation models for determination of gear output torque from different magnetic gear types are analysed. These analytical calculations models are used together with optimisation tools in order to improve the performance of investigated magnetic gear types. Experimental test gears are designed to validate the calculation models.

The first gear type is the very basic magnetic spur gear, which reminds most of all of the traditional mechanical spur gear, the difference is basically that magnetic teeth is replacing mechanical teeth. A magnetic version of the spur gear with a gearing of 1:4 will be able to reach an active torque density of approximately 24 [Nm/l]. Corresponding mechanical spur gears examples with a gearing of 1:5 are found and these gears have a total torque density of 16 to 24 [Nm/l].

The second analysed gear type is the magnetic version of the traditional cycloidal gear. This magnetic gear type is searched and only a single reference [74] is found and that is why the combination of a cycloidal gear and a magnetic gear are considered as an innovative supplement to magnetic gear technology. A magnetic cycloidal gear is designed with a gearing of 1:21 and a calculated active torque density of 142 [Nm/l]. Measurement from this gear has resulted in a measured total torque density of 23 [Nm/l]. Mechanical versions of this gear type are found with total torque density in the 16 to 31 [Nm/l] range. The third and last gear technology that is investigated is a gear that reminds of a planetary gear. Research shows that this gear technology is also one of better technologies regarding torque density.

[1] Torque density is defined on page 10.

Dansk resumé

Denne afhandling omhandler design og udvikling af magnetiske gear. Formålet med projektet er at udvikle viden og beregningssoftware til magnetiske gear. Der anvendes stærke NdFeB magneter og en magnetiske gear teknologi hvilket vil give et seriøst alternativ til klassiske mekaniske gear. De nye magnetiske gear forventes blandt andet at have et stor moment-volumen forhold, samt at være med høj virkningsgrad og vedligeholdes frie. I projektet fremstilles der to test gear, som efterfølgende testes for at verificerer modeller udviklet i dette projekt.

Indledningsvis er der fortaget et litteratur studie af magnetiske gear, for at få en ide om teknologiske status for magnetiske gear. Der er desuden foretaget en analyse af mekaniske gear for at finde frem til hvilken performance karakteristik der findes for mekaniske gear.

Nogle af de gear typer som blev fundet i undersøgelsen af de magnetiske gear er blevet udvalgt til videre undersøgelse. Analytiske beregnings modeller til bestemmelse af udgangsmomentet for forskellige typer af magnetiske gear er analyseret. Disse analytiske modeller er brugt sammen med optimeringsværktøjer med henblik på at forbedre ydelse af den aktuelle gear type. Eksperimentelle test gear er designet for at validere beregnings modellerne. Den første gear type er et helt simpelt magnet gear der minder meget om et traditionelt tandhjuls gear, der er dog den forskel at der er magnetiske tænder i stedet for mekaniske tænder. En magnetisk version af et traditionelt tandhjulsgear med en gearing på 1:4 vil kunne opnå en aktiv moment densitet på omtrent 24 [Nm/l], hvis moment og ydre dimensioner er designet med lignende proportioner som de eksperimentelle test gear. Tilsvarende mekaniske tandhjuls gear eksempler med gearing på 1:5 er fundet og disse gear har en moment densitet på 16 til 24 [Nm/l].

Den anden type som er analyseret er en magnetisk version af den det traditionelle cyclo gear. Der er søgt efter denne gear type og kun en enkelt reference [74] er fundet, derfor kan kombinationen af cycloid gearet og det magnetiske gear betragtes som et innovativt tiltag inden for magnetisk gear teknologi. Et magnetisk cycloid gear er designet med en gearing på 1:21 og en beregnet aktiv moment densitet på 142 [Nm/l]. Målinger fra dette gear har resulteret i en målt total moment densitet på 23 [Nm/l]. Mekaniske versioner af denne type er fundet med en total moment densitet i størrelsesorden 16 til 31 [Nm/l]. Tredje og sidste type som er analyseret er et magnet gear som minder meget om det mekaniske planet gear. Forskning har vidst at denne gearteknologi også er en af de bedre teknologier hvad angår moment densitet.

Contents

Chapter 1 Introduction

1.1 Project motivation

The basic idea of a gearing is to convert mechanical power from one rotational speed and torque to another speed and torque. Many applications require power input with a high torque and low revolution speed. An example can be a conveyer belt for a production machine. Drive shaft for the conveyer belt must pull a relative heavy load with relative low angular velocity. Power sources for mechanical systems are often available with high speed and low torque. Examples of such a power source can be an electrical machine or a combustion engine. These machines have a relatively low torque and runs at high rotational speeds. The problem is often lack of torque from the source drives. The physical size of a direct drive electrical machine able to drive a conveyer belt directly will typically be too large and expensive. A more cost effective solution will be to place a transmission between the conveyer belt and the electrical machine. This transmission will be able to convert the electrical machine power from a low torque to high torque on the conveyer belt with almost the same power level. Mechanical gears are often used for such transmission purposes. These gears have often a high torque capability and relatively high efficiency and that is why these transmissions are a good choice for many applications. A magnetic gear is also a transmission device that can transform low torque and high rotational speed to a high torque low rotational speed. Magnetic gears can also achieve high efficiency, but a high torque capability can be hard to achieve unless carefully considerations are made regarding magnetic gear technology and design. That is why torque density is a major issue for the magnetic gear technology. Cost and amount of magnetic material is also rightly linked. Many of the known magnetic gear technologies are documented through patents, and only a few of these technologies are well documented in scientific papers. One of scientific papers that have caused attention to the magnetic gear technology is a paper about a high performance magnetic gear published in 2001 by Atallah and Howe [1]. This gear technology will have a significantly high torque density and has therefore increased possibility to utilize magnetic gears for industrial applications. Increased interest for the magnetic gear technology has made it possible to set up funds for magnetic gear research.

1.2 Basics of magnetic and mechanical gears

A gear can be defined as a mechanism that transfers torque from one shaft to another shaft by the use of magnets or mechanical teeth. Some mechanical gears are very similar to magnetic gears for instance the magnetic spur gear. The similarity of these two gear types is shown on Figure 1.1.

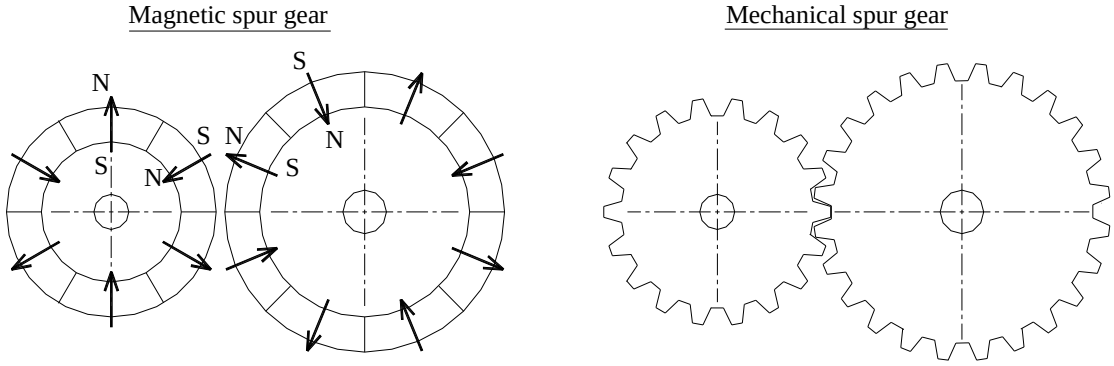

Figure 1.1 A sketch of a magnetic spur gear with permanent magnets and a mechanical spur gear.

The traditional mechanical gear uses steel teeth's to transfer torque. Gear wheel teeth have physically contact with each other, and there will be wearing on the tooth flanges. The magnetic gear does not have the same wear, because there is no direct contact. Permanent magnets on the gearing wheels transfer the torque between the two wheels. Since the magnetic gear does not have direct contact, there will be a fictive torsion spring effect between gear wheels. The torsion spring effect can be explained by imaging one wheel fixed and the other wheel is rotated a small angle. Then there will be a certain torque interaction between the gear wheels depending on angle displacement of the second wheel. This phenomenon is illustrated on Figure 1.2 where a magnetic gear consisting of a driving gear wheel and a driven gear wheel is shown. The torsion spring phenomenon is similar to the well known torque angle characteristic effect in synchronous machines.

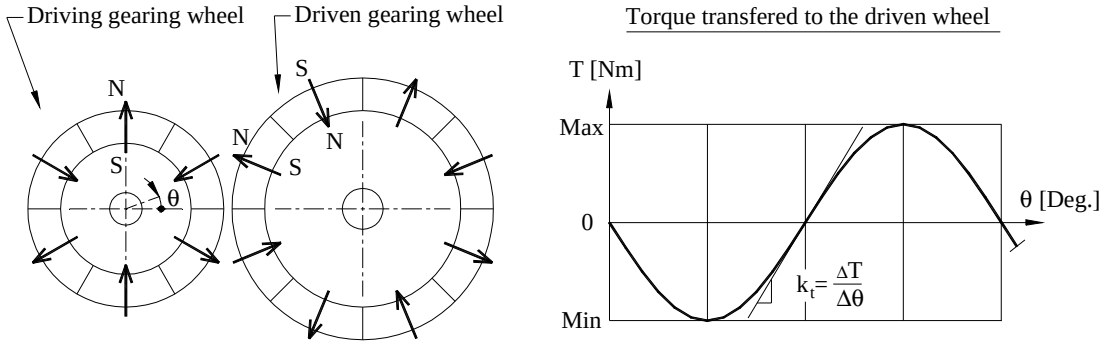

Figure 1.2 A magnetic gear and a torque diagram, where the torque versus turning angle on the driving gear wheel is shown.

A magnetic gear will have a torque limitation T_{max} where the gear will reach the maximal torque. If the applied torque is increased further than this point, there will be a problem because the gear wheels will slip. The slip effect can not be allowed for most of the known applications used for gearing purposes. A magnetic gear must therefore operate somewhat under the T_{max} limitation. However some applications like a spindle machine have a mechanical fuse included in the design. The torque limitation can be an advantage in such applications where the drive system is protected by the torque limitation. The torsion spring k_t for a magnetic gear will not be constant because it is the rate of change in torque divided by the angle change. Mechanical gears will often have a backlash instead of a spring constant.

Gearing relationship R_g depends on the number of magnets N_{pole1} on the drive wheel and N_{pole2} on driven wheel. This relationship can be shown as equation (1.1). Most gear systems have a gearing relationship R_g which is greater than one, which corresponds to high revolutions on the input shaft and low revolutions on the output shaft. Gearing relationship equation is valid for mechanical gears also if the number of magnet poles are replaced of number of teeth's on each gearing wheel.

$$R_g = \frac{N_{pole2}}{N_{pole1}} \tag{1.1}$$

Torque density is a performance criterion used in the electrical machines literature, where a torque per unit rotor volume or torque per total unit volume is given. Performance criterion like this can also be applied to magnetic gears. A gear with permanent magnets has a certain amount of rotor volume and this volume versus the maximum transferred torque is here defined as the active torque density (1.2). The active torque density ρ_A is suitable for comparing different types of magnetic gears with each other. The volume V_A is in this case volume of the rotors.

$$\rho_A = \frac{T_{max}}{V_A} \tag{1.2}$$

It can be necessary to compare the torque density for magnetic gears with mechanical gears. A better torque density measure for magnetic gears is defined for that purpose. This is the total torque density ρ_R shown in (1.3).

$$\rho_R = \frac{T_{max}}{V_T} \tag{1.3}$$

Mechanical gears have a corresponding torque density factor (1.4), which is calculated from the rated nominal torque T_{Nom}.

$$\rho_T = \frac{T_{Nom}}{V_T} \tag{1.4}$$

Volume V_T which is used in these equations is the total outer gear volume. Since gearboxes often have rounding and different shapes extruded from the base curvature, it can be a rather complicated calculation. That is why volume calculation is an approximated volume surrounding the gearbox excluding the gear axles. A simple gearbox illustration on Figure 1.3, shows where the total outer gear volume V_T is defined.

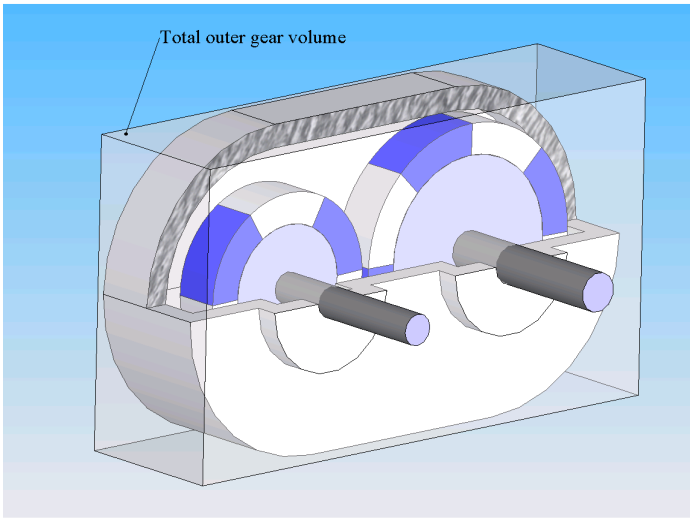

Figure 1.3 An illustration of the total outer gear volume V_T surrounding a magnetic gear used to define total torque density.

Mechanical and magnetic gears have a certain efficiency. This efficiency is defined as the relationship between power at the output shaft divided with the power at the input shaft (1.5).

$$\eta = \frac{P_{Out}}{P_{in}} \tag{1.5}$$

Summary

A simple magnetic gear is presented together with performance criteria for such gear. Performance criterion is comparable to mechanical gears. A state of the art analysis of the mechanical gears is made to clarify the performance characteristic for mechanical gears regarding torque density and efficiency. Another state of the art analysis is made to find state of the art regarding magnetic gears. A summary of these two analyses are described in the following sections.

1.3 State of the art analysis - Summary

This report deals with a magnetic gear which basically is a combination of two engineering topics, namely mechanic and magnetic. Magnetic analysis are normally performed by people with an electromechanically or physics background and gears are normally developed and analysed by people with a mechanical background. Efforts is made to clarify the state of the art – Mechanical gears to introduce a reader with a electromechanical background to mechanical gears and a state of the art - Magnetic gears is made to introduce a reader from the mechanical background to the topic of magnetic gears. A summary of these two analyses is presented in the following. The two analyses are placed at the end of this chapter.

Summary of the state of the art - Mechanical gears

The state of the art analysis – Mechanical gears are a description of the most common gear types used in the industry. These gears are analysed regarding torque density and efficiency. Five different gear types are analysed, and these are:

- Spur gear/helical gear
- Planetary gear
- Cycloidal gear
- Harmonic drive
- Worm gear

The analysis shows that these gears have a relatively high torque density. 300 [kNm/m^3] is not unrealistic for the helical drive and 250 [kNm/m^3] is obtainable for the mechanical planetary gears if the input speed is lower than 500 [RPM]. The analysis also shows that there is a reduction in torque density down to 210 [kNm/m^3] if the input reference speed is 1500 [RPM]. The cycloidal gear type has a torque density close to the planetary gear. Spur gears and worm gears have typically the lowest torque density. Efficiency is best for the planetary type and spur gears type. These types have efficiencies up to 98, 5% and 99% respectively. Cycloidal, helical and worm gears have normally lower efficiencies. The analysis of the mechanical gears reveal also that planetary gears is one of the best gear choices if a high torque density is wanted together with high efficiency.

Summary of the state of the art - Magnetic gears

The state of the art analysis - Magnetic gears indicate that there are many ideas and concepts about magnetic gear technology. Most of these concepts are documented in patents, and only a minor part of them are documented in scientific papers. The analysed magnetic gears are divided in two categories namely:

- Magnetic gears with closely spaced magnets
- Flux guided magnetic gear mechanisms

The magnetic gear technology with closely spaced magnets is one of the simplest magnetic gear technologies which are similar to the mechanical spur gear. There are many different types of magnetic gears with closely spaced magnets, types with different magnetisations direction, types with different axis position and direction. Flux guided magnetic gears are another magnetic gear type which is found among patents and papers. These magnetic gear types consist of a permanent magnet rotor that guides the magnetic flux in iron segments. The other output rotor is driven by this altering flux and a magnetic gear is therefore present. Gear types are also found in many different configurations. Some of these configurations have parallel axis and other configurations will transform a rotational motion to a linear motion. Other flux guided magnetic gears versions have similarities to the mechanical planetary gear. Common for most of the magnetic gear publications and patents is that very little is written about their torque relative to their volume, and that is one of the main problems of magnetic gears. One of the first magnetic gear publications found where the torque density is specified is a high-performance magnetic gear [1]. This paper claims that it is possible to achieve a torque density of approximately 100 [kNm/m^3], which is approximately 10 times higher than the torque density of a traditional electrical machine.

Scientific papers use often FEM calculations to estimate the torque output and these calculations are compared with physical measurements in some cases. Analytical models of magnetic gears is not so common among the publications; however analytical models are often the best choice when the purpose is to optimise torque because they are often less time consuming than FEM models.

1.4 Problem statement

The project motivation describes that mechanical gears are often used for power transmission purposes. A more unconventional way to transmit power is to use a magnetic gear. Characteristic for the two gear types is outlined in basics of magnetic and magnetic gears in terms of gearing relationship and torque density. With the gear characteristic in mind a thorough investigation of existing gear references is considered to be fundamental in order to contribute with new research. Following statement is therefore required:

1. Determine state of the art for magnetic gear technologies, and also technologies from traditional mechanical gears.

State of the art analysis has shown that magnetic gears are rather weak compared to traditional mechanical gears when it comes to torque density. Calculation tools for predicting or optimising torque is therefore important for designing magnetic gears in order to compete with the existing mechanical gear market. The state of the art analysis - magnetic gears has shown that numerical Finite Element Method (FEM) are commonly used for magnetic gear analysis. These modelling methods are fast to develop for new gear concepts but these models are relatively slow regarding calculation time. Analytical models are on the other hand slow to develop for new gear concepts but fast regarding computation time. Following statement is then found essential:

2. Develop analytical and numerical calculation models of permanent magnetic gears. The purpose of the calculation models is to be able to estimate torque in an early stage for magnetic gear design process.

An experimental test gear model is included in some of the scientific papers from the state of the art analysis which is used for verifying the calculated results. Efficiency measurements and experience gathered from prototype design are also useful for the magnetic gear evolution. This is the reason why following statement is included:

3. Develop two experimental magnetic gear models. The purpose with the test models is to compare the theoretical results with experimental test models and to gain practical experience.

Visions for this project are also to develop magnetic gears able to fit to a wide range of applications.

1.5 Restrictions in the scope of this work

There are many performance parameters which can be compared for gears. However to limit the scope of the project, following parameters are excluded:

- Speed
- Efficiency
- Power
- Moment of inertia
- Thrust loads
- Starts per hour
- Life time
- Ambient temperature
- Weight
- Price
- Shock factor
- Acoustic noise
- Loss models
- Torque oscillations

Gears are used for many different applications and are driven by different power sources. These different applications will not always run smooth and the gear must therefore be able to resist a certain level of shock. This is the reason why the gear designer has the possibility to specify a shock factor to reduce nominal torque. A shock factor will depend on the drive machine and the driven application. For instance a one-cylinder combustion engine will result in a much higher shock factor than an electrical machine. Shock factor is not treated in this thesis.

Another performance parameter which is not included is acoustic noise. Mechanical gears have sometimes problems with acoustic noise and many initiatives are often done to prevent that. The noise and vibrations is most dominant for high loads and high speeds.

There is found many interesting gear types in the state of the art analysis regarding magnetic gear which can be modelled and build. However it takes time to build and develop that kind of models and it is decided to limit the amount of analysed gear models.

Models developed are only useful for static analysis to design gears taking into account maximum torque capacity. Static loss model can also analyse the power losses in gear parts; however these models are also outside the scope of this thesis.

Torque oscillations in magnetic gear can occur. Such oscillations are from energy conversions between rotor inertia parts and magnetic spring's torsion, like simple springs and mass system. These kinds of oscillations are not analysed in this thesis.

1.6 Description of the individual chapters

The documentation of the research accomplished to fulfil project statements is collected into the following 5 chapters.

Chapter 1, Introduction
Motivation and an introduction to mechanical and basic magnetic gear are presented. State of the art analysis summaries for both mechanical gears and magnetic gears are described. A problem statement describes scope of work with the project aims and restrictions. Individual chapter descriptions are also included.

Chapter 2, Magnetic spur gear
This chapter describes development of analytical expression for permanent magnetic spur gear torque calculations. The analytical calculation is verified with a physical test model and FEM calculations. Optimisation by which the analytical expressions are used is performed to determine an obtainable level of torque density. Test model is made and test is performed to validate the analytical expressions.

Chapter 3, Magnetic cycloidal gear
A new type of magnetic gear is proposed. An analytical model for torque calculation is developed for a magnetic cycloidal gear. Optimisations are performed with analytic models to determine obtainable level of a torque density. Also a test model is developed and tested to determine the performance of a magnetic cycloidal gear in terms of efficiency and torque density.

Chapter 4, Planetary magnetic gear
The history of planetary magnetic gears is introduced with a chronological description of found references. Basic and improved design theory for this gear type is also described. 2D FEM models of planetary magnetic gear are used to analyse the planetary magnetic gear regarding maximum output torque and parametrical change of segmentation duty cycle.

Chapter 5, Conclusion

A general summary together with magnetic conclusions is completed. The main contributions of this thesis are identified and suggestions for future work are given.

1.7 State of the art -Mechanical gears

Mechanical gears have been used for centuries and have therefore gone through a development ever since. There exist many different gear technologies, and these technologies are used for many different applications. This section introduces common technologies and their performance regarding torque density and efficiency. A simple investigation is made to find the torque density for mechanical gears. Data for the different gear types is mainly found from a search on the internet. It was originally the idea to search gears with low middle and high gearing relationship, and search for minimum three gears manufactured by different manufactures. The found data will represent an approximate part of the existing mechanical gear market. In the search for gears is the gearing interval of 1-15 defined as the low gearing relationship. Middle and high gearing in the interval of 16-30 and 31-150 respectively are also searched. All of the mechanical gears is picked out of random chosen torque sizes. It is not possible to find three gears of every gear types; however the results of this analysis will still be used to give an insight into mechanical gears performance. There are also problems finding all gear types with gearing in these exact gearings limits. This must be noted in the final mechanical gear type comparison, which is described at the end of this section.

Torque density:
Specific gear types are picked out from data sheets, and it is the purpose to calculate a torque density for different gearing, from information about torque and dimensions used. An example of torque density calculation and volume estimation on the basis of dimensions is shown on Figure 1.4. This example is the mechanical spur gear type (C11 2P-4.9-P90) [2]. Output torque for this spur gear is T_{Nom} 48 [Nm]. The overall torque density for this gear is estimated in (1.6) to approximately 16 [kNm/m^3].

Volume and torque densities for the other gear types are estimated with similar approach, where a primitive volume replaces the often rather complicated volume part.

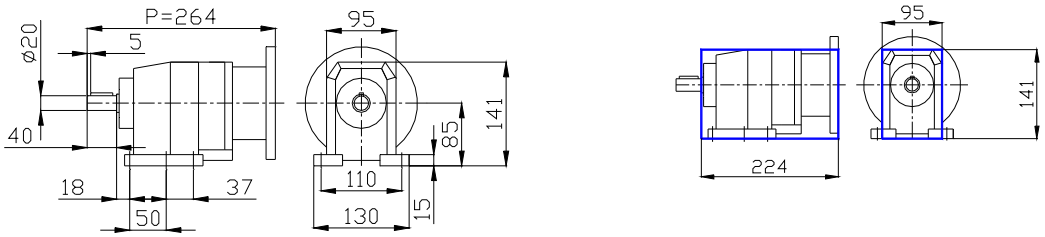

a) b)

Figure 1.4 a) Sketch with physical dimensions in mm. b) Sketch, where an estimated gear volume is illustrated with blue colour.

$$\rho_T = \frac{T_{Nom}}{V_T} = \frac{48}{0.224 \cdot 0.095 \cdot 0.141} \approx 16 \cdot 10^3 \left[\frac{Nm}{m^3}\right] = 16 \left[\frac{Nm}{l}\right] \tag{1.6}$$

Efficiency

The total efficiency of a gear is calculated by the power ratio between the output shaft and the input shaft. Precise mechanical gear efficiency is not possible to calculate. However there exist rules of thumb for estimating a total theoretical gear efficiency, which depends on power losses in bearings, seals, lubrication and gearing in it self. The total theoretical gear efficiency is estimated by multiplying theoretically efficiencies for each gearing stage. The theoretical gear efficiency is less accurate than a measurement and does not include any information about rotational speed, which means that it can only be thought of as a theoretical efficiency at nominal speed and torque. Gear manufacturers should inform about measured gear efficiency instead of a theoretically estimated efficiency in the data sheet. Efficiency is a competitive parameter and that is the reason why efficiencies from datasheets are expected to be optimistic.

1.7.1 Mechanical spur gear and the helical gear

The mechanical spur gear type is one of the most simple gear topologies. A sketch of this gear type is illustrated on Figure 1.5 a). Another variant of this technology is the helical gear type Figure 1.5 b). The two gear technologies are often used in mechanical gear boxes.

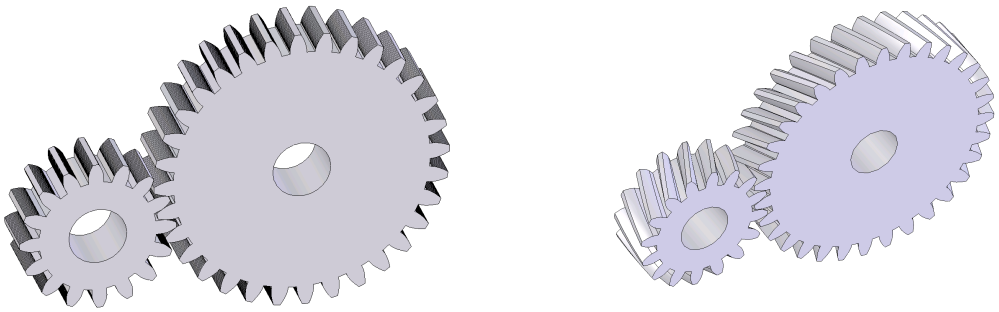

a) b)

Figure 1.5 a) A mechanical spur gear. b) A Mechanical helical gear.

The gearing for helical and spur gears are not so often larger than 6 [3], because the large wheel will become unnecessary large if larger gearing is chosen. The torque density is calculated for the helical gears and the data are gathered from 3 different manufacturers. Different gearing intervals are chosen with different gear torque ratings. Some of the best gears are picked out of the manufacturer data sheets regarding torque density. The results from helical gears are shown in the following Table 1.

Type	**Ref.**	**R_g**	**T**	**Speed**	**Stage**	**ρ_T**	**η**
[-]	[no.]	[-]	[Nm]	[RPM]	[-]	[Nm/l]	[%]
C11 2P-4.9-P90	[2]	1:4.9	48	1400	2	16	95
C11 2P-20,6_P80	[2]	1:20.6	82	1400	2	27	95
C41 2P-44,8-P90	[2]	1:44.8	500	1400	2	51	95
C100 3P-150,4-P132	[2]	1:150.4	12000	1400	3	83	93
12,8 R17 CT71D	[4]	1:5.09	51	[-]	2	17	-
12,8 R17 CT71D	[4]	1:19.71	85	[-]	2	28	-
12,13 R67 CT 71D	[4]	1:28.13	540	[-]	2	56	-
12,13 R67 Ct71D	[4]	1:158,14	600	[-]	3	63	-
RD02	[5]	1:5.276	38	1400	2	24	96
RD02	[5]	1:21.533	51	1400	2	33	96
RD02	[5]	1:48.667	35	1400	2	23	96
RD03	[5]	1:324.444	36	1400	3	23	94

Table 1 Torque density and efficiency comparison of mechanical helical gears.

The gearing power loss from a single stage spur gear or helical spur gear can be calculated from general gear efficiencies known from the mechanical literature [6]. A mechanical spur gear will have a gear efficiency of 98% to 99% if the gear friction is taken into account. Another variant is helical gear. These gears have a force reacting on the axial bearings and therefore a lower efficiency, typical about 96% to 98%. Advantages for the helical gear are lower noise, more teeth are active at the same time and this type can carry higher load than a corresponding spur gear.

1.7.2 Mechanical planetary gear

The mechanical planetary gear is another common used gear technology. This gear type has 2 degrees of freedom (2-DOF), while two inputs are needed to obtain a single output, unlike the previous described spur gear type with only 1-DOF [6]. An exploded view of a planetary gear is illustrated on Figure 1.6. The gear technology consist primary of an inputs shaft, a ring part and an output shaft. The gear becomes 1-DOF if one of the three parts is fixed; in this shown example, the ring is held stationary. Working principle for this gear is to rotate the input shaft and hereby rotate planet gear wheels, which are connected to a driven output shaft.

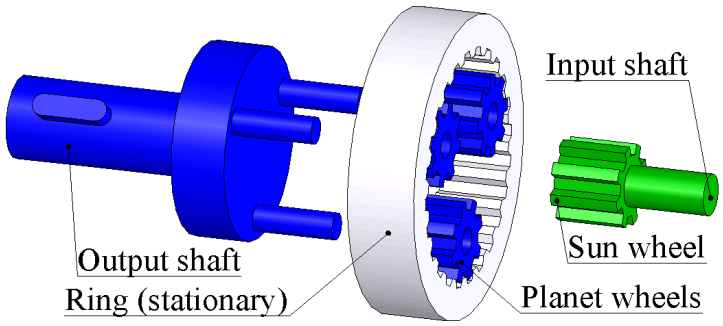

Figure 1.6 Mechanical planetary gear (exploded view).

The torque density is calculated for planetary gears from 3 different manufacturers. The results are shown in Table 2.

Type	**Ref.**	**R_g**	**T**	**Speed**	**Stage**	**ρ_T**	**η**
[-]	[no.]	[-]	[Nm]	[RPM]	[-]	[Nm/l]	[%]
PLS90 HP	[7]	1:5	220	500	1	265	98
PLS90 HP, 2 stage	[7]	1:20	220	2000	2	189	95
PLS60 HP, 2 stage	[7]	1:64	120	5000	2	103	95
SP +100, 1 Stage	[8]	1:5	105	4500	1	48	98,5
SP +100, 2 Stage	[8]	1:20	105	4500	2	60	96,5
SP +100, 2 Stage	[8]	1:100	65	4500	2	37	96,5
P501SPN0050	[9]	1:5	200	2000	1	92	95-97
P812SPN0200	[9]	1:20	743	2000	2	119	95-97
P812SPN1000	[9]	1:100	800	2000	2	128	95-97

Table 2 Torque density and efficiency comparison of mechanical planetary gears.

Torque density is extremely high for the “PLS90 HP” gear type and the theoretical efficiency for this gear type is also noticeable high. The torque density seems to vary a lot for different gear types and also for different manufacturers. The reason for this can be that the gear housing is made in different sizes and in order to limit the gear box manufacturers costs, there might be compromise in choosing a big gearbox house where a smaller model can fitted in.

1.7.3 Mechanical cycloidal gear

The mechanical cycloidal gear is another 2-DOF gear. This gear consists of an input shaft with an eccentric Figure 1.7. An eccentric pulley drives the mover and it has an outer toothed rim shape connected to the ring. Connection point between the toothed rim and the mover will move when the eccentric pulley is rotated. There is different number of teeth on the mover and ring. If the difference of number of teeth between mover teeth and ring teeth is larger than one, the mover will be indexed backward relative to the stationary ring, each time the eccentric pulley has moved one revolution. The output shaft is driven by the mover by a number of columns. These columns have a tangential connection to the 3 holes in the mover, which will rotate the output shaft.

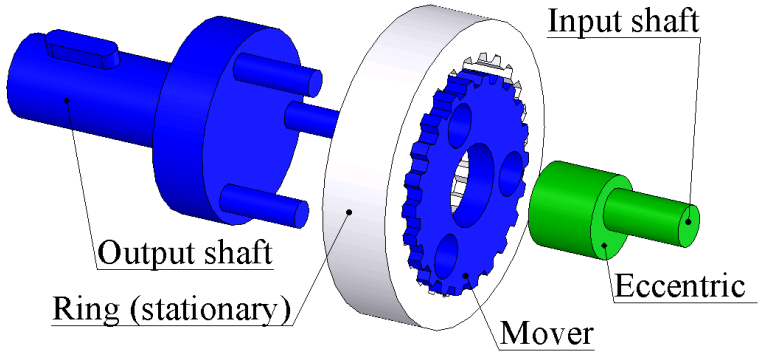

Figure 1.7 Mechanical cycloidal gear (exploded view).

The torque density is calculated for 3 different cycloidal gear manufacturers with different gearing and gear sizes. The results are shown in Table 3.

Type	**Ref.**	**R_g**	**T**	**Speed**	**Stage**	**ρ_T**	**η**
[-]	[no.]	[-]	[Nm]	[RPM]	[-]	[Nm/l]	[-]
Servo 110-Series	[10]	1:11	132	1500	1	111	-
Servo 110-Series	[10]	1:29	200	1500	1	168	-
Servo 110-Series	[10]	1:87	200	1500	1	168	-
6160 (p. A-142)	[11]	1:6	695	1450	1	76	-
6060 (p. A-140)	[11]	1:21	13	1450	1	15	-
6065 (p. A-140)	[11]	1:21	26	1450	1	31	-
6145 (p. A-142)	[11]	1:21	1450	1450	1	159	-
6145 (p. A-142)	[11]	1:87	1200	1450	1	132	-
2C115	[12]	1:6	1920	1135	1	64	95
2D255	[12]	1:21	10600	1165	1	173	95
2K225	[12]	1:87	109000	1165	1	181	95

Table 3 Torque density and efficiency comparison of mechanical cycloidal gears.

It can be seen that the torque density is generally high for cycloidal gears with high gearing relationship and not so high at very low gearing relationships. Gears with the same gearing relationship seem also to have different torque densities. The cycloidal gears efficiencies are specified to 95%, which is lower than the planetary gear.

1.7.4 Harmonic drive

The harmonic drive is another 2-DOF gear variant. The functional principle for this gear type (Figure 1.8) is explained in the following. An ellipse is connected to the input shaft. The ellipse is connected to a flexspline, which is made of a flexible material. The flexspline is deformed to an ellipse shape because the input shaft ellipse part is inserted. The flexspline is directly connected to the output shaft (not shown in Figure 1.8). Teeth on the ring and flexspline are only in connection with each other at two points. There is a different number of teeth's on flexspline and the ring, and this will force the flexspline to rotate relative to the ring, when the input shaft rotates. Figure 1.8 illustrate the ellipse as a solid primitive, but for real harmonic drives, roller bearings are used between ellipse and flexspline for minimise the friction.

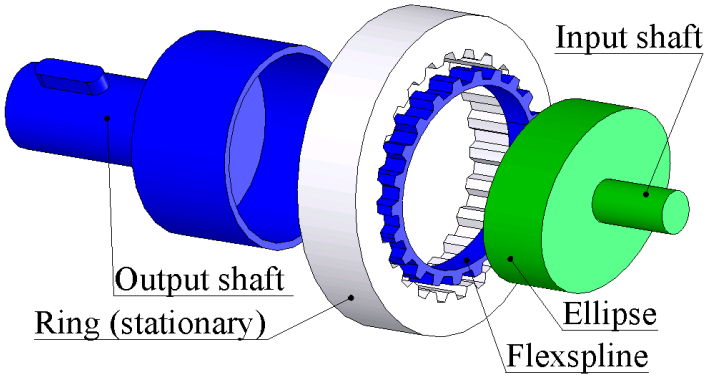

Figure 1.8 Mechanical harmonic drive (exploded view).

The torque densities are calculated for 4 harmonic drives from the same manufacturer. The manufacturer has only gears with gearing relationship between 1:50 and 1:160, which indicates that the gearing principle is not suitable for gearing relationships under 1:50. The torque density results are shown in Table 4. Nominal torque for the 1:160 gearing relationship is not available in the data material and that is why the Table 4 shows gearing relationship up to 1:120.

Type	**Ref.**	**R_g**	**T**	**Speed**	**Stage**	**ρ_T**	**η**
[-]	[no.]	[-]	[Nm]	[RPM]	[-]	[Nm/l]	[-]
RGH 20	[13]	1:50	40	500	1	188	-
RGH 20	[13]	1:120	63	500	1	297	-
RGH 25	[13]	1:50	62	500	1	176	-
RGH 25	[13]	1:120	106	500	1	302	-

Table 4 Torque density comparison of mechanical harmonic drives.

The harmonic drives have a high torque density. The efficiency is not specified in the data sheet for the current gear type. However efficiencies for other harmonic drive types produced by the same producer is rated from approximately 83% and down to 50% efficiency. These efficiencies are also rated at 500[RPM] input speed.

1.7.5 Mechanical worm gear

Worm gear is also a very common gear type that is used in gear applications. Worm gears exist in many configurations. In order to explain the simple function principle for a worm gear, there are made an illustration of this on Figure 1.9. The gear has the input shaft with an Archimedes spline. Spline interacts with teeth's which are on output shaft wheel, torque are hereby transferred from the input shaft to the output shaft with a certain gearing relationship.

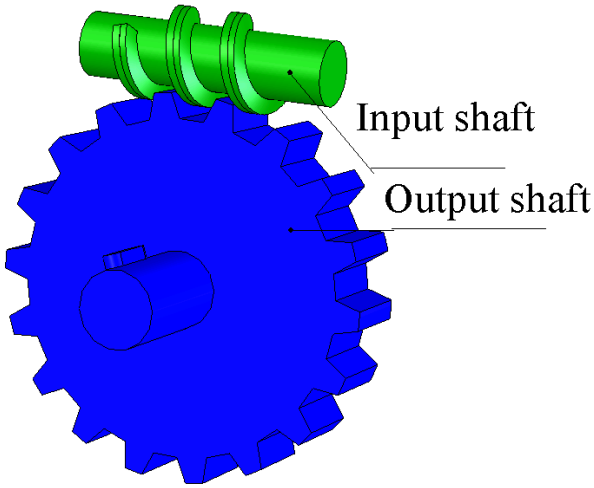

Figure 1.9 Mechanical worm gear.

The torque density is calculated for drives produced by 3 different manufacturers and the results are shown in Table 5. Gearing relationship of this gear type is up to 1:100 per stage.

Type	**Ref.**	**R_g**	**T**	**Speed**	**Stage**	**ρ_T**	**η**
[-]	[no.]	[-]	[Nm]	[RPM]	[-]	[Nm/l]	[-]
RT28	[14]	1:7	18	1400	1	33	-
RT70	[14]	1:20	194	1400	1	40	-
RT150	[14]	1:100	1120	1400	1	29	-
224B	[15]	1:5	74	1750	1	26	-
224B	[15]	1:20	127	1750	1	45	-
224B	[15]	1:100	73	1750	1	26	-
DB961	[16]	1:5	2274	1450	1	33	96
DB961	[16]	1:20	3386	1450	1	49	90
DB961	[16]	1:100	2588	1450	1	38	68

Table 5 Torque density comparison of mechanical worm gears.

Worm gears have relative low torque density and low efficiency. Worm gears are often self locking gear mechanisms, which mean that it is a type gear which can only be forced from the input shaft side, and not from the output side. Backlash adjustment is an extra alternative feature for worm gears and these gears can be adjusted down to zero backlash. This feature can be an advantage for control applications.

1.7.6 Summary

Torque density data from the different mechanical gears are plotted in Figure 1.10 a) in order to compare the different gear types.

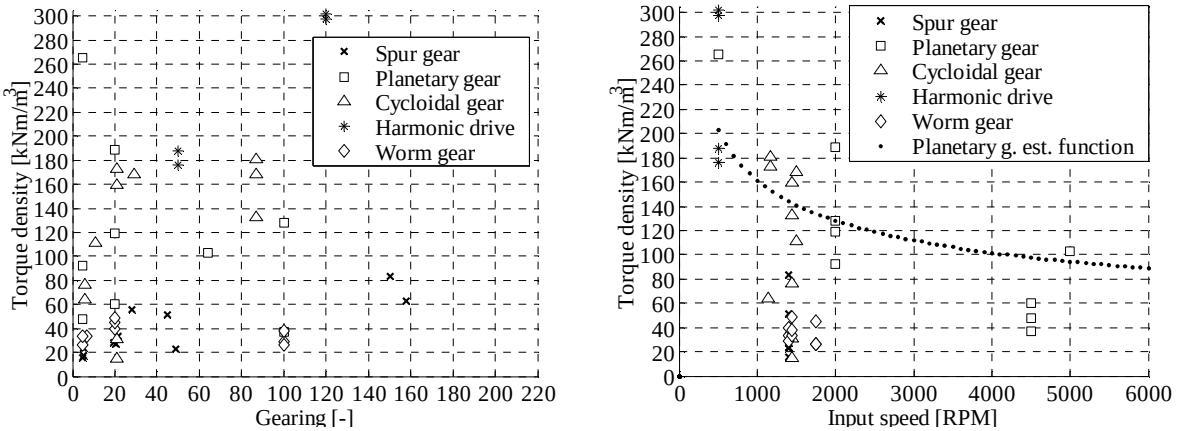

a) b)

Figure 1.10 a) Calculated torque density versus gearing of different mechanical gears. b) Calculated torque density versus input speed of different mechanical gears.

There are large differences between the different gear types. Spur gear, helical gears and worm gears have low torque densities. Planetary gears and cycloidal gears have higher torque densities and harmonic drives seem to have the highest torque density. It must be noticed that the output torque of a mechanical gear is dependent on input shaft speed at where the specific gear is rated at. For instance the torque data for the harmonic drive is specified for a input speed of 500 [RPM] with a torque output at 40 [Nm]. The same gear have torque rated at 28 [Nm] and 22 [Nm] at respectively 1500 [RPM] and 3000 [RPM], which will give 210 [kNm/m^3] and 165 [kNm/m^3]. Another planetary gear is also torque rated at a speed of 500 [RPM]. This gear has a rated torque density of 265 [kNm/m^3] which is quite high. This gear will convert less torque if the gear is operated at higher speed. One planetary gear producer [9] has even included an estimation calculation function for calculating maximum torque as a function of operating speed (1.7) so there is a connection between torque outputs and input speeds. The equation calculates the maximum output torque T_{2NX} at input speed n_1, with a rated speed of 2000 [RPM] and a torque rated at T_{2N}. This function is illustrated on Figure 1.10 b) in terms of torque density.

$$T_{2NX} = \frac{T_{2N}}{\sqrt[3]{\frac{n_1}{2000}}} \tag{1.7}$$

This equation is only directly valid for gear types from this specific gear producer, but the equation might also be valid for other planetary gear as an estimate of a torque. The equation will have to be modified with another reference speed of 500 [RPM] instead of 2000 [RPM], if this equation is used to estimate the torque density of previous described

gear with 265 [kNm/m^3]. Such estimation will result in a torque density of 184 [kNm/m^3] for a rotation speed at 1500 [RPM]. This example indicates that maximum calculated torque densities are dependent of the input velocity. If a rule of thumb for maximum torque densities of mechanical gears in general shall be deduced from this analysis. Then it will not be likely to achieve a torque density of greater than 210 [kNm/m^3] for a gear with a speed of 1500 [RPM] on the input shaft. Gears limited to 500 [RPM] will probably reach a higher maximum torque density up to 300 [kNm/m^3].

The torque density analysis must be thought of as a rough method to estimate an approximate torque density performance so that the reader can get an idea of approximate torque densities available for mechanical gears in general. These torque densities can be compared to torque densities of magnetic gears, however since the torque density of mechanical gears is a function of gearing relationship, manufacturer and torque size it is not possible to make this comparison with only a few gear boxes to represent all mechanical gears which are available. A proper torque density comparison between magnetic gears and mechanical gears can therefore only be made with a larger number of mechanical gearboxes rated at same torque and speed.

There is also a paper [17], where different mechanical gears are compared. The paper concludes that planetary gears are better when it comes to efficiency. Another conclusion is that cycloidal gears are not so suitable for gearing below 1:50. Final conclusion is that the helical gears have efficiencies of approximately of 80%.

Mechanical spur gear and helical gear efficiencies are often very high rated in the literature [6], sometimes as high as 99%. The gears found in this small analysis are also rated very high. Distributors of mechanical spur and helical gears specify efficiencies in the interval 93% to 96%. Planetary gear types are stated to achieve efficiencies from 95% to 98.5%, and cycloidal gear types are stated to achieve efficiencies of 95%. Worm gears have the worst efficiency, down to 68%. All these efficiencies can only be thought of as guiding efficiencies, because there is typically no experimental documentation from the distributor behind these numbers. Gear efficiencies depend also on more parameters like rotational speeds and temperature, so if gear must be compared with each other, there must be performed experiments where these parameters are measured.

1.8 State of the art -Magnetic gears

State of the art magnetic gears are completed in the light of a search in the library databases and patent databases. The magnetic gears search has resulted in different types of magnetic gear technologies. These different technologies are structured into following categories:

- Magnetic gears with closely spaced magnets
- Flux guided magnetic gear mechanisms

The technologies which are found in the searched literature is visualised with computer-rendered images for supporting understanding of function principles. Different materials in these models are computer-rendered with different colour. Magnets are rendered with blue and light grey and the meaning of this is to indicate magnetic north and south pole configuration. A yellow colour represents non-magnetic material, and the green colour represents a magnetically conducting material such as iron.

1.8.1 Magnetic gears with closely spaced magnets

There exist many magnetic gears which can be categorised into the category of magnetic gears with closely spaced magnets. This gear type has typically a magnetic interaction in between magnets on two or more axes. The technology is with the two magnetic gear wheels covered with magnets on the surfaces. These magnets interact with each other and they create a driving force on drive magnet wheel. One example is the very simple radial magnetic spur gear, documented in a couple of books, papers and patents. Furlani, E. P. [18],[19] have developed an equation for the torque of two radial magnetised gear wheels Figure 1.11 a). The torque from the equation is compared with a FEM model, which is based on the same assumptions as in the torque equation. Torque equation and the FEM analysis model show very good agreement.

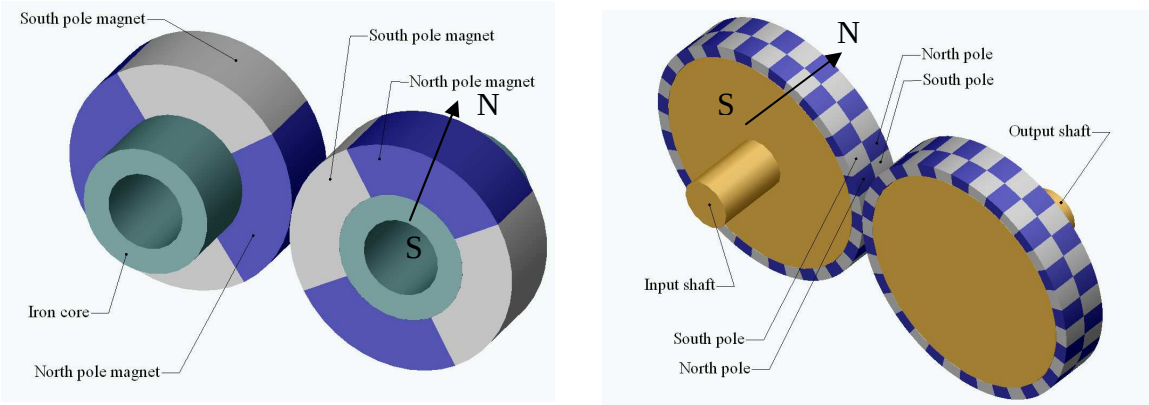

a) b)

Figure 1.11 a) Simple radial magnetic spur gear [18]. b) Magnetic spur gear with magnetisation in the axial direction [20].

A magnetic gear similar to this type is found in a paper [21], where it is described how a radial polarised magnetic spur gear can be optimised to give a maximum torque. The optimisation is accomplished by the use of a FEM software program. In this paper there is no experimental result that verifies the FEM simulations, but in a previous paper [22] from the same authors there is a single experimental test where simulated FEM results are verified. This paper shows there is good agreement with the FEM calculated torque and the experimental results. Another paper [23] also describes the magnetic gear types with closely spaced magnets, where the distance between the magnetic wheels versus the output torque are analysed with an experimental test. A related paper [24] is a description of an experimental test with 3 radial magnetic spur gears. An analytic expression of the output torque is one of the results and this expression is compared with measured torque values as a function of the distance between magnetic gear wheels. Also a patent [20] describes a magnetic gear wheel. This configuration is different, because every single tooth in the magnetic gear wheel has a north and a south pole with axial magnetisation, which is seen on Figure 1.11 b). With this principle the magnetic flux will not follow a direction, which is in the same axis as the previous discussed magnetic spur gear, but instead will a magnetic flux be pointed towards the same axes as gear wheels axes. The technology might increase the magnetic flux and hereby increase the maximum torque for the magnetic gear.

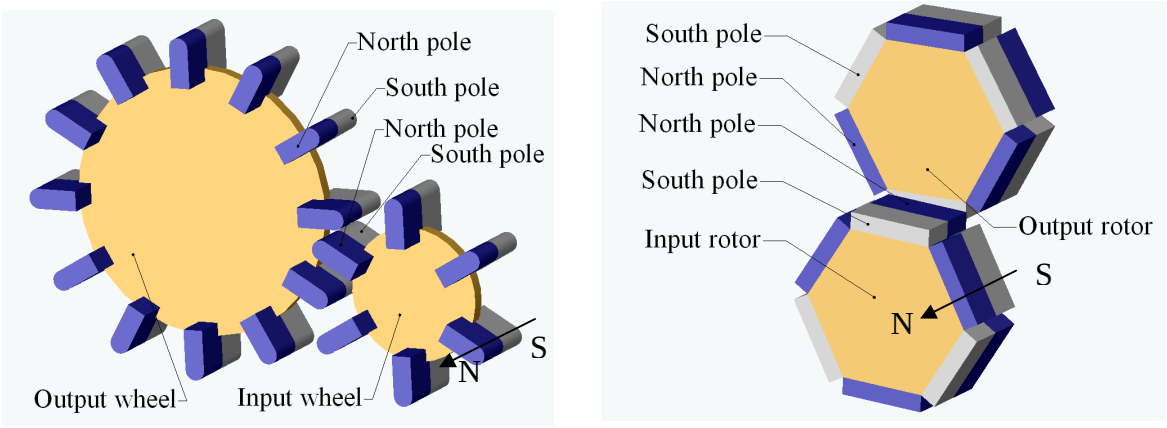

a) b)

Figure 1.12 a) Spur gear with overlapping magnets and axial aligned magnetisation [25]. b) Axially magnetised gear wheels with offset [26].

Another patent [25] describes a magnetic gear equipped with magnets in which the repulsion force is a core detail. This type of gear has all magnets turned with the magnetisation in the same axial direction and not the radial direction Figure 1.12 a). Axial magnetisation will in this configuration try to keep an equal distance between magnetic teeth. There is a mechanical contact between the teeth if the torque is too high in this configuration. Another gear with axial oriented magnets is shown on Figure 1.12 b). This gear is described in a paper [26]. This type of magnetic gear consists of two rotors with permanent magnet on the outer face. The paper has a description of a semi-numerical method to calculate torque. The method is based on numerical integration. Another magnetic gear with magnetisation pointing in axial shaft direction is found in [27], Figure 1.13 a). The paper describes a magnetic gear with a gearing relationship of

3 and a torque of 5.5 [Nm]. The same authors have also written a paper [28], where super conductors are used instead of permanent magnets.

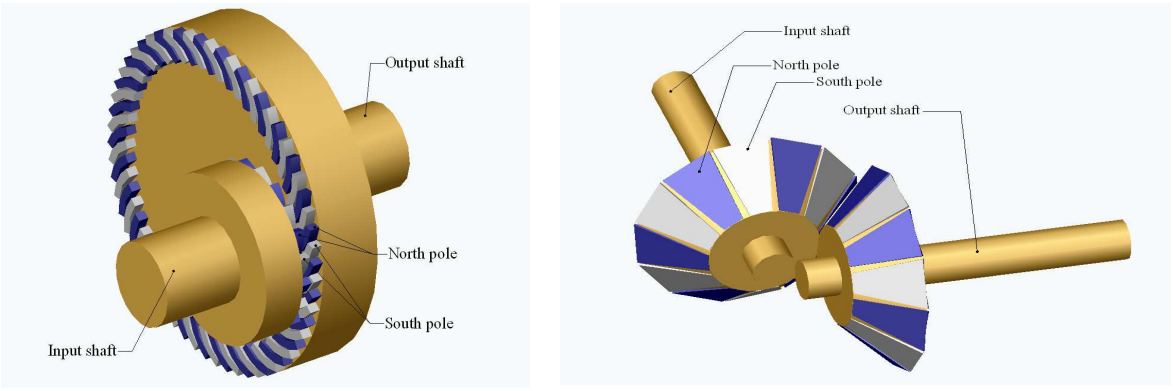

a) b)

Figure 1.13 a) Magnetic gear with magnetisation directed in axial shaft direction [27]. b) Magnetic gear similar to the mechanical bevel gear [29].

There is a description of a magnetic gear similar to the mechanical bevel gear in a paper [29]. The gear consists of two conical wheels, which is covered with shifting north and south poles as show on Figure 1.13 b). Experimental tests are performed in the paper, from which it can be concluded that the transferred torque is increased as the distance between the conical gear wheels is made smaller. Only experimental results are represented in this paper.

In a paper [30] a magnetic worm gear is described. The gear configuration consists of a worm and a worm wheel, which is shown on Figure 1.14 a). The input worm wheel is magnetised with north and south poles and also worm wheel is magnetised. The paper describes experimental results from a gearing with gearing 1:33. This gear can deliver a maximal torque of 11.5 [Nm]. The magnetic worm gear has a less complicated geometry unlike the mechanical gear which has noticeable advanced geometry and it makes this type difficult to manufacture. However the magnetic worm gear is difficult to magnetise.

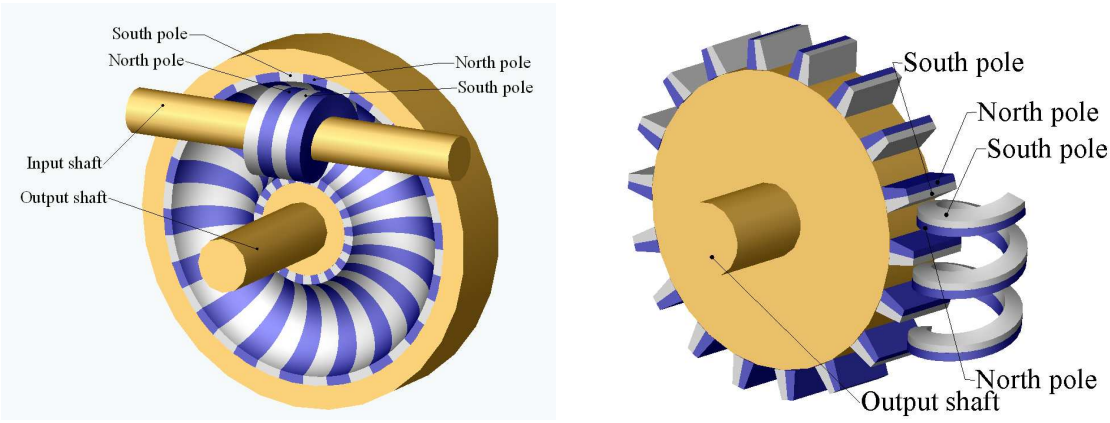

a) b)

Figure 1.14 a) Magnetic worm gear with simple geometry [30]. b) Magnetic gear similar to the worm gear type [31].

In paper [32] from the same author, there is a description of a experimental test where the worm gear has a gearing of 38:66 and the transferred torque is 2.4 [Nm]. In a patent [31] there is a description of a magnetic gear similar to the mechanical worm gear.
The worm is formed a like an Archimedean screw with helical tooth flanges, as shown on Figure 1.14 b). The worm gear flanks are magnetised with magnetic north and south poles. Worm wheel teeth are also magnetised with north and south poles. At the place where wheels flanges interact, there is a magnetic north pole against a magnetic north pole and the magnetic south pole configuration is arranged in the same way. This configuration will force the worm gear wheel to positioning where there is an equal air gap between magnetic pole tooth flanges. This type of gear configuration has the property of making contact between the flanges, when a high load is applied.

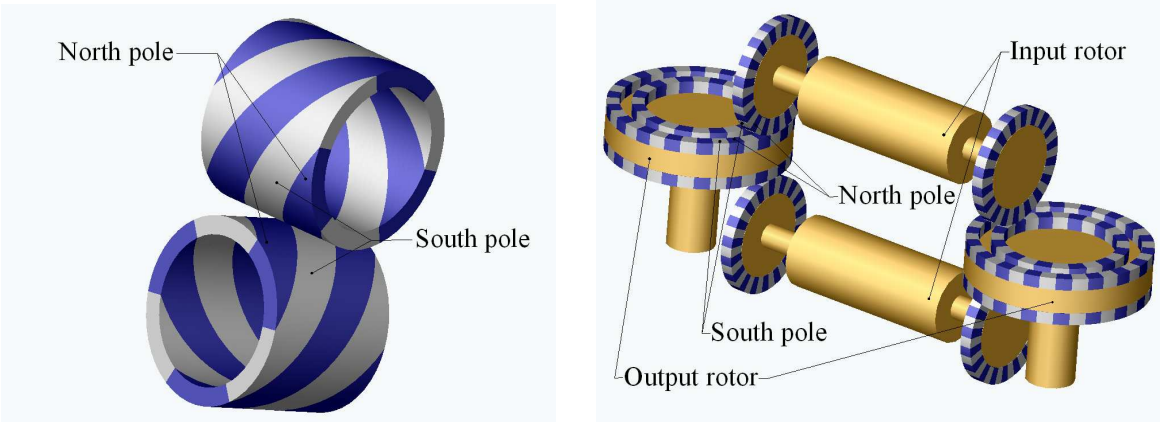

a) b)

Figure 1.15 a) Perpendicular axis gear [33]. b) Variable magnetic gear with two output shafts [34].

A paper [33] describes a gearing with perpendicular axes Figure 1.15 a). The gear consists of two magnet wheels, which is radial magnetised with screw magnetic north and south poles. Influences of different design parameters are investigated by the use of a FEM software. The investigated parameters are screw angle, flux distribution, number of poles, thickness in the magnetised direction, and overhang length. The torque measured from an experimental setup is 0.357 [Nm]. The patent [34] describes a variable magnetic gear consisting of two driving shafts and two driven shafts Figure 1.15 b), which is coupled together with PM magnets. These types of gear are originally intended for airplane applications, with two propellers outputs. Changes in gearings relationship are conducted at the driving shafts. They can shift axial position, and the gearings relationship will be changed, because diameter and number of poles on the driven part can hereby be changed. The gear shift mechanism is similar to mechanical gearboxes with several stages.

A magnetic version of a harmonic gear is recently purposed in [72]. This drive is predicted to obtain an active torque density of op to 110 [kNm/m^3]. Practical implementation of this drive has similarities to the cycloidal gear which is described in this thesis.

1.8.2 Flux guided magnetic gear mechanisms

The previous described magnetic gears have magnets with close spacing so that the magnetic flux travels from a magnet to an air gap and further to another magnet. Other gear types have iron elements included. These gears will typical operate by moving the main flux. In a patent [35] a magnetic gear with parallel shafts is presented. The gears consist of two shafts, which are magnetised with north and south poles. In between these shafts there are iron segments that guide the magnetic flux. The basic principle for the magnetic transmission is shown on Figure 1.16 a).

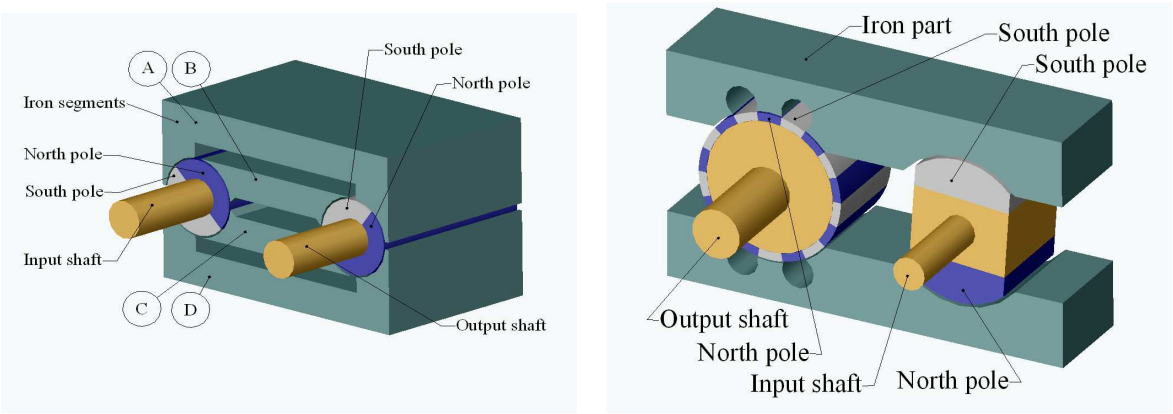

a) b)

Figure 1.16 a) Flux guided magnetic gear with a gearing relationship of 1:1 [35]. b) Flux guided magnetic gear with a gearing relationship of 1:n_p, n_p=9 [36].

In a situation, where the flux guided magnetic gear is shown Figure 1.16 a), the main magnetic flux will passes through two of the segments marked with B and D, and in the other segments A and C, the magnetic flux will be less. In another situation when the magnetic wheels are rotated to a position where north and south direction on the wheels is vertical, then the magnetic flux will be equally distributed in the two circuits. If the axles are rotated further, the main magnetic flux will follow a path that pass segment A and C, and in the other segments the magnetic flux will be less. This design will have gearing relationship of 1:1.

Another patent [36] describes a flux guided magnetic gear, with the gearing relationship of 1:n_p, where n_p is the number of pole pairs on the output shaft rotor. This transmission gear also consists of two shafts with rotors, which will guide flux through two iron segments. Figure 1.16 b) illustrates the magnetic transmission gear. This gear type has only a single phase and for this reason there might be operation problems. Other versions of magnetic gears with tooth segments are also found [37]. This gear uses electro magnets to create magnetic flux in iron segments Figure 1.17 a). The reason for using electro magnets is because this gear is from the early days of permanent magnet history.

A linear version of a flux moving mechanism is also presented in a patent [38]. The linearly gear is shown on Figure 1.17 b). The gear type consists of a driving shaft where permanent magnets are fastened. Furthermore there are some iron segments to guide the magnetic flux. The linear part consists of iron segments with teeth. When the driving shaft is rotated, will magnetic flux be forced to pass through certain iron segments, and the resulting adjusted position between iron segments and track will be where majority of magnetic flux passes through.

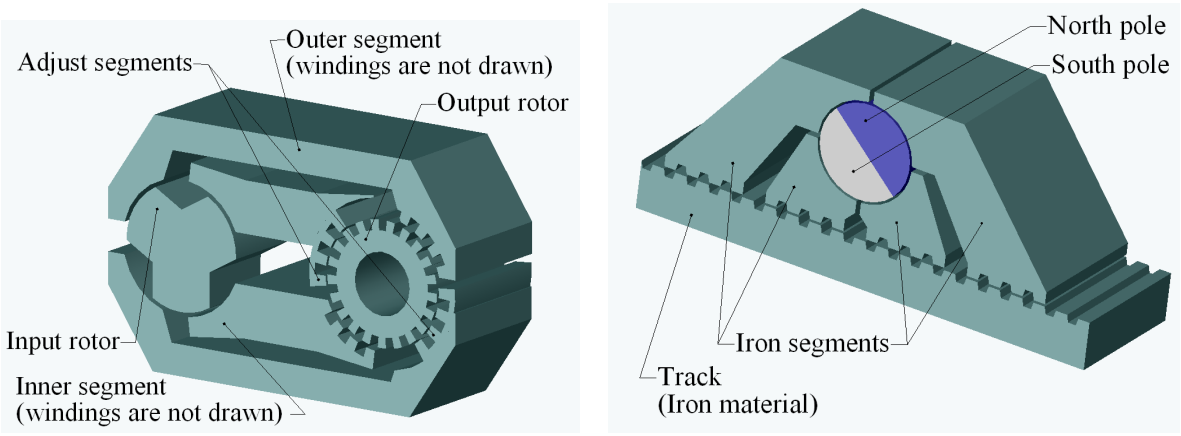

a) b)

Figure 1.17 a) Flux moving gear mechanism with electro magnets [37]. b) Linear magnetic gear [38].

A patent [39], describes a more compact flux moving mechanism. In this patent there is described different gearing with different configurations regarding the number of segments and the number of permanent magnets on the output shaft and input shaft. The patent is also with different shape examples for the middle steel segment part. One of the gear configurations is shown on Figure 1.18 a).

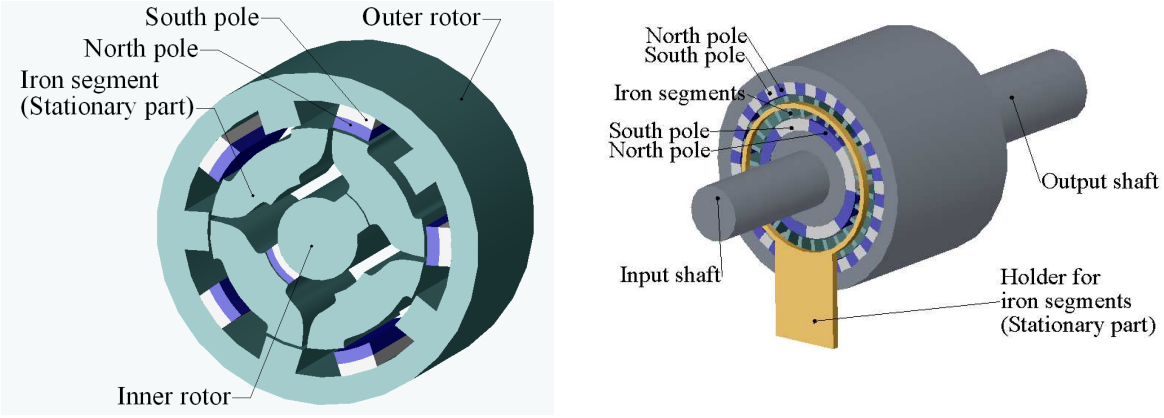

a) b)

Figure 1.18 a) Magnetic gear similar to the mechanical planetary gear type [39]. b) High performance magnetic gear [1].

In publication [1] a planetary magnetic gear described and an illustration of this gear is shown on Figure 1.18 b). This gear has a similarity to a mechanical planetary gear. The basic structure of this gear type is like the previous described gear because the magnetic fluxes are also forced to pass through certain segments and with a certain angle. The magnetic flux path has different shape and different magnitude, and hereby also different energy contents. Flux shift in shape and magnitude is driven by torque from the input shaft. The magnetic flux will change most in iron core segments. The output shaft will be driven by flux changes in the iron core segments. Another magnetic gear with the function principle similar to the mechanical planetary gear shown on Figure 1.6 is described in [75]. Permanent magnets are replaced by mechanical teeth not only on the central input shaft but also at the outer ring and planet wheels. A simulation study has shown a relatively high active torque density at nearly 100 [kNm/m^3] with a relative small air gap distance of only 0.5 mm. Estimation of the measured active torque density is approximately (4.4 x 3)/ (π x 0.047^2 x 0.040) = 47.6 [kNm/m^3] for a configuration type with 3 planet gear wheels, similar to the configuration shown on Figure 1.6.

There exist many references to planetary magnetic gear versions and they can be found in chapter 4 where search results from this magnetic gear type is presented in chronological order.

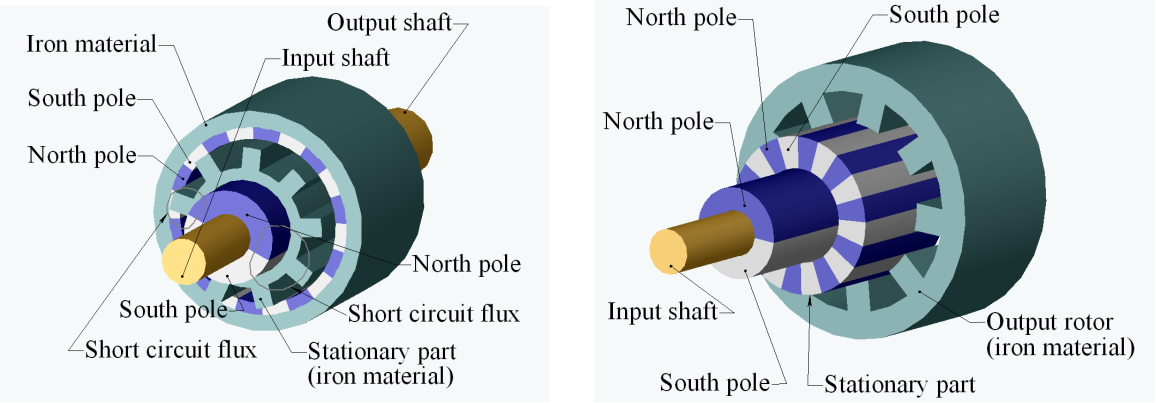

a) b)

Figure 1.19 a) Ackermann's patent with middle part made in iron [40]. B) Ackermann´s patent with outer part made in iron [41].

A patent [40], which most of all is similar to the planetary magnetic gear type is Ackermann's patent from 1997. An outline drawing from the patent is shown on Figure 1.19 a). The basic mode of operation is similar to previous described high performance magnetic gear. Ackermann's patent gives a good understanding of function with a series of pictures. This gear has a problem with short circuiting flux at the inner rotor. However this problem is solved by a newer patent from Ackermann [41], which is shown on Figure 1.19 b). This patent minimises the short-circuiting with a steel output rotor. But a magnetic ring with high stack is not easy to make.

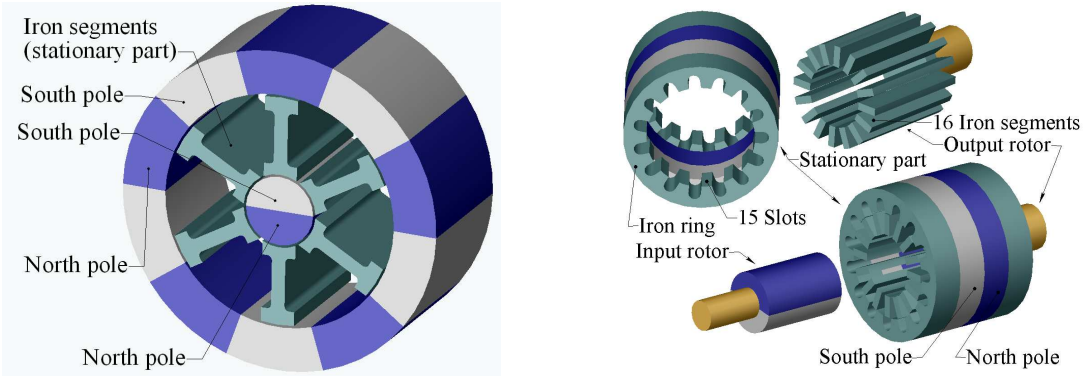

a) b)

Figure 1.20 a) Martin's version of the planetary magnetic gear [35]. b) Magnetic planetary gear, with high gearing relationship [35].

Similar gear types are also described in the patent of Martin Jr. T. B [35]. This gear is shown on Figure 1.20 a). The gear is very similar to the high performance magnetic gear described previously. The iron segments in this version are very thin. This might increase the flux density in the iron segments and hereby cause saturation in the iron, however there were not developed neodymium magnets in 1960, which explains the design with thin iron segments. Segments are also relatively elongated here and this will cause unnecessary long flux paths. Same patent by Martin [35] describes a technology which has a high gearing of 1:16. An illustration sketch for showing function principle is pictured on Figure 1.20 b). The gear consists of a 2-poled inner magnetised rotor, an output shaft with iron segments and an outer stationary part with permanent magnets and iron rings to guide the magnetic flux. The stationary part has iron rings with 15 segments and the output rotor has 16 iron segments. The principal function for this gear works as following. If the inner rotor is rotated to a position, where magnet north pole direction is at "12 o clock", it will induce that upper half of the output shaft iron elements to be magnetised with a north pole magnetisation. North pole magnetisation of the iron elements will be attracted to the magnetised south pole in the upper half of the stationary part. When the rotor has rotated one round, then the output shaft rotated the 1/16 round caused by magnetisations shift in iron segments.

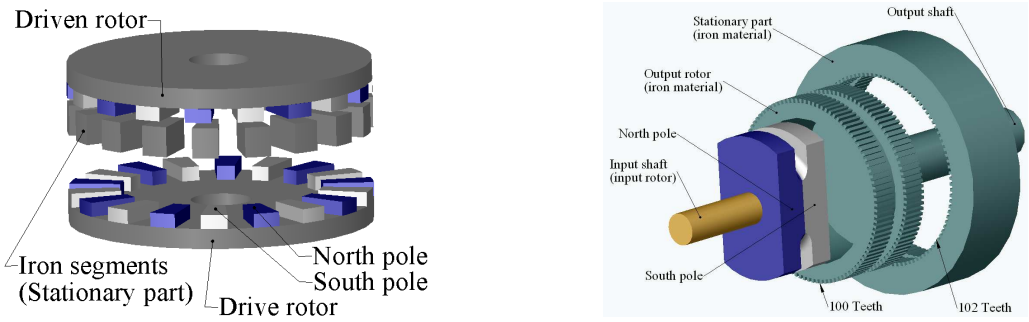

a) b)

Figure 1.21 a) Axial version of the planetary alike gear [42]. b) The patent [43] describes a magnetic version of a harmonic drive [43].

The flux guided principle is also found in a patent [42]. Function of principle for this patent is similar to the magnetic planetary gear type described; however this version is modified to operate axially. The gear is illustrated in Figure 1.21 a). It consists of two rings, which are magnetised with north and south poles on the side of the magnetic ring. The two rotate around the same axis and the magnet elements are faced against each other. A segmented steel plate is placed between the two magnetic rings and this segmented plate transfers the torque. This axial type is also described in [73] with a predicted torque density of 70 [kNm/m^3]. Another flux moving mechanism [43] consists of 3 parts. Two of these parts are made of iron materials and the third is made of permanent magnet material. This gear has an input rotor part which consists of a permanent magnet and an output rotor made of iron material Figure 1.21 b). The stationary outer part is also an element of iron and this element has 102 teeth on the inside. The output rotor has 100 teeth on the outside. When one tooth from the stationary part is aligned to a tooth on the output rotor, there will also be an alignment 180 [°] from this place. When zero torque is applied, the rotor will ensure this precise alignment between the output rotor and the stationary part. If the rotor north pole starts at “12 a clock” on the stationary outer part and rotates a clockwise rotation it will result in a rotation increment at the output shaft by 2 teeth. Because the output shaft has 100 teeth, then there will be a gearing of 50. It is stated that this type of gear principle can be designed to achieve high gearing.

Chapter 2 Magnetic spur gear

This chapter describes the development of an analytical expression for calculating the torque of a permanent magnetic spur gear. The analytical calculation is verified with a physical test model and FEM calculations. Optimisations with the analytical expressions are performed to determine an obtainable level of torque density.

2.1 An existing gear theory for radial magnetisation

The radial magnetised spur gear is one of the most commonly analysed magnetic gears. This gear type is analysed analytically in [18], [19], and also by the use of FEM calculation methods. The calculation time for a FEM model is often larger than for an analytical calculation routine. This is why the analytical calculation is preferred. Radial magnetised magnets are often more expensive to manufacture than parallel magnetised magnets, so parallel magnets can be an alternative to radial magnetised magnets. Analytical calculation expressions for parallel-magnetised spur gears are searched in the literature and appropriate literature for analysing magnetic spur gears is not found. However these expressions will be developed on the basis of radial magnetisation gear theory with parallel magnetisation.

2.2 Improved theory for parallel magnetisation

This section describes the improved theory behind a modified version of the Furlani gear equations. Figure 2.1 shows the source magnet and drive magnet, which is used in the theoretical description. The explanation of this theory is split into two parts. The first part is where Boundary Value Problem (BVP) theory is used to obtain a free space field solution for the source magnet. In second calculation part the drive magnets are reduced to an equivalent current density distribution and the torque is computed under considering the current density distribution is under external influence field from the source magnet.

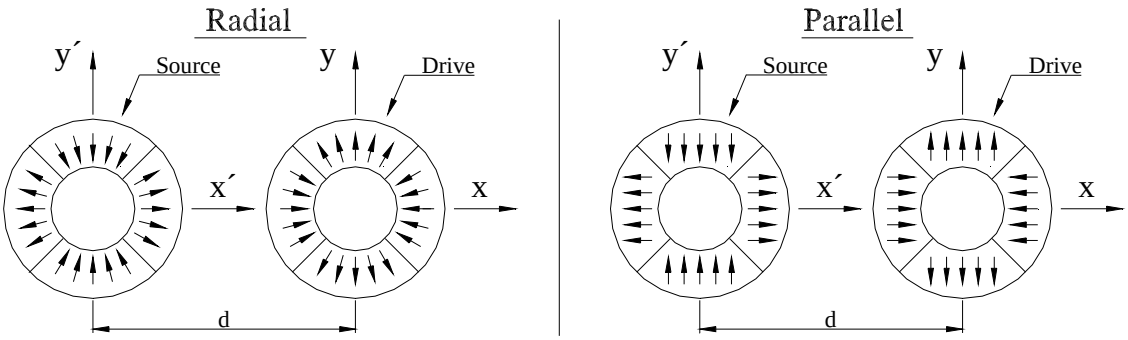

Figure 2.1 Source and drive magnet sketch for radial and parallel magnetised gear.

The free space field solution is a rather complicated subject, which is why this topic is explained in a separate section called “The free space field solution”. The essential result from this section is to be able to express the B-field as a function of coordinate position. The free space solution is defined for the source magnet. The drive magnet has no influence on this solution i.e. the relative permeability is assumed to be one. At the end of “The free space field solution” section there is a transformation of the defined B-field into the drive magnet coordinate system, where the torque is calculated. The drive magnet is reduced to an equivalent current density distribution which is explained in the section “Equivalent surface current density determination”, where a permanent magnet is substituted with a current density distribution. The current densities are present at the outer surface of each magnet pole on the drive magnet side. Since it is a surface current density distribution it is expressed per units distance at the surfaces. The torque is finally calculated in the last section “Torque expression”, where there is an integration of the torque expression along the surfaces of the drive magnets. The torque integration expression uses the B-field solution of the source magnet and the equivalent current density distribution of the drive magnet to calculate torque, and that is the coupling part between source and drive magnet.

2.2.1 The free space field solution

E. P. Furlani has previously described the free space solution of a radial magnetised pole pieces. Documentation for this theory is explained in [18] and this theory is the foundation for developing a new expression. In the explanation of parallel gear theory, there is used the same terminology and approach as for the radial formulation. The new expression describes the B-field distribution for a parallel-magnetised magnetic spur gear. Analytical calculation expressions for parallel magnetised magnets with arc shape is searched in the literature and there is found parallel magnetised arc magnet expressions, where there is included back iron in the stator and rotor [44] [45]. Intensions for these equations are that they are to be used for electrical machines purpose that is the reason why these expressions are not directly applicable for formulation of B-field. It is therefore necessary to develop a parallel magnetisation expression.

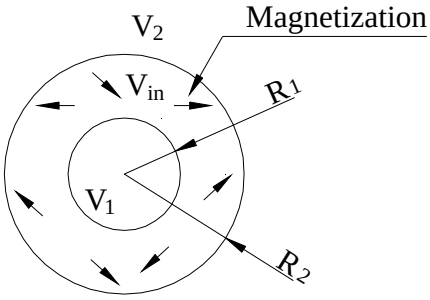

Figure 2.2 Arbitrary magnetised cylinder

One of the ideas of developing a parallel magnetised expression is to use the formulation of an arbitrary magnetised cylinder [18] and "magnetise" this formulation with a parallel magnetisation expression (2.8) instead of a radial magnetisation expression [18]. The first step is to develop this parallel magnetisation expression and rewrite it so it can be used in the arbitrary formulation. This expression can be written as a vector field expression with radial and tangential parts (2.8). The expression for the parallel magnetisation is found in [46], where the magnetisation unit vectors exist in both radial and tangential direction unlike in [18].

$$\mathbf{M_s}(r,\phi) = M_r \cdot \hat{\mathbf{r}} + M_\phi \cdot \hat{\boldsymbol{\varphi}} \tag{2.8}$$

Radial magnetisation and tangential magnetisation are expressed as Fourier expressions. The period in the Fourier expressions can not be the same for the radial magnetisation [18] and for the new parallel expressions (2.8)(2.9)(2.10) which take its basis in [46], because expressions in [18],[19] is defined for number of poles, the new parallel expressions has to be modified from $(i\phi)$ period to another period by substituting parallel magnetisation expressions from [46] with "$\frac{1}{2}iN_p$" where it is "i" in [46] because pole pairs are used in expressions from [46].

$$\begin{aligned} M_r(\phi) &= \sum_{i=1,3,5}^{\infty} M_{ri} Cos(\tfrac{1}{2} iN_p \phi) \\ M_\phi(\phi) &= \sum_{i=1,3,5}^{\infty} M_{\phi i} Sin(\tfrac{1}{2} iN_p \phi) \end{aligned} \tag{2.9}$$

$$\begin{aligned} M_{ri} &= \frac{B_r}{\mu_0 \pi} \cdot \frac{2N_p}{1-(\frac{1}{2}iN_p)^2} \left[\sin\left(\frac{\pi}{N_p}\right) \cos\left(\frac{\pi}{2} i\right) - \tfrac{1}{2} iN_p \cos\left(\frac{\pi}{N_p}\right) \sin(\frac{\pi}{2} i) \right] \\ M_{\phi i} &= \frac{B_r}{\mu_0 \pi} \cdot \frac{2N_p}{1-(\frac{1}{2}iN_p)^2} \left[\cos\left(\frac{\pi}{N_p}\right) \sin\left(\frac{\pi}{2} i\right) - \tfrac{1}{2} iN_p \sin\left(\frac{\pi}{N_p}\right) \cos(\frac{\pi}{2} i) \right] \end{aligned} \tag{2.10}$$

Notice that this expression is not valid for one set of pole pair when $N_p = 2$, because this will give an infinite number.

The trigonometric Fourier functions are used to define the coefficient D_i found in [19]. This coefficient is found by inserting the magnetisation $\mathbf{M_s}$ vector into the volume charge density expression ρ_m which is defined in [19]. This expression can be understood as source term for the boundary value problem formulation. This procedure

is similar to the procedure which is used for finding the radial magnetisation expression in [18], but the magnetisation expression is now different so (2.14) will not be the same as in [18]. The substitution of $\mathbf{M_s}$ and reduction of the expression are shown in (2.13).

$$\rho_m = -\frac{\mu_0}{\mu}\nabla \cdot \mathbf{M_s} \tag{2.11}$$

Remember that divergence [19] of a vector field is (2.12).

$$\nabla \cdot \mathbf{A} = \frac{1}{r}\frac{\partial(rA_r)}{\partial r} + \frac{1}{r}\frac{\partial A_\phi}{\partial \phi} + \frac{\partial A_z}{\partial z} \tag{2.12}$$

$$\begin{aligned}
\rho_m &= -\frac{\mu_0}{\mu}\left(\frac{1}{r}\frac{\partial(rM_r)}{\partial r} + \frac{1}{r}\frac{\partial M_\phi}{\partial \varphi} + \frac{\partial M}{\partial z}\right) \Rightarrow \\
\rho_m &= -\frac{\mu_0}{\mu}\frac{1}{r}\left(M_r + \frac{\partial M_\phi}{\partial \phi} + 0\right) \Rightarrow \\
\rho_m &= -\frac{\mu_0}{\mu}\frac{1}{r}\left(\sum_{i=1}^{\infty} M_{ri}\cos\left(\tfrac{1}{2}iN_p\phi\right) + \frac{\partial\sum_{i=1}^{\infty} M_{\phi i}\sin\left(\tfrac{1}{2}iN_p\phi\right)}{\partial\phi}\right) \Rightarrow \\
\rho_m &= -\frac{\mu_0}{\mu}\frac{1}{r}\left(\sum_{i=1}^{\infty} M_{ri}\cos\left(\tfrac{1}{2}iN_p\phi\right) + \sum_{i=1}^{\infty}\tfrac{1}{2}iN_pM_{\phi i}\cos\left(\tfrac{1}{2}iN_p\phi\right)\right) \Rightarrow \\
\rho_m &= -\frac{\mu_0}{\mu}\frac{1}{r}\left(\sum_{i=1}^{\infty}\left(M_{ri} + \tfrac{1}{2}iN_pM_{\phi i}\right)\cos\left(\tfrac{1}{2}iN_p\phi\right)\right)
\end{aligned} \tag{2.13}$$

The $\frac{\partial M_z}{\partial z}$ term disappears, because the model is a 2D model. Finally the expression for D_i is written as (2.14).

$$D_i(r) = -\frac{\mu_0}{\mu}\frac{\left(M_{ri} + \frac{1}{2}iN_pM_{\phi i}\right)}{r} \tag{2.14}$$

The D_i expression is substituted into the source term integrals, which lead to two large expressions S_{hi} and S_i. These expressions are substituted into matrix solutions (2.40).

Equation (2.14) includes the absolute permeability (2.15) found in [19]. This absolute permeability can be calculated from the relative permeability μ_r and the permeability of air μ_0. Equation (2.15) is also used in Table 10 to define the relative permeability for a permanent magnet material.

$$\mu = \mu_r \cdot \mu_0 \tag{2.15}$$

The surface charge density $\gamma_m^{(k)}$ is another source term which goes into the boundary value problem formulation, and it must also be substituted into matrix result by a coefficient term $B_i^{(k)}$. Generally there are used the index k = 1 for the inner magnetic field (Figure 2.2) and k = 2 for the outer magnetic field and index "in" for the magnetic material part. The surface charge density is written like (2.16), which is formulated by a similar way as shown in [18], but derived with another magnetisation $\mathbf{M_s}$:

$$\begin{aligned}
\gamma_m^{(k)} &= \mu_0(-1)^{(k)}\hat{\mathbf{r}}\cdot\mathbf{M_s}(r,\phi) \\
\gamma_m^{(k)} &= \mu_0(-1)^{(k)}\hat{\mathbf{r}}\cdot\left(\sum_{i=1}^{\infty}M_{ri}\cos\left(\tfrac{1}{2}iN_p\phi\right)\cdot\hat{\mathbf{r}}+\sum_{i=1}^{\infty}M_{\phi i}\sin\left(\tfrac{1}{2}iN_p\phi\right)\cdot\hat{\boldsymbol{\varphi}}\right) \\
\gamma_m^{(k)} &= \mu_0(-1)^{(k)}\sum_{i=1}^{\infty}M_{ri}\cos\left(\tfrac{1}{2}iN_p\phi\right)
\end{aligned} \tag{2.16}$$

The radial magnetisation term is the only term which is included in the surface charge density, because the tangential term becomes zero caused by the dot product $\hat{\mathbf{r}}\cdot\hat{\boldsymbol{\varphi}}=0$. The surface current densities will give the following $B_i^{(k)}$ coefficients, which are substituted into matrix expression.

$$B_i^{(k)} = \mu_0(-1)^{(k)}M_{ri} \tag{2.17}$$

The next step is to formulate the equations used to solve the boundary value problem. These equations take its basis in boundary conditions [18]. At media interface there are boundary conditions for the magnetic flux density **B** and the magnetic field strength **H**. One of these boundary conditions (2.18) describes the change rate of scalar potential in the surface normal outward direction at the boundary surface. The other boundary conditions (2.19) describe that magnetic scalar potential φ_m^{in} at a certain point on the boundary surface at a radius R_k must be the same as scalar potential $\varphi_m^{(k)}$.

$$\mu\frac{\partial\phi_m^{in}}{\partial n}-\mu_0\frac{\partial\phi_m^{(k)}}{\partial n}=\gamma^{(k)} \qquad at \qquad r=R_k \qquad (k=1,2) \tag{2.18}$$

$$\phi_m^{(in)}=\phi_m^{(k)} \qquad at \qquad r=R_k \qquad (k=1,2) \tag{2.19}$$

The scalar potential ϕ_m must be differentiated regarding the normal outward direction of the rotor. Expressions for these fields come from the radial magnetisation formulation [18]. But it is necessary to correct these expressions to fit into the parallel magnetisation description. Periodic term is modified to a period of "$\frac{1}{2}iN_p$".The harmonic period for the radial expression uses "i" instead. However this is not possible in this case because the period must follow magnetisation expressions (2.9) and (2.10) these expressions has a period defined by $\frac{1}{2}iN_p$. That is the reason why, this period is modified for the parallel-magnetised expression. Many of the expressions in [18] will have to change the period in order to be able to fit with the new magnetisation expressions (2.8).

$$\boldsymbol{\phi}_m^{in}(r,\boldsymbol{\phi})=\sum_{i=0}^{\infty}\left[V_i^{in}(r)\sin(\tfrac{1}{2}iN_p\boldsymbol{\phi})+U_i^{in}(r)\cos(\tfrac{1}{2}iN_p\boldsymbol{\phi})\right] \tag{2.20}$$

$$\phi_m^{(1)}(r,\phi) = \sum_{i=0}^{\infty} r^{\frac{1}{2}iN_p}\left[V_i^{(1)}(r)\sin(\tfrac{1}{2}iN_p\phi) + U_i^{(1)}(r)\cos(\tfrac{1}{2}iN_p\phi)\right] \tag{2.21}$$

$$\phi_m^{(2)}(r,\phi) = \sum_{i=0}^{\infty} r^{-\frac{1}{2}iN_p}\left[V_i^{(2)}(r)\sin(\tfrac{1}{2}iN_p\phi) + U_i^{(2)}(r)\cos(\tfrac{1}{2}iN_p\phi)\right] \tag{2.22}$$

$$\rho_m(r,\phi) = \sum_{i=0}^{\infty}\left[C_i(r)\sin(\tfrac{1}{2}iN_p\phi) + D_i(r)\cos(\tfrac{1}{2}iN_p\phi)\right] \tag{2.23}$$

$$\gamma_m^{\,k}(\phi) = \sum_{i=0}^{\infty}\left[A_i^{(k)}\sin(\tfrac{1}{2}iN_p\phi) + B_i^{\,k}\cos(\tfrac{1}{2}iN_p\phi)\right] \tag{2.24}$$

Solutions written in (2.20) (2.21) (2.22) come from the general 2D solution of a BVP [18], but with a correction of the periodic term. The volume charge density and the surface charge density can also be expressed as Fourier series (2.23) and (2.24). These densities can physically be understood as input sources to the system.

Inside of the magnet where there exists a magnetic material. (2.25) must be solved for this material. Following must also be solved outside (2.26). There is used a method to separate the variables used to solve these equations and this method is the same as used in [18], so expressions from (2.25) to (2.39) are also modified regarding the periodic term.

$$\nabla^2\phi_m^{\,in} = -\rho_m \tag{2.25}$$

$$\nabla^2\phi_m^{\,k} = 0 \qquad (k = 1,2) \tag{2.26}$$

The constants $C_i(r)$, $D_i(r)$,$A_i^{(k)}$ and $B_i^{(k)}$ can be determined once the magnetisation $\mathbf{M_s}$ is specified. Following ordinary differential equations for the unknown coefficients $V_i^{in}(r)$ and $U_i^{in}(r)$ are found by substituting (2.20) and (2.23) into (2.25).

$$\frac{d^2V_i^{in}}{dr^2} + \frac{1}{r}\frac{dV_i^{in}}{dr} - \frac{(\frac{1}{2}iN_p)^2}{r^2}V_i^{in} = -C_i(r) \tag{2.27}$$

$$\frac{d^2U_i^{\,in}}{dr^2} + \frac{1}{r}\frac{dU_i^{\,in}}{dr} - \frac{(\frac{1}{2}iN_p)^2}{r^2}U_i^{\,in} = -D_i(r) \tag{2.28}$$

$$\frac{d^2f}{dr^2} + \frac{1}{r}\frac{df}{dr} - \frac{(\frac{1}{2}iN_p)^2}{r^2}f = g(r) \tag{2.29}$$

With homogeneous solutions $f_1(r) = r^{\frac{1}{2}iN_p}$ and $f_2(r) = r^{-\frac{1}{2}iN_p}$.

Solution: There is used a method of variation of parameters with a general solution form of (2.27) and (2.28). Where c_1 and c_2 are constants and $W(f_1, f2) = f_1 f_2' - f'_2 f_1$ is the Wronskian. This method is used to solve (2.27) and (2.28).

$$f(r) = c_1 f_1(r) + c_2 f_2(r) - f_1(r)\int_{R_1}^{r} \frac{f_2(\eta)g(\eta)}{W(f_1, f_2)(\eta)}d\eta + f_2\int_{R_1}^{r} \frac{f_1(\eta)g(\eta)}{W(f_1, f_2)(\eta)}d\eta \tag{2.30}$$

$$V_i^{in}(r) = E_i r^{\frac{1}{2}iN_p} + F_i r^{-\frac{1}{2}iN_p} - \frac{1}{iN_p}\int_{R_1}^{r} \eta\left[\left(\frac{r}{\eta}\right)^{\frac{1}{2}iN_p} - \left(\frac{\eta}{r}\right)^{\frac{1}{2}iN_p}\right] C_i(\eta)d\eta \tag{2.31}$$

$$U_i^{in}(r) = P_i r^{\frac{1}{2}iN_p} + Q_i r^{-\frac{1}{2}iN_p} - \frac{1}{iN_p}\int_{R_1}^{r} \eta\left[\left(\frac{r}{\eta}\right)^{\frac{1}{2}iN_p} - \left(\frac{\eta}{r}\right)^{\frac{1}{2}iN_p}\right] D_i(\eta)d\eta \tag{2.32}$$

The unknown coefficients $V_i^{(k)}$, $U_i^{(k)}$ (k=1,2) and Q_i are determined by adding the boundary conditions from (2.19) and (2.18). This will result in the following group of simultaneous equations, which can be used to determine $U_i^{(k)}$, P_i, and Q_i.

$$\mu_0 U_i^{(2)} \tfrac{1}{2}iN_p R_2^{-(\frac{1}{2}iN_p+1)} + \mu P_i \tfrac{1}{2}iN_p R_2^{\frac{1}{2}iN_p-1} - \mu Q_i \tfrac{1}{2}iN_p R_2^{-(\frac{1}{2}iN_p+1)} - \frac{\mu \frac{1}{2}iN_p}{R_2}\hat{S}_i = B_i^{(2)} \tag{2.33}$$

$$U_i^{(2)} R_2^{-\frac{1}{2}iN_p} = P_i R_2^{\frac{1}{2}iN_p} + Q_i R_2^{-\frac{1}{2}iN_p} - S_i \tag{2.34}$$

$$U_i^{(1)} R_1^{\frac{1}{2}iN_p} = P_i R_1^{\frac{1}{2}iN_p} + Q_i R_1^{-\frac{1}{2}iN_p} \tag{2.35}$$

$$\mu_0 U_i^{(1)} \tfrac{1}{2}iN_p R_1^{\frac{1}{2}iN_p-1)} - \mu P_i \tfrac{1}{2}iN_p R_1^{\frac{1}{2}iN_p-1} + \mu Q_i \tfrac{1}{2}iN_p R_1^{-(\frac{1}{2}iN_p+1)} = B_i^{(1)} \tag{2.36}$$

$$\hat{S}_i = S_{hi} = \frac{1}{iN_p}\int_{R_1}^{R_2} \eta\left[\left(\frac{R_2}{\eta}\right)^{\frac{1}{2}iN_p} + \left(\frac{\eta}{R_2}\right)^{\frac{1}{2}iN_p}\right] D_i(\eta)d\eta \tag{2.37}$$

$$S_i = \frac{1}{iN_p}\int_{R_1}^{R_2} \eta\left[\left(\frac{R_2}{\eta}\right)^{\frac{1}{2}iN_p} - \left(\frac{\eta}{R_2}\right)^{\frac{1}{2}iN_p}\right] D_i(\eta)d\eta \tag{2.38}$$

The first term in (2.33) is a result of differentiating boundary (2.18) with the $\varphi_m^{(2)}$ expression substituted in to this equation. The next terms can be identified from differentiation of φ_m^{in}, which will give a differentiated expression for U_i^{in} (2.32). The fourth term in (2.33) is not straight forward to recognise, but it also comes from differentiation. This differentiation process is easiest to identify on (2.30) and not on (2.32).

Boundary conditions (2.19) are used to define (2.34). (2.35) is also found from boundary condition (2.19), but the last part of the equation with the integration expression is missing because the integration is from R_1 to R_1 so this part of the integration becomes zero. Boundary condition (2.18) is also used to define (2.36), where an integration part also disappears.

(2.33) to (2.36) can be written in matrix form. Matrix expression (2.39) is used to determine $U_i^{(k)}$, P_i and Q_i coefficients. A similar matrix expression can be used to find coefficient $V_i^{(k)}$, E_i and F_i.

$$\begin{bmatrix} 0 & 1 & \frac{\mu}{\mu_0} R_2^{\,iN_p} & -\frac{\mu}{\mu_0} \\ 0 & 1 & -R_2^{\,iN_p} & -1 \\ 1 & 0 & -1 & -R_1^{\,-iN_p} \\ 1 & 0 & -\frac{\mu}{\mu_0} & \frac{\mu}{\mu_0} R_1^{\,-iN_p} \end{bmatrix} \cdot \begin{bmatrix} U_i^{(1)} \\ U_i^{(2)} \\ P_i \\ Q_i \end{bmatrix} = \begin{bmatrix} R_2^{\frac{1}{2}iN_p+1}\left(\frac{\mu}{\mu_0}\frac{S_{hi}}{R_2} + \frac{2B_i^{(2)}}{\mu_0 iN_p}\right) \\ -R_2^{\frac{1}{2}iN_p} S_i \\ 0 \\ R_1^{-\frac{1}{2}iN_p+1}\frac{2B_i^{(1)}}{\mu_0 iN_p} \end{bmatrix} \tag{2.39}$$

One of the solution for matrix expression leads to an expression $U_i^{(2)}$ (2.40), where S_{hi}, S_i, $B_i^{(1)}$ and $B_i^{(2)}$ must be substituted into this matrix.

$$\begin{aligned} U_i^{(2)} &= \frac{U_i^{(2),num}}{U_i^{(2),den}} \\ U_i^{(2),num} &= -\Big[-R_2^{(\frac{2}{2}N_p i+1)}\mu_0 R_2^{(N_p i)} R_1^{(-N_p i)}\mu S_{hi} N_p i - 2R_2^{(\frac{1}{2}N_p i+1)}\mu_0 R_2^{(N_p i)} R_1^{(-N_p i)} B_2 R_2 \\ &+ R_2^{\left(\frac{1}{2}N_p i+1\right)}\mu_0\mu S_{hi} N_p i + 2R_2^{(\frac{1}{2}N_p i+1)}\mu_0 B_2 R_2 - R_2^{(\frac{1}{2}N_p i+1)}\mu^2 R_2^{(-N_p i)} S_{hi} N_p i \\ &- 2R_2^{(\frac{1}{2}N_p i+1)}\mu R_2^{(N_p i)} R_1^{(-N_p i)} B_2 R_2 - R_2^{(\frac{1}{2}N_p i+1)}\mu^2 S_{hi} N_p i - R_2^{(\frac{1}{2}N_p i+1)}\mu B_2 R_2 \\ &+ \mu R_2^{\left(\frac{1}{2}N_p i\right)} S_i R_2 N_p i\mu_0 R_2^{(N_p i)} R_1^{\left(-N_p i\right)} + \mu R_2^{\left(\frac{1}{2}N_p i\right)} S_i R_2 N_p i\mu_0 \\ &+ \mu^2 R_2^{\left(\frac{1}{2}N_p i\right)} S_i R_2 N_p i R_2^{\left(N_p\right)} R_1^{\left(-N_p i\right)} - \mu^2 R_2^{(\frac{1}{2}N_p i)} S_i R_2 N_p i - 4\mu R_2^{(\frac{1}{2}N_p i+1)} B_1 R_2\Big] \\ U_i^{(2),den} &= \Big[\Big[2\mu\mu_0 R_2^{\,N_p i} R_1^{(-N_p i)} + 2\mu\mu_0 + R_2^{(N_p i)} - \mu^2 \\ &+ \mu_0^{\,2} R_2^{(N_p i)} R_1^{(-N_p i)} - \mu_0^{\,2}\Big]\Big[R_2\left(N_p i\right)\Big]\Big] \end{aligned} \tag{2.40}$$

The solution to coefficient $U_i^{(2)}$ from matrix expressions can be solved by the following procedure [18]: There is given a magnetisation $\mathbf{M_s}(r,\phi)$, which can be used to determine coefficients for the surface and volume charge densities $C_i(r)$, $D_i(r)$, $A_i^{(k)}$, $B_i^{(k)}$. After that, $D_i(r)$ and $B_i^{(k)}$ are substituted into (2.39), and $C_i(r)$, $A_i^{(k)}$ into the corresponding equation for coefficient $V_i^{(k)}$, E_i and F_i. Now there are two sets of decoupled equations for the unknown coefficients $U_i^{(k)}$, P_i , Q_i and $V_i^{(k)}$, E_i, F_i. These equations are solved for $U_i^{(k)}$ and $V_i^{(k)}$. These coefficients are substituted into (2.21) and (2.22) to get the desired field solution.

The substitution of variables $B_i^{(k)}$ and $D_i(r)$ leads to a large expression, which can be reduced to (2.41), which is part of the new parallel magnetisation formulation.

$$U_i^{(2)} = -2\mu_0 \frac{H_{ri}}{L_i} M_{ri} - 2\mu_0 \frac{H_{\phi i}}{L_i} M_{\phi i} \tag{2.41}$$

$$\begin{aligned} H_{ri} = {} & R_2\mu_0\left(R_2^{(N_p i)}\right)^{\frac{3}{2}} N_p i + 2R_1^{(N_p i)}\sqrt{R_2^{N_p i}}\,R_2\mu - R_1^{(N_p i)}\sqrt{R_2^{(N_p i)}}\,R_2\mu_0 N_p i \\ & -2\sqrt{R_1^{(N_p i)}}\,\mu R_1 R_2^{(N_p i)} N_p i - 2R_2\mu\left(R_2^{(N_p i)}\right)^{\frac{3}{2}} + 4\sqrt{R_1^{(N_p i)}}\,R_2^{(N_p i)}\mu_0 R_1 \\ & +R_1^{(N_p i)}\sqrt{R_2^{(N_p i)}}\,R_2\mu N_p i - 2R_1^{(N_p i)}\sqrt{R_2^{(N_p i)}}\,R_2\mu_0 \\ & -2R_2\mu_0\left(R_2^{(N_p i)}\right)^{\frac{3}{2}} + R_2\mu\left(R_2^{(N_p i)}\right)^{\frac{3}{2}} N_p i \end{aligned} \tag{2.42}$$

$$\begin{aligned} H_{\phi i} = {} & -R_2\mu_0\left(R_2^{(N_p i)}\right)^{\frac{3}{2}} N_p i - 4\sqrt{R_1^{(N_p i)}}\,\mu R_1 R_2^{(N_p i)} \\ & -R_2\mu\left(R_2^{(N_p i)}\right)^{\frac{3}{2}} N_p i + 2R_1^{(N_p i)}\sqrt{R_2^{(N_p i)}}\,R_2\mu - 2R_1^{(N_p i)}\sqrt{R_2^{(N_p i)}}\,R_2\mu_0 \\ & +R_1^{(N_p i)}\sqrt{R_2^{(N_p i)}}\,R_2\mu N_p i + 2\sqrt{R_1^{(N_p i)}}\,R_2^{(N_p i)}\mu_0 N_p i R_1 + 2R_2\mu\left(R_2^{(N_p i)}\right)^{\frac{3}{2}} \\ & +2R_2\mu_0\left(R_2^{N_p i}\right)^{\frac{3}{2}} - R_1^{(N_p i)}\sqrt{R_2^{(N_p i)}}\,R_2\mu_0 N_p i \end{aligned} \tag{2.43}$$

$$\begin{aligned} L_i = {} & \left[\left(-2 + N_p i\right)\left(2 + N_p i\right)\left[-2\mu\mu_0 R_2^{(N_p i)} - 2\mu\mu_0 R_1^{(N_p i)}\right.\right. \\ & \left.\left. -\mu^2 R_2^{(N_p i)} + \mu^2 R_1^{(N_p i)} - {\mu_0}^2 R_2^{(N_p i)} + {\mu_0}^2 R_1^{(N_p i)}\right]\right] \end{aligned} \tag{2.44}$$

The magnetic field strengths $\mathbf{H^{(1)}}$ and $\mathbf{H^{(2)}}$ in the regions V_1 and V_2 at the outside the magnet, and $\mathbf{H^{(in)}}$ inside the magnet can be represented in terms of scalar potentials $\varphi_m^{\,in}$, $\varphi_m^{(1)}$, and $\varphi_m^{(2)}$. The minus gradient of these potentials will result in magnetic field strength vector fields which are represented by (2.45). Flux density vectors (2.46) in the free space can be calculated by multiplying these field strengths like in [18].

$$\mathbf{H^{in}} = -\nabla {\varphi_m}^{(in)} \qquad \mathbf{H^{(k)}} = -\nabla \varphi_m^{(k)} \qquad (k = 1,2) \tag{2.45}$$

$$\mathbf{B^k} = \mu_0 \cdot \mathbf{H^k} \quad (k = 1,2) \tag{2.46}$$

$$B_r^{(2)}(r,\phi) = \mu_0 \sum_{i=1,3,5..}^{\infty} \tfrac{1}{2} i N_p r^{-\left(\frac{1}{2} i N_p + 1\right)} U_i^{(2)} \cos\left(\tfrac{1}{2} N_p i \phi\right) \tag{2.47}$$

$$B_\phi^{(2)}(r,\phi) = \mu_0 \sum_{i=1,3,5..}^{\infty} \tfrac{1}{2} i N_p r^{-\left(\frac{1}{2} i N_p + 1\right)} U_i^{(2)} \sin\left(\tfrac{1}{2} N_p i \phi\right) \tag{2.48}$$

(2.47) and (2.48) are used to describe the field solution for the source magnet in the (x´, y´) coordinate system (Figure 2.1).

The expressions (2.47) and (2.48) are renamed to respectively $B_{r'}^{ext}(r',\phi')$ and $B_{\phi'}^{ext}(r',\phi')$ which corresponds to the prime coordinate system for source magnets. These field solutions are transformed into the coordinate system to the drive magnet by the use of the following transformation equations. This procedure is similar to the one used in [18].

$$r'(r,\phi) = \sqrt{r^2 + 2rd\cos(\phi) + d^2} \tag{2.49}$$

$$\phi'(r,\phi) = \arctan\left(\frac{r\sin(\phi)}{r\cos(\phi) + d}\right) \tag{2.50}$$

The source magnet field solution $B_{r'}^{ext}(r',\phi')$ and $B_{\phi'}^{ext}(r',\phi')$ is transformed to act as an external field on the drive magnet coordinate system [18], which result in (2.51) and (2.52).

$$\begin{aligned} B_x^{ext}(r,\phi) = {} & B_{r'}^{ext}\left(r'(r,\phi),\phi'(r,\phi)\cos\left(\phi'(r,\phi)\right)\right) \\ & -B_{\phi'}^{ext}\left(r'(r,\phi),\phi'(r,\phi)\sin\left(\phi'(r,\phi)\right)\right) \end{aligned} \tag{2.51}$$

$$\begin{aligned} B_y^{ext}(r,\phi) = {} & B_{r'}^{ext}\left(r'(r,\phi),\phi'(r,\phi)\cos\left(\phi'(r,\phi)\right)\right) \\ & -B_{\phi'}^{ext}\left(r'(r,\phi),\phi'(r,\phi)\sin\left(\phi'(r,\phi)\right)\right) \end{aligned} \tag{2.52}$$

Source field solution is used in the torque expression for the drive magnet, which is explained in the torque expression section.

2.2.2 Equivalent surface current density determination

An equivalent surface current density is a current density distribution, which will give the same magnetic field as a permanent magnet. A simple example can be a rectangular permanent magnet. This type of magnet can be replaced with two equivalent current densities Figure 2.3. Surface current densities are often used to model permanent magnets. Examples where this has occurred can be found in the following papers [47], [48], [49], [50], [51], [52].

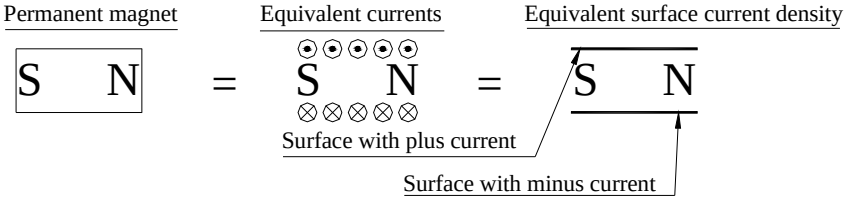

Figure 2.3 Equivalent surface current for a simple rectangular shape.

A permanent magnet can be replaced with a number of currents directed in and out of paper direction. This is illustrated with Figure 2.3, where a number of equivalent currents will replace a magnet at top and bottom of a surface. These equivalent currents will create a magnetic field distribution similar to a permanent magnet. This simple example has just few equivalent currents, but if there are an infinite number of equivalent currents, there will be an equivalent surface current density. The surface current density is per unit length. The drive magnet wheel pole pieces can be reduced to an equivalent current density distribution in a similar way as described previously in [18]. The same method can be used to define an expression for a parallel magnetisation. The previous method for radial expression [18] uses the mathematic cross product of the surface normal vector together with the radial magnetisation vector M_r. This will give the surface current density at top surface, shown in Figure 2.4. In case of a radial magnetisation then there will be the same magnetisation for M_s and M_r. However for the new parallel magnetisation formulation the magnetisation M_s is there needed a projection in radial direction to give radial magnetisation M_r at top side of the magnet shown in Figure 2.4. This projection is therefore included into the equations to get a parallel expression.

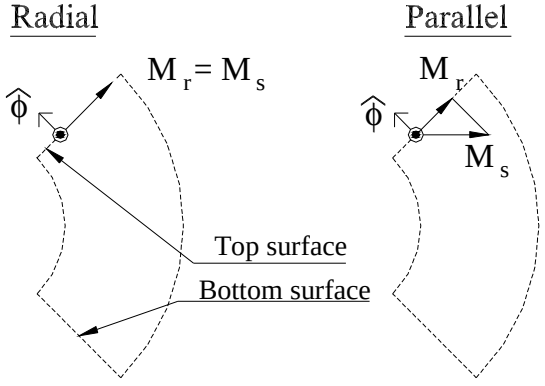

Figure 2.4 Magnetisation vectors for a radial and a parallel magnetised pole piece at top surface.

The current density expression for drive magnet top and bottom surface is described by expression (2.53). The new part of this expression is the cross product projection which is not necessary in [18].

$$\mathbf{j_m}(p,r,\boldsymbol{\phi}) = \begin{cases} M_s \cos\left(\dfrac{\boldsymbol{\pi}}{N_{pole}}\right)\hat{\mathbf{z}} & \begin{cases} R_1 \le r \le R_2 \\ \boldsymbol{\phi}_2(p) = \boldsymbol{\phi} + \dfrac{\boldsymbol{\pi}}{N_{pole}}(1+2p) \end{cases} \\ -M_s \cos\left(\dfrac{\boldsymbol{\pi}}{N_{pole}}\right)\hat{\mathbf{z}} & \begin{cases} R_1 \le r \le R_2 \\ \boldsymbol{\phi}_1(p) = \boldsymbol{\phi} - \dfrac{\boldsymbol{\pi}}{N_{pole}}(1+2p) \end{cases} \end{cases} \qquad p = 0,1,2...(N_{pole}-1 \tag{2.53}$$

A current density expression is also found for the curved pole piece surfaces. This is calculated in almost the same way as for the top and bottom surfaces. Magnetisation M_s must be projected into the tangential direction illustrated in Figure 2.5. It will result in a tangential magnetisation M_ϕ. Tangential magnetisation must then be crossed with the surface normal vector, which will result in the current density at curved surface. This current density is not needed in [18], because a tangential magnetisation is zero and a cross product of a zero vector gives zero. So this part of the parallel magnetisation expression formulation is also new.

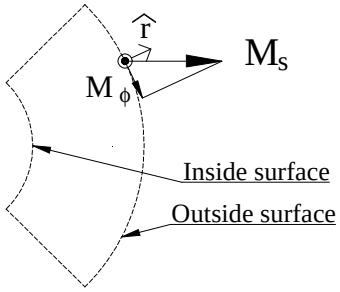

Figure 2.5 Magnetisation vectors for a parallel magnetised pole piece at the inside and outside surfaces.

Current density for the inside and outside surface can then be expressed by the following expression:

$$\mathbf{j_m}(p,r,\boldsymbol{\phi},\boldsymbol{\theta}) = \begin{cases} M_s \sin(\boldsymbol{\theta})\hat{\mathbf{z}} & \begin{cases} r = R_2 \\ \boldsymbol{\phi}_1(p) \le \boldsymbol{\theta} \le \boldsymbol{\phi}_2(p) \Rightarrow \\ \boldsymbol{\phi} - \dfrac{\boldsymbol{\pi}}{N_{pole}}(1+2p) \le \boldsymbol{\theta} \le \boldsymbol{\phi} + \dfrac{\boldsymbol{\pi}}{N_{pole}}(1+2p) \end{cases} \\ -M_s \cos(\boldsymbol{\theta})\hat{\mathbf{z}} & \begin{cases} r = R_1 \\ \boldsymbol{\phi}_1(p) \le \boldsymbol{\theta} \le \boldsymbol{\phi}_2(p) \Rightarrow \\ \boldsymbol{\phi} - \dfrac{\boldsymbol{\pi}}{N_{pole}}(1+2p) \le \boldsymbol{\theta} \le \boldsymbol{\phi} + \dfrac{\boldsymbol{\pi}}{N_{pole}}(1+2p) \end{cases} \end{cases} \tag{2.54}$$

The inner radial surface is expressed in the same way, but with an opposite sign, because surface normal vector $\hat{\mathbf{r}}$ is pointed in opposite direction and that is why cross product is directed in the opposite direction.

2.2.3 Torque expression

In order to determine drive magnet torque the first thing to do is to reduce the system to a distribution of equivalent volume and surface current densities $\mathbf{J_m}$ and $\mathbf{j_m}$. The torque expression (2.55) consists of two integrals where the V and S are respectively volumes and surfaces of the magnets.

$$T = \int_V \mathbf{r} \times (\mathbf{J_m}(r,\phi) \times \mathbf{B}_{ext}) r dr d\phi dz + \int_S \mathbf{r} \times (\mathbf{j_m} \times \mathbf{B}_{ext}) da \tag{2.55}$$

Since $\mathbf{J_m} = \nabla \times \mathbf{M} = 0$, the first volume integration becomes zero [18], the only remaining part is then the surface contributions to the torque expression. This expression contains an equivalent surface current density factor for drive magnet, which is described in the section "Equivalent surface current density determination". All surface current densities must be crossed with the external $\mathbf{B_{ext}}$ flux density field from the source magnet to create a torque on the drive magnet, this cross product is illustrated with an isometric sketch on Figure 2.6.

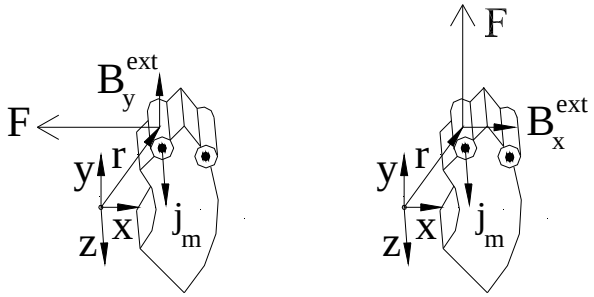

Figure 2.6 Illustration of calculated torque by integrating the cross product of current densities and B-fields at magnet boundaries.

The current j_m in the z direction must be crossed with the source field flux density B_y^{ext}, which results in a force acting on r. This force will create a positive torque around the z-axis. Same current must also be crossed with B_x^{ext}, which also result in a positive torque around the z-axis. All current densities crossed with the external field must be integrated around the surface of the magnet. The radial integration and tangential integration is described in the following.

Radial surface integration

The radial integration is performed with steps in the radial direction and this integration is done on the plane surface of the magnet piece. A new torque expression (2.56) is derived when the current expression is substituted into the torque expression. This procedure is also similar with [18] so following expressions (2.56) to (2.60) is almost the same expressions as used in [18].

$$T_r(\phi) = 2M_s \cos\left(\frac{\pi}{N_{pole}}\right) L \sum_{p=0}^{N_{pole}-1} (-1) \int_{R_1}^{R_2} r\left[\cos\left(\phi_{edge}(\phi,p)\right) B_x^{ext}\left(r, \phi_{edge}(\phi,p)\right)\right. \\ \left. + \sin\left(\phi_{edge}(\phi,p)\right) B_y^{ext}\left(r, \phi_{edge}(\phi,p)\right)\right] dr \tag{2.56}$$

Times 2 M_s comes from integration of 2 surface current densities at the same time. One current density comes from the current surface integration. The second one comes from integration of the neighbouring magnet. Magnetisations of these surfaces are constant, and that is why these quantities are outside the integration sign. The integration is calculated along a straight line. This line lies on a certain angle in drive magnet coordinate system, which depends on the drive magnet turning angle, and magnetic pole number p.

$$\phi_{edge}(\phi, p) = \phi + \frac{\pi}{N_{pole}}(1+2p) \tag{2.57}$$

Integral can be calculated by the use of Simpson's integration method, which involves:

$$S_r(q) = \begin{cases} \frac{1}{3} & (q=0) \\ \frac{4}{3} & (q=1,3,5,...) \\ \frac{2}{3} & (q=2,4,6,...) \\ \frac{1}{3} & (q=N_r) \end{cases} \tag{2.58}$$

$$r = R_1 + \frac{q}{N_r}(R_1 - R_2) \quad (q = 0,1,2,...,N_{r)}) \tag{2.59}$$

N_r is the radial mesh coefficient (must be an even number).

The final radial torque expression with the use of Simpson's integration method becomes:

$$T_r(\phi) = \frac{2M_s \cos\left(\frac{\pi}{N_{pole}}\right) L(R_2 - R_1)}{N_r} \sum_{p=0}^{N_{pole}-1} \sum_{q=0}^{N_p} (-1)^p S_r(q) r(q) \\ \times\left[\cos\left(\phi_{edge}(\phi,p)\right) B_x^{ext}\left(r(q), \phi_{edge}(\phi,p)\right)\right. \\ \left. + \sin\left(\phi_{edge}(\phi,p)\right) B_y^{ext}\left(r(q), \phi_{edge}(\phi,p)\right)\right] \tag{2.60}$$

Tangential surface integration

Tangential surface integration is performed at the two radial surfaces. Torque expression for the outer surface leads to expression (2.61), which is new for a parallel magnetisation formulation.

$$T_{t2}(\phi)=\frac{M_s LR_2{}^2}{N_t}\sum_{p=0}^{N_{pole}-1}(-1)^p\int_{\theta_1}^{\theta_2}\sin(\theta)\cdot$$
$$\left[\cos\left(\theta+p\frac{2\pi}{N_{pole}}+\phi\right)B_x{}^{ext}\left(\theta+p\frac{2\pi}{N_{pole}}+\phi\right)\right. \tag{2.61}$$
$$\left.+\sin\left(\theta+p\frac{2\pi}{N_{pole}}+\phi\right)B_y{}^{ext}\left(\theta+p\frac{2\pi}{N_{pole}}+\phi\right)\cdot d\theta\right]$$

Once again there is used the Simpson's method to evaluate the integral, and this will lead to the following expression.

$$T_{t2}(\phi)=\frac{M_s LR_2{}^2\left(\frac{2\pi}{N_{pole}}\right)}{N_t}\sum_{p=0}^{N_{pole}-1}\sum_{q=0}^{N_t}(-1)^p S_r(q)\sin(\theta(q))$$
$$\left[\cos\left(\theta(q)+p\frac{2\pi}{N_{pole}}+\phi\right)B_x{}^{ext}\left(R_2,\theta(q)+p\frac{2\pi}{N_{pole}}+\phi\right)\right. \tag{2.62}$$
$$\left.+\sin\left(\theta(q)+p\frac{2\pi}{N_{pole}}+\phi\right)B_y{}^{ext}\left(R_2,\theta(q)+p\frac{2\pi}{N_{pole}}+\phi\right)\right]$$

Where:

$$\theta(q)=\frac{-\pi}{N_{pole}}+\frac{q}{N_t}\frac{2\pi}{N_{pole}} \tag{2.63}$$

A similar expression for the torque T_{t1} is necessary to calculate along the inner radius R_1 of the drive magnet, but with a negative sign. The total torque from the drive can then be calculated as the sum of surface integrations:

$$T(\phi)=T_r(\phi)+T_{t1}(\phi)+T_{t2}(\phi) \tag{2.64}$$

The analytical solution part is described in (2.41) - (2.44) and (2.49) - (2.52). This part will calculate the flux on the outside of drive magnets with a complete field solution. The same field solution can be obtained by FEM, but this will require longer computation time if the model have too many nodes. The second part of the expression is the numerical part of the integration. This part is (2.60) for the radial integration and (2.62) for one of the two tangential integrations. All three integrations for the torque expressions can be written in (2.64).

The torque expressions for a parallel and a radial magnetised spur gear are programmed into a software program where the algorithm is tested and there is also a 2D FEM calculation for verifying the results. Software program and 2D FEM calculations are shown in the following sections.

2.3 Software program description

The magnetic spur gear program is a software program developed in this thesis in order to design magnetic gears. For torque calculations the software uses the radial analytical equations defined by Furlani [18] and extended analytical equations for parallel magnetisation. The program is built in a Borland Builder 3 environment [54]. A screenshot from the program is shown in Figure 2.7. The screenshot is marked with 5 numbers, which corresponds to 5 regions explained in the following section.

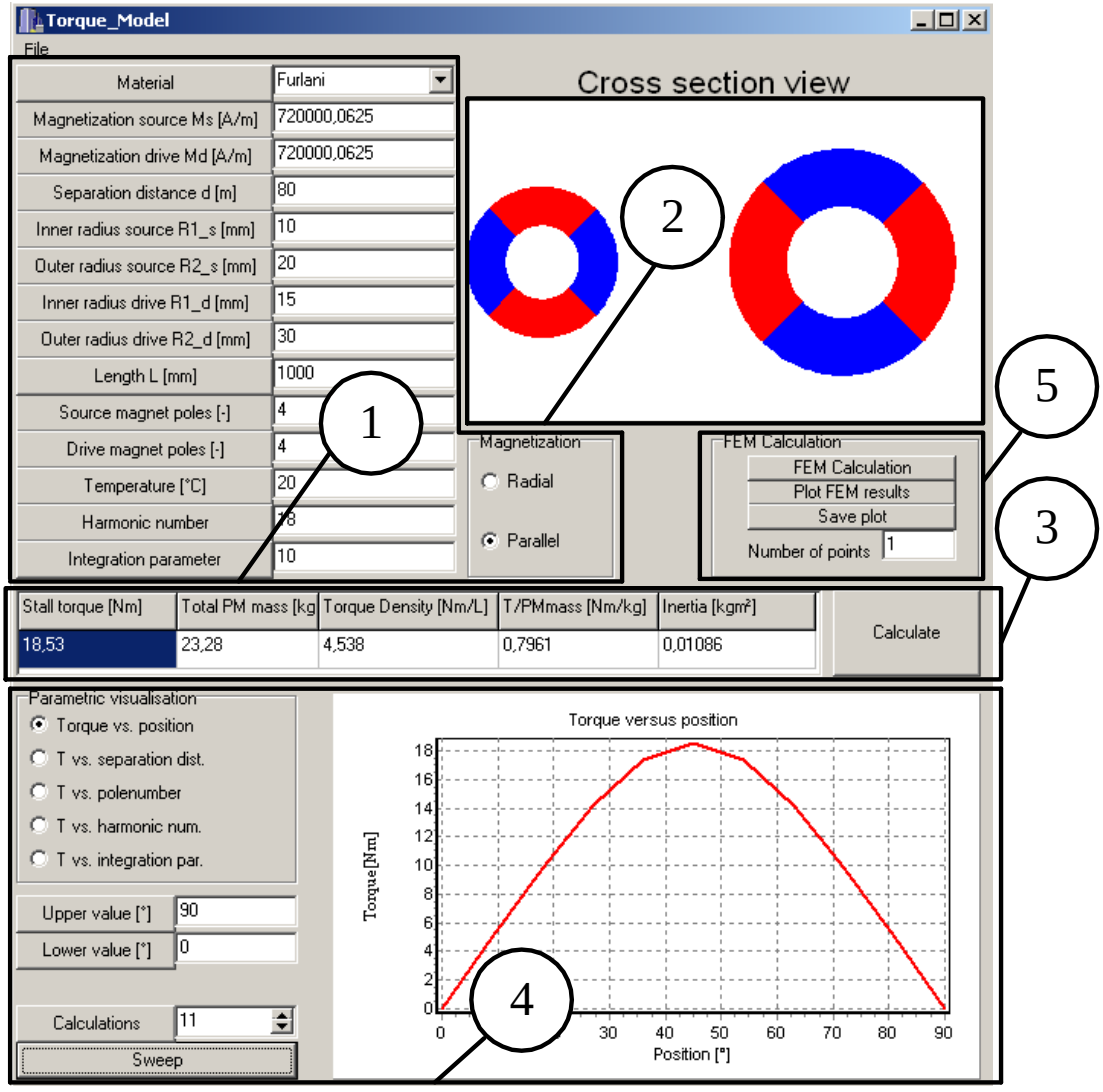

Figure 2.7 Screenshot from the magnetic spur gear program.

The first region of the graphical user interface is the design parameter input region. The input parameters are gear dimensions, physical magnetic properties and the simulation parameters. The second region shows cross-section of a magnetic gear, this region is updated when new gear dimensions is entered. The third region can perform a single torque calculation, at an angle where torque between magnetic wheels is maximal. The total permanent magnet mass, torque per unit volume, and torque per unit mass and

inertia are also calculated. The fourth region can perform a parametric visualisation of a chosen parameter. Parameters which are possible to choose among is torque versus angular position, torque versus separation distance between the wheels, drive wheel pole numbers versus source pole numbers, and torque versus pole number. The fifth region can perform a Finite Element Model calculation [53]. In the following section a more detailed description of the five regions in the graphical user interface is done.

First region- design parameters

Permanent magnet magnetisation is one of the design parameters, used in the calculations. Data for permanent magnet magnetisation is located in a material file, where all material parameters are stored. It is possible to load these parameters from this magnetisation file by picking material name which corresponds to pre defined material properties. Program user can modify the material properties by editing material file and add a new material. From the material file a temperature coefficient k_t and a magnetic magnetisation M_s is calculated. Equations for these calculations are:

$$M_s = M_d = \frac{B_r}{\mu_r \mu_0} \cdot k_t \tag{2.65}$$

$$k_t = 1 + \left(\frac{T_{coeff}}{100} \right) \cdot (T - 20) \tag{2.66}$$

A screen shot of a cross-section from the GUI is shown in Figure 2.8. The figure shows a source magnet and a drive magnet with attached dimension variables. Those dimension variables are listed in the nomenclature list Table 19.

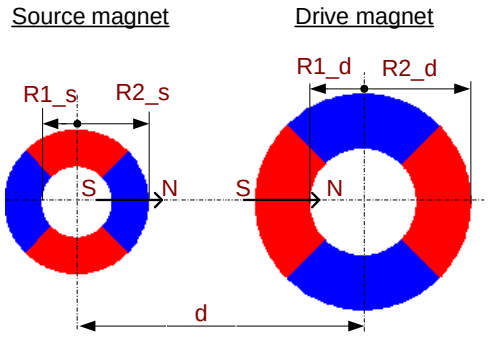

Figure 2.8 Gear model cross-section.

Third region - Single torque calculation

The torque transforming capability depends on drive magnet rotation angle. A plot of the torque versus angle is approximately a sinusoidal function. The highest torque point on this function corresponds to the stall torque. Angle $\theta_{Stall\ torque} = \frac{180°}{N_{poleD}}$ for the stall torque calculation is calculated from the number of poles on the drive magnet wheel. Stall torque is calculated at stall angle $\theta_{Stall\ torque}$ by the use of the analytical equations. The total mass of permanent magnet material is calculated from the magnet volume and magnet material density. The torque density and the torque per unit mass are calculated from (2.67) and (2.68) respectively. The torque density gives an idea of magnetic gear performance and the torque per unit mass gives an idea of how efficient the magnetic material is utilised. The last calculation in the single torque calculation is an inertia

calculation. This is simply a calculation of the total inertia converted to drive magnet side.

$$T_{Dens} = \frac{T_{Stall}}{V_A} = \frac{T_{Stall}}{\pi \cdot L \cdot (R_{2s}{}^2 + R_{2d}{}^2)} \tag{2.67}$$

$$T_{mass} = \frac{T_{Stall}}{m_{PM}} = \frac{T_{Stall}}{\rho_{PM} \cdot \pi \cdot L \cdot (R_{2s}{}^2 - R_{1s}{}^2 + R_{2d}{}^2 - R_{1d}{}^2)} \tag{2.68}$$

Fourth region - Parametric visualisation
The parametric visualisation region has 5 options:

- Torque versus position
- Torque versus separation distance
- Torque versus pole number
- Torque versus harmonic number
- Torque versus integration number

It is possible to make a torque versus angular position calculation when specifying angular position interval and the number of calculations. The software program can plot torque versus angular position in a graph by calculating several torque values at different angles.

Stall torque are calculated for different distance between magnet wheels, this is the torque versus separation distance calculation. There is specified a separation distance interval and torque plot is made step by step through a number of calculations.

Gearing relationship N_g is normally specified as a number in the mechanical gear terminology. Gearing from a high revolution axle to a low revolution axle is the most common gearing type used for mechanical gears. This type of gear will have a gearing relationship N_g, which is equal to the number of mechanical teeth on the large gear wheel divided by the number of teeth on the small gear wheel. This number is greater than 1 when gear input speed is higher than gear output speed. The terminology from mechanical gears is adapted to the magnetic gears and hereby gearing relationship from (2.69).

$$N_g = \frac{N_{poleD}}{N_{PoleS}} \tag{2.69}$$

Gearing relationship is normally known by gear designer. That is why this gearing relationship number must be typed into the program in the field beside the text “Gearing N [-]”.When the gearing is fixed and when it is greater or equal to one is it possible to do a parametrical sweeping through different pole configurations and keep the gearing relationship constant. But not every pole number configurations are valid, that is why different drive pole numbers are tried out. Torques at valid drive pole numbers configurations are calculated. The torque versus pole number procedure is used to find the amount of poles for the current configuration. First of all, there must be specified a gearing relationship as mentioned before. Diameters for source and drive wheel must

also be chosen and somehow be scaled so that the radius relationship between the source wheel and the drive wheel are close to the gearing relationship, because highest torque is often obtained for this parameter relationship. The torque versus pole number calculation will calculate the torque at different pole numbers and the gear designer can then choose pole configurations that give the highest torque.

Torque versus harmonic number is a calculation check which will show if there is used enough harmonic components in the description of the B-field. It is important to ensure that an appropriate harmonic number is chosen. This value can be found by sweeping through torque versus harmonic calculation. Torque will be calculated at different harmonic numbers. The sensible harmonic number can be found where the calculated torque seems to converge to a constant value.

Torque versus integration number is a calculation check, which is performed to ensure that the number of torque integrations is enough. The torque is calculated for different integration numbers, and when the torque converges to a constant value, a reasonable integration number is found.

Fifth region – FEM calculation

The fifth region is the FEM calculation procedure which will activate a FEM calculation programme called FEMM [53]. The FEM calculation procedure is used together with torque versus angular position calculation procedure and this will also calculate torque versus position and plot results with a number of points. Input parameters for the FEM model are similar to parameters used for the analytical calculation method and this is the way the FEM calculation is verified with the analytical expression. The calculated values can be compared after the “plot FEM results” procedure is activated, which will plot the FEM results together with previous analytical calculated results. It is also possible to save the verification plot by choosing “Save plot”.

The developed software program can be used to calculate torque for radial and parallel magnetised spur gears with different parametric input parameters.

2.4 Magnetic spur gear optimisation

An analytical expression is developed for the torque calculation of a parallel magnetisation. And this expression is programmed into the previous described software program, where the torque can be calculated for different input parameters. The radial magnetisation expression is also programmed into the software program and these expressions are used to "semi" optimise the spur gear regarding the torque density. Different input parameters are chosen and the torque is calculated in many operation points. Final dimension parameters are chosen when the highest torque density is obtained. Radial magnetisation expression is first used to semi optimise a magnetic spur gear torque, because parallel magnetisation expression was not finally developed at that point of time when the prototype was designed. Parallel magnetisation expression is later used in the computerised optimisation process. Both optimisations are also described in this chapter.

Semi optimisation

There is used a trial and error method to find the initial design for a magnetic spur gear test model. The radial magnetisation algorithm [18] is used to calculate torque density with different input parameters. A gearing relationship of 1:4 is chosen for this design. Approach for choosing the input parameters is done by setting some variables to constant values and then try to change other variables. The approach is continued until calculated design results indicate that optimal design is reached. The result of semi optimisation procedure gave the following design variable lengths:

$R_{2s} = 29 \cdot 10^{-3}[m]$; $R_{1s} = 16 \cdot 10^{-3}[m]$; $R_{2d} = 100 \cdot 10^{-3}[m]$; $R_{1d} = 90 \cdot 10^{-3}[m]$;$N_p$=10 [-] N_{pole}= 40 [-].

These design variables gave the best results for this semi optimisation procedure.

Computerised optimisation process

The computerised optimisation is formulated as a general optimisation problem [55] with a cost function (2.70), equality constrains (2.71), inequality constrains (2.72), and a number of constants, shown in Table 6. The cost function is set up as the torque density of magnetic spur gear with torque calculation from parallel magnetisation expressions developed in this chapter (2.64), and volume which is set to the entire area of two gear wheel times a constant length. The optimisation procedure routine is a minimisation routine and the torque function $T(R_{2s,} R_{1s,} R_{2d,} R_{1d})$ is set up with a negative sign in the cost function. It is also necessary to have an equality constrain for limitation of permanent magnet material used. Permanent magnet area constrain is setup to be the same area as for semi optimisation. Inequality constrains is also included for minimisation routine. The outer radius has to be greater than the inner radius in g_1 and g_2. The smallest radius for the gear wheels has to be greater than a certain value in g_3 and g_4.

$$f(x) = f(x_1, x_2 ..., x_n) \quad \Rightarrow$$
$$f(R_{2s}, R_{1s}, R_{2d}, R_{1d}) = \frac{-T(R_{2s}, R_{1s}, R_{2d}, R_{1d})}{L\pi({R_{2s}}^2 + {R_{2d}}^2)} \tag{2.70}$$

$$h_j(x) = (x_1, x_2, ...x_n) = 0 \quad \Rightarrow$$
$$h_1(R_{2s}, R_{1s}, R_{2d}, R_{1d}) = 0.0078 - \pi({R_{2s}}^2 - {R_{1s}}^2 + {R_{2d}}^2 - {R_{1d}}^2) = 0 \tag{2.71}$$

$$g_i(x) = g_i(x_1, x_2, ...x_n) \le 0 \quad \Rightarrow$$
$$g_1(R_{2s}, R_{1s}) = R_{1s} - R_{2s} + 5 \cdot 10^{-3} \le 0$$
$$g_2(R_{2d}, R_{1d}) = R_{1d} - R_{2d} \le 0 \tag{2.72}$$
$$g_3(R_{2d}) = 20 \cdot 10^{-3} - R_{1d} \le 0$$
$$g_4(R_{1s}) = 2 \cdot 10^{-3} - R_{1d} \le 0$$

The following constants are used for the computerised optimisation procedure.

Symbol	**Optimisation constants**		
	Description	***Size***	***Units***
g	Air gap between magnet wheels	$1 \cdot 10^{-3}$	[m]
L	Length/height of the magnets	$20 \cdot 10^{-3}$	[m]
B_r	Remanence flux	1.183	[T]
$H_c = M_s$	Coercivity	936892	[A/m]
i	Harmonic parameter, max value.	11	[-]
$N_r = N_t$	Torque integration parameter	10	[-]
μ_0	Permability for air regions	$4 \cdot \pi \cdot 10^{-7}$	[Tm/A]
$\mu = B_r/H_c$	Absolut permability, magnets	$12.63 \cdot 10^{-7}$	[Tm/A]
$\mu_r = \mu/\mu_0$	Relative permability, magnets	1.0048	[-]
N_p	Number of source magnets	10	[-]
N_{pole}	Number of drive magnets	40	[-]
ϕ	Angle for the maximum torque	4.5	[Deg.]

Table 6 Constants used for the computer optimisation procedure.

A constrained non linear minimisation routine is performed to find the optimal dimensions for the magnetic spur gear. The minimisation routine gives the following result:

$R_{2s} = 24 \cdot 10^{-3}[m]$; $R_{1s} = 7.3 \cdot 10^{-3}[m]$; $R_{2d} = 78.5 \cdot 10^{-3}[m]$; $R_{1d} = 64.8 \cdot 10^{-3}[m]$

Comparison of semi and computerised optimisation

Semi optimisation is originally optimised with the radial magnetisation algorithm. The result from this optimisation would give a torque density of 24.4 [kNm/m^3]. If computerised optimisation with parallel magnetisation algorithm is used then it will result in 26.7 [kNm/m^3] which is a little bit higher. The dimensions for the two types are shown in Figure 2.9 with two illustrations for visualising size changes using a semi optimisation approach a) and a computerised approach b).

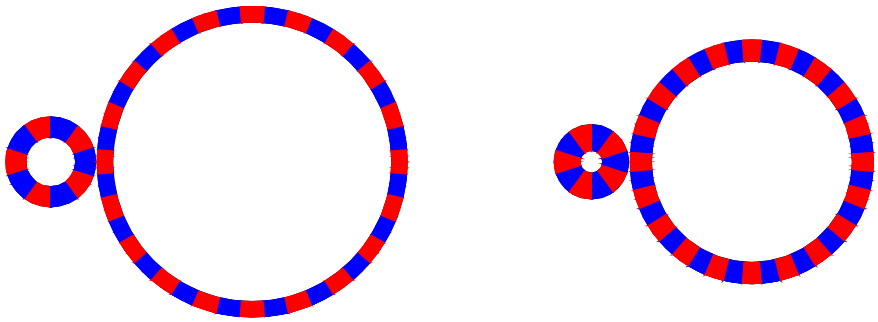

a) b)

Figure 2.9 a) Illustration sketch of the semi optimised gear b) Illustration sketch of the computerised optimisation.

The optimisation routine will try to optimise magnetic gear torque density and it will use the specified amount of material at the best possible way for the given degrees of freedom available. The amount of permanent magnet material for the two optimisations is the same for both. But the computerised optimisation finds a better way to utilise the volume by choosing a small diameter on the small rotor. The gear is changed in size downwards which results in a reduced overall volume and hereby also a higher torque density. However this optimisation is only performed with a 10:40 pole number combination and other combinations are also available if 1:4 gearing relationship are to be investigated. Then other pole combinations are also optimised with previous described algorithm and even higher torque density is obtained. The results from this optimisation are shown in Table 7.

Source poles	**Drive poles**	**Turn angle**	**Area constrain**	**Radius constrain**	**Torque density**
N_p	N_{pole}	ϕ	A_{const}	R_{1s}	ρ_A
[-]	[-]	[Deg.]	[m^2]	[m]	[kNm/m^3]
12	48	3.75	$78 \cdot 10^{-4}$	$2 \cdot 10^{-3}$	23.41
10	40	4.5	$78 \cdot 10^{-4}$	$2 \cdot 10^{-3}$	26.70
8	32	5.63	$78 \cdot 10^{-4}$	$2 \cdot 10^{-3}$	31.05
6	24	7.5	$78 \cdot 10^{-4}$	$2 \cdot 10^{-3}$	37.31
4	16	11.25	$78 \cdot 10^{-4}$	$2 \cdot 10^{-3}$	47.47

Table 7 Results from the computer optimisation process with different pole numbers.

The optimisation shows that pole number combination of 4:16 will give a much higher torque density. And a 2:8 pole configuration might even result in higher torque however

it is not possible to use the developed algorithm for a lower pole number than 4 because this will give numerical problems for the developed algorithm so configurations with lower pole numbers than 4 on a source magnet rotor are not analysed.

The very promising 4:16 pole configuration has the following dimension results:
$R_{2s} = 19.6 \cdot 10^{-3}[m]$; $R_{1s} = 2.0 \cdot 10^{-3}[m]$; $R_{2d} = 55.5 \cdot 10^{-3}[m]$; $R_{1d} = 31.3 \cdot 10^{-3}[m]$

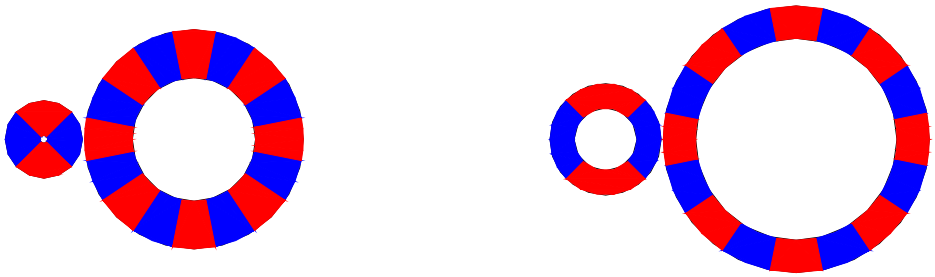

a) b)

Figure 2.10 a) Illustration sketch of the optimised 4:16 configuration. b) Illustration sketch of the optimised 4:16 configuration with a 16 [mm] R_{1s} inequality constraint.

4:16 pole configuration Figure 2.10 a) must have a very small shaft radius on the source magnet rotor. This shaft radius R1s is equal to 2 [mm] for optimised result. And this dimension is equal to the inequality constrain set in the optimisation routine (2.72). But a shaft with 2 [mm] radius will not be strong enough to support bearing load at axle ends. That is the reason why another optimisation with a larger limitation on the inner radius R1s for source wheel shaft is performed. This radius inequality constraint is set to 16 [mm] for second optimisation analysis, shown in Table 8.

Source poles	**Drive poles**	**Turn angle**	**Area constrain**	**Radius constrain**	**Opt. Torque density**
N_p	N_{pole}	ϕ	A_{const}	R_{1s}	ρ_A
[-]	[-]	[Deg]	[m^2]	[m]	[kNm/m^3]
12	48	3.75	$78 \cdot 10^{-4}$	$16 \cdot 10^{-3}$	23.0944
10	40	4.5	$78 \cdot 10^{-4}$	$16 \cdot 10^{-3}$	25.5878
8	32	5.625	$78 \cdot 10^{-4}$	$16 \cdot 10^{-3}$	28.3967
6	24	7.5	$78 \cdot 10^{-4}$	$16 \cdot 10^{-3}$	31.3594
4	16	11.25	$78 \cdot 10^{-4}$	$16 \cdot 10^{-3}$	34.6383

Table 8 Result table for optimising with different magnet pole combinations.

Magnetic configuration with 4:16 magnetic poles and with a 16[mm] R_{1s} inequality constraint radius has the following size results, which is illustrated on Figure 2.10 b):
$R_{2s} = 28.2 \cdot 10^{-3}[m]$; $R_{1s} = 16.0 \cdot 10^{-3}[m]$; $R_{2d} = 67.5 \cdot 10^{-3}[m]$; $R_{1d} = 51.1 \cdot 10^{-3}[m]$

Influence from calculations with different amount of magnetic material is also investigated in this analysis. This analysis is only performed with 4:16 pole configuration. The result of this analysis is shown in Table 9.

Source poles	**Drive poles**	**Turn angle**	**Area constrain**	**Radius constrain**	**Torque density**
N_p	N_{pole}	ϕ	A_{const}	R_{1s}	ρ_A
[-]	[-]	[Deg]	[m^2]	[m]	[kNm/m^3]
4	16	11.25	$30 \cdot 10^{-4}$	$16 \cdot 10^{-3}$	20.60
4	16	11.25	$60 \cdot 10^{-4}$	$16 \cdot 10^{-3}$	31.00
4	16	11.25	$90 \cdot 10^{-4}$	$16 \cdot 10^{-3}$	36.46
4	16	11.25	$120 \cdot 10^{-4}$	$16 \cdot 10^{-3}$	39.80
4	16	11.25	$150 \cdot 10^{-4}$	$16 \cdot 10^{-3}$	42.05
4	16	11.25	$180 \cdot 10^{-4}$	$16 \cdot 10^{-3}$	43.67
4	16	11.25	$210 \cdot 10^{-4}$	$16 \cdot 10^{-3}$	44.89
4	16	11.25	$240 \cdot 10^{-4}$	$16 \cdot 10^{-3}$	45.84

Table 9 Results from an optimisation with different area constrains.

Tendency illustration on Figure 2.11 shows that optimal torque density is increased if more magnetic material is put into the magnet wheels.

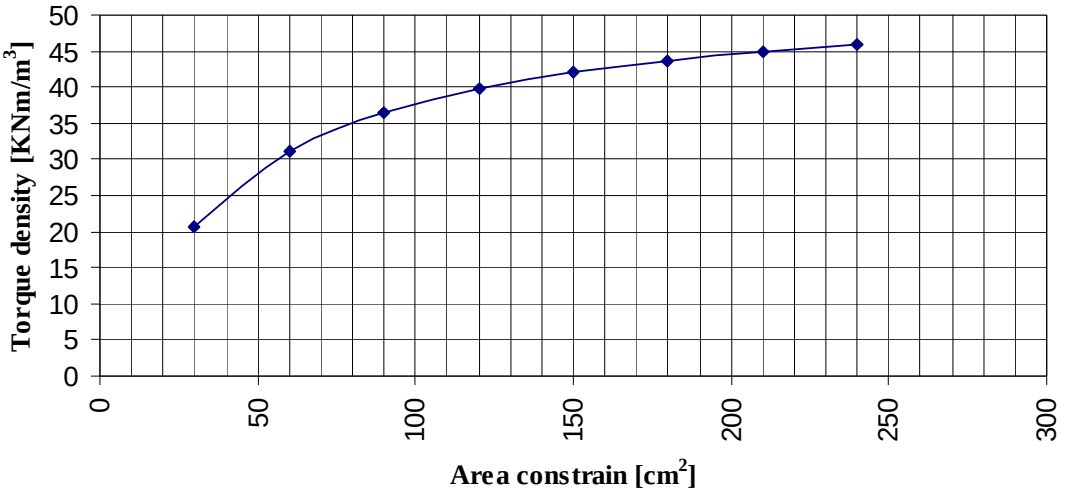

Figure 2.11 Torque densities versus area constrains.

Connection between the amounts of used magnetic material versus optimal obtainable torque density is not linear. So adding extra material for large gear will not necessarily result in same torque density effect as adding extra material on small gear. There is therefore a saturation tendency in terms of area constraint and torque density performance.

Summary for the optimisation

A magnetic gear is optimised with a manual semi optimisation method and a computerised optimisation method. The results from computerised method seem to be a very powerful tool for optimising magnetic spur gears. A torque density of 34.6 [kNm/m^3] is calculated for a magnetic gear with the same limitation on magnetic material and another limitation on the inner radius of the small gear wheel. Result from the computerised optimisation is slightly larger than semi optimisation routine which only is 24.4 [kNm/m^3].

Higher torque density is possible to reach if more material are used for gear and higher torque density might be possible to obtain if lower pole number is used on the source wheel. Adding a larger amount of magnetic material will not necessarily result in an increase in torque density even though the gear is optimised by a computer optimisation. There will also be a dependency of the absolute amount of magnetic material used for the chosen design. A gear with a small amount of magnetic material will therefore get a relatively large increase in torque density while a gear with a relatively large amount of magnetic material will get a relatively small increase in torque density, when the same amount of magnetic material is added to optimisation calculation routine. Magnetic spur gear functions does not allow lower pole number than 4 so there is a limitation for possible pole combinations. Gear configurations with lower magnetic pole number than 4 are not performed because of the limitations in magnetic spur gear functions. Further investigations can be done in this area in order to optimise the torque density performance.

2.5 2D FEM model

Magnetic spur gear is modelled in FEM software [53]. The FEM program can run a script code used for creating the model of the specific problem. Parameters similar to those used in analytical calculations are automatic picked in the script code. Definition of all physical parameter and dimensions occur at program start. The next part of the script code model describes the source magnet poles and these poles are split into smaller pieces, and this property is used to model a pseudo magnetisation. Drive magnets are modelled in a similar way as the source magnets; however these magnets can be rotated, which corresponds to a certain load angle. There are placed circles on the outside of the magnets. These circles are used for calculating the torque at the drive magnet. Maxwell stress tensor is used for torque calculation in these circles. Figure 2.12 shows the content in the FEM model. The FEM model uses furthermore a boundary condition with two circles. The left circle shown on Figure 2.12 contains the magnet wheels, and the magnetic field potential at the circle periphery is equal to the magnetic field potential at the circle periphery in right circle. This boundary condition at circle periphery will give a more accurate solution because the surroundings will be almost infinity. The way this is done is called the Kelvin transform.

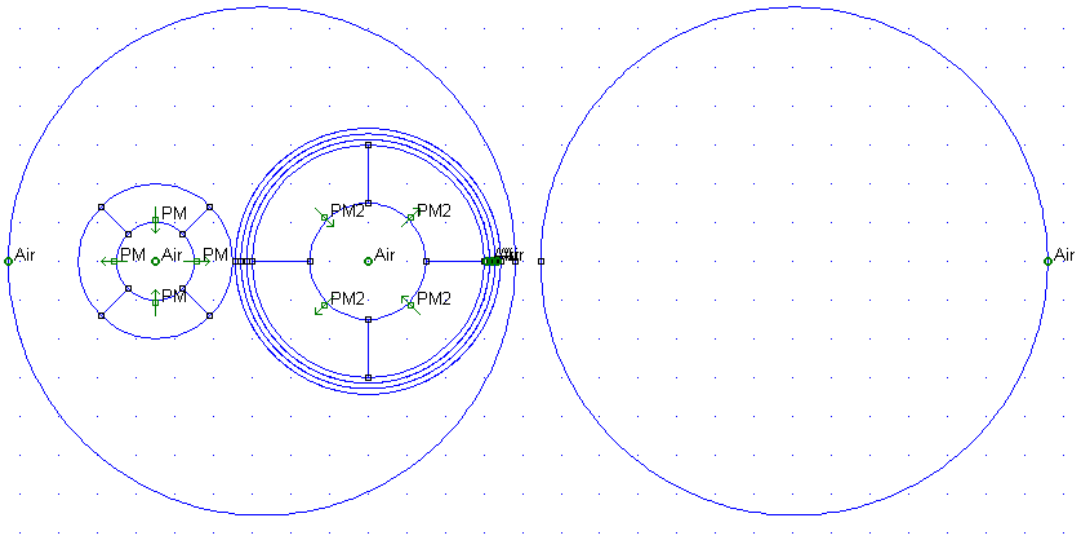

Figure 2.12 Screenshot from A 2D FEM model.

The torque calculation is made with a program call to a post processor, when the solver has calculated the B-field for the entire system. The torque can automatically be calculated for different angle rotations of drive magnets, which means the torque can be expressed as a function of the angle rotation for the drive magnet.

Information about model content is listed in: Table 10

Symbol	Dimensions for models		
	Description	***Size***	***Units***
R_{2s}	Outer radius, source magnets	$29 \cdot 10^{-3}$	[m]
R_{1s}	Inner radius, source magnets	$16 \cdot 10^{-3}$	[m]
R_{2d}	Outer radius, drive magnets	$100 \cdot 10^{-3}$	[m]
R_{1d}	Inner radius, drive magnets	$90 \cdot 10^{-3}$	[m]
d	Distance between center points	$130 \cdot 10^{-3}$	[m]
L	Length/height of the magnets	$20 \cdot 10^{-3}$	[m]
B_r	Remanence flux	1.183	[m]
$H_c = M_s$	Coercivity	936892	[A/m]
i	Harmonic parameter, max value.	19	[-]
$N_r = N_t$	Torque integration parameter	10	[-]
μ_0	Permability for air regions	$4 \cdot \pi \cdot 10^{-7}$	[Tm/A]
$\mu = B_r/H_c$	Absolut permability, magnets	$12.63 \cdot 10^{-7}$	[Tm/A]
$\mu_r = \mu/\mu_0$	Relative permability, magnets	1.0048	[-]
N_p	Number of source magnets	10	[-]
N_{pole}	Number of drive magnets	40	[-]

Table 10 FEM calculation and analytical calculation parameter list.

The magnetisation values for the source and drive magnets are specified in a datasheet from the supplier [62]. The relative permeability for source magnets is calculated (2.73) from the supplier data sheet.

$$\mu_r = \frac{B_r}{\mu_0 H_c} \tag{2.73}$$

The mesh size depends on the problem size. For a large problem, there will be large mesh elements. The number of elements will depend on the specific problem.

2.6 3D FEM model

3D magnetic spur gear model is modelled in order to clarify 3D end effect influences relative to 2D FEM model results. The 3D model is made in opera [56]. A screenshot of the Opera model is shown on Figure 2.13.

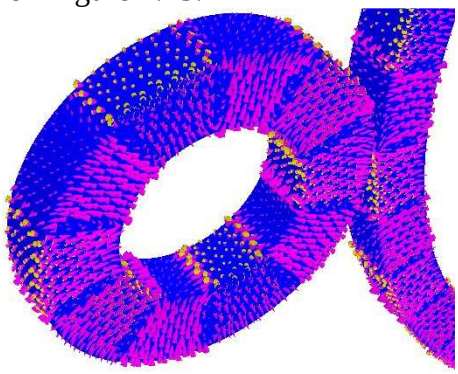

Figure 2.13 B-field vector plot from the 3D magnetic spur gear model.

The 3D model consists of permanent magnets, and air surroundings. Parameters for the 3D model are similar to the parameters used in the 2D model. These parameters are listed in Table 10. Output torque for the 3D model is calculated with the Maxwell stress tensor method which is similar to 2D calculation method. 3D Maxwell stress tensor method integrates around a circular path just outside the rotor where a torque is calculated.

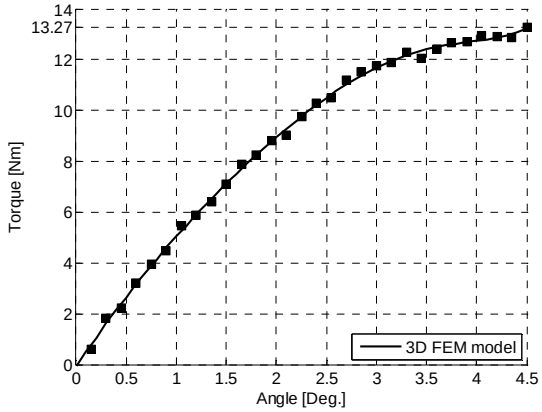

Figure 2.14 Torque results from the 3D spur gear model.

Torque results show that the maximum torque is approximately 13.3 [Nm] from the 3D magnetic spur gear model.

2.7 Experimental test model

Experimental test model Figure 2.15 of a magnetic spur gear is designed in order to verify theoretical results. Test model design is made with two aluminium rotors where neodymium magnets are embedded inside. Rotor manufacturing is done in several steps. Custom-made neodymium magnets are glued on aluminium rotors and an aluminium ring is pressed over for covering magnets and a final manufacturing procedure is performed on outer rotor surface. Model parts for the other test model parts are primary made of aluminium except bolts. The small rotor is placed on a moveable unit in order to be able to adjust the separation distance. The first test made is a static test where the small rotor is blocked and the other rotor is forced to rotate in small steps. Torque is calculated for every step made. Torque transducer is placed between drive unit and the large gear wheel.

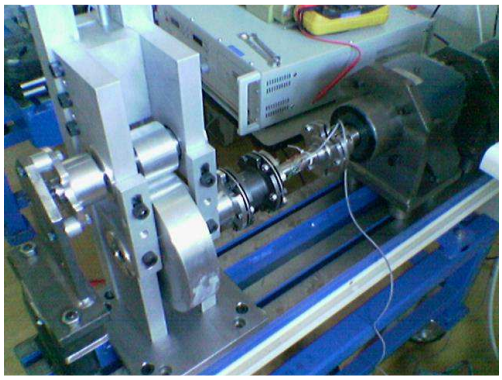

Figure 2.15 Magnetic spur gear test model and test rig for static test.

The torque transducer is calibrated with static weight in order to give accurate measured results. First measurement is performed with a separation distance of 1 [mm] between wheel magnets. The measurement results are shown on Figure 2.16.

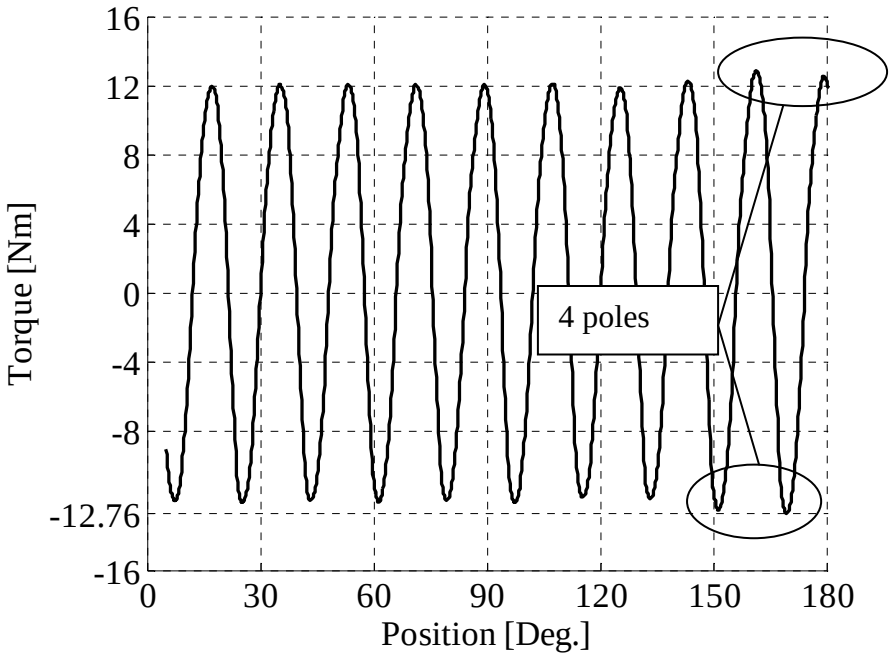

Figure 2.16 Torque versus rotation position at separation distance of 1[mm].

The maximum torque does not seem to vary very much for the different poles shown in the graph except for 4 poles, where the lowest value is -12.76 [Nm]. This low value is probably caused by a small radial displacement of a few magnets.

2.8 Verification and comparison of results

There are several magnetic spur gear models. These models are analytical models of the parallel and radial magnetised magnetic spur gears. A 2D FEM model, a 3D model, and finally an experimental prototype model of a parallel magnetised spur gear is presented. Models with the same number of dimensions should give the same results so it is possible to compare and verify these models with each other. The 2D FEM models can therefore be verified with a 2D analytical model, which is shown in 2.8.1. The experimental test model is a 3D model. This experimental test model is not possible to compare and verify with 2D analytical model without model differences. However these two models are compared in order to estimate differences and this is done in 2.8.8, and finally a comparison of all 3 models is done in 2.8.9.

2.8.1 Verification of the analytical models with 2D FEM models

The analytical parallel and radial magnetisation models are verified with the FEM models. Model verification is accomplished with different input parameters regarding dimensions and pole numbers. Input parameters are set differently in 5 different cases in order to compare models at different input parameters. Two kinds of instances are chosen regarding dimensions and pole numbers.

First dimensional case is set to similar dimensional parameters as the magnetic spur gear example modelled by E. P. Furlani. The second and third cases have the same dimensions as the final prototype. Fourth and fifth cases have similar dimensions as the example modelled by E. P. Furlani.

The purpose in verifying the analytical model with different input parameters is partly to verify and partly to visualise some of modelling limitations regarding material permeability. The different calculation cases are listed in following list:

1. Calculation example verified by E. P. Furlani
2. Prototype example with parallel magnetisation
3. Prototype example with radial magnetisation
4. E. P. Furlani example with parallel magnetisation
5. E. P. Furlani example with high permeability in the source magnet

These cases are described in the following sections.

2.8.2 Calculation example verified by E. P. Furlani

E. P. Furlani formulated the analytical calculation method [18] for radial magnetised spur gear. These expressions are verified by E. P. Furlani with a FEM program and there are found good agreement in the results. Same analytical expressions are also implemented in software program and they are verified with the FEM software. The result of this analysis is shown in Figure 2.17.

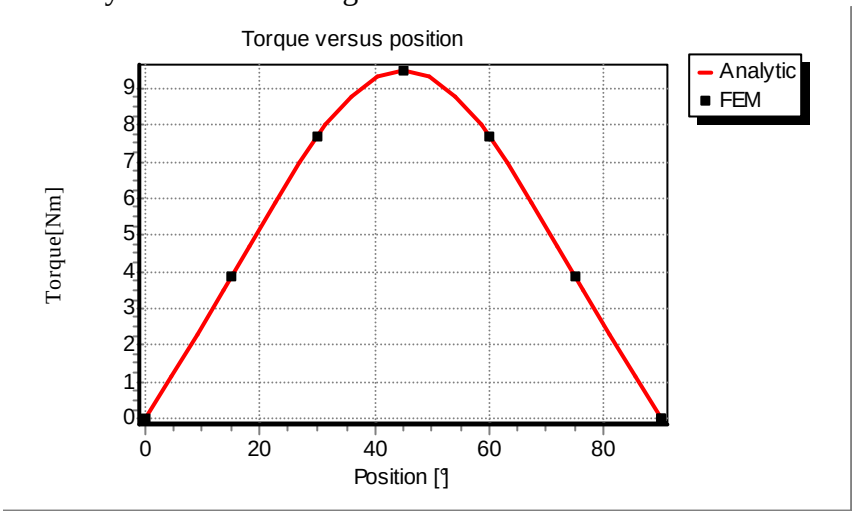

Figure 2.17 Radial magnetisation equations verified with FEM (Same example as E. P. Furlani used [18]).

The graph on Figure 2.17 describes calculated torque versus rotation angle for drive magnet when the analytical expressions are used and when FEMM program calculates the torque. There is a good agreement between analytical expression and FEM calculation for this example. The maximum torque is 9.5 [Nm] and this is equal to the results obtained by E. P. Furlani. From these results, it is concluded that the equation for the radial magnetisation are correct implemented in the software program and it is also concluded that the FEM model is correct modelled.

2.8.3 Prototype example with parallel magnetisation

There is a laboratory prototype of a magnetic spur gear with parallel magnetised magnets Figure 2.15. In section 2.2 there is developed an analytical torque expression for this parallel magnetised spur gear type. The verification result for this example is shown in Figure 2.18. Material parameters specified for this verification is obtained from the material supplier. The harmonic number used in this case is 15.

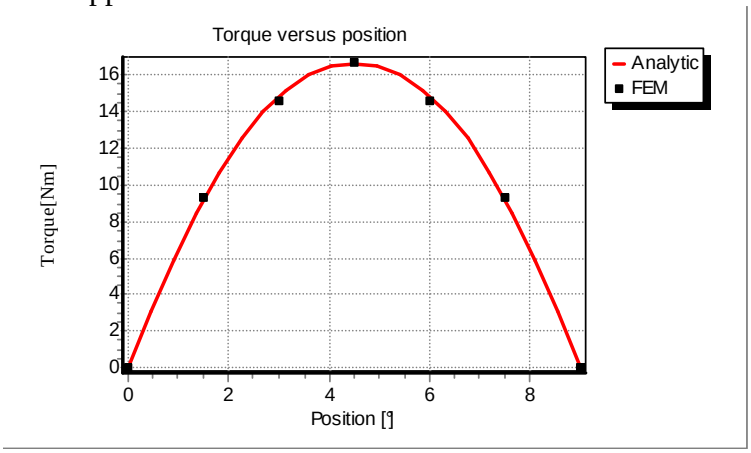

Figure 2.18 Verification results from the prototype example with parallel magnetisation.

The magnetic spur gear prototype dimensions and pole numbers is analysed with parallel magnetisation expression and there are agreements between the analytical calculated result and the FEM calculated result.

2.8.4 Prototype example with radial magnetisation

The magnetic prototype is also calculated with a radial magnetisation. These results are shown in Figure 2.19. The harmonic number used for this model is 35.

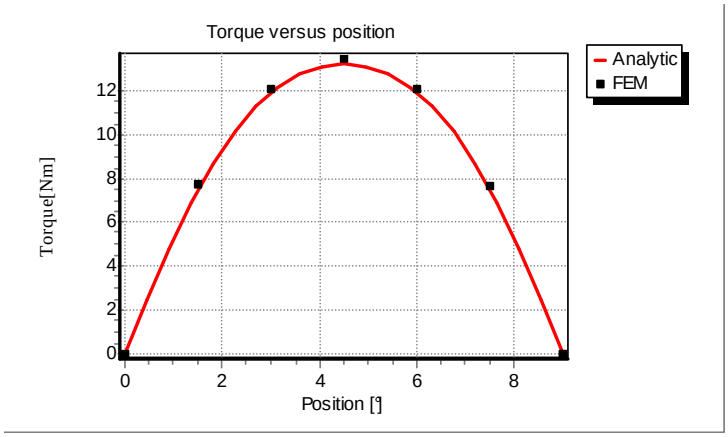

Figure 2.19 Verification results from the prototype example with radial magnetisation.

This calculation shows also good agreement between the analytical model and the FEM calculation.

2.8.5 E. P. Furlani example with parallel magnetisation

Another example with parallel magnetisation and similar design variables as the Furlani example is calculated in order to visualise the influence of high relative permeability on the source magnet.

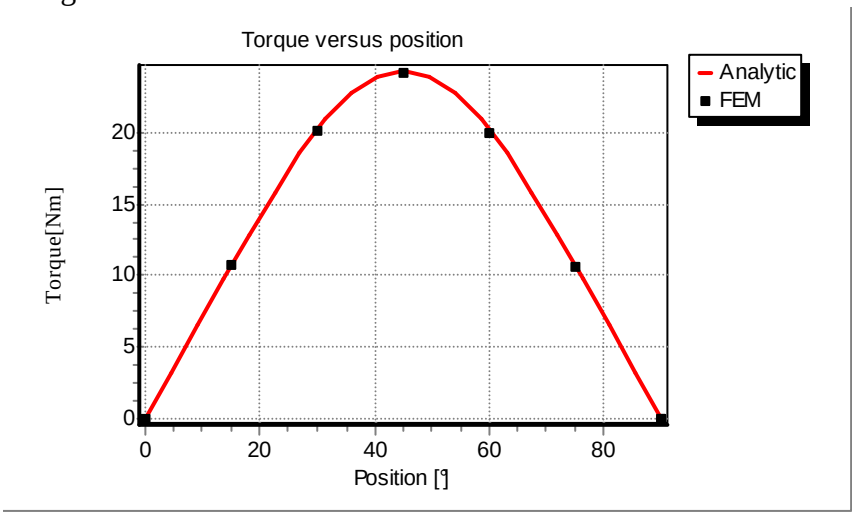

Figure 2.20 Parallel magnetisation for Furlani example with twice the permeability μ_r = 2 on source and μ_r = 1 on drive magnet.

Analytical parallel magnetisation expression seems to calculate the same torque value as FEM model, when the relative permeability is set to μ_r = 1 at the drive magnet. Even if relative permeability is increased to 10 or 100 for the source there will still be equality between analytical and FEM model. This is shown in Figure 2.21 for μ_r = 10 at source magnet.

2.8.6 E. P. Furlani example with high permeability in the source magnet

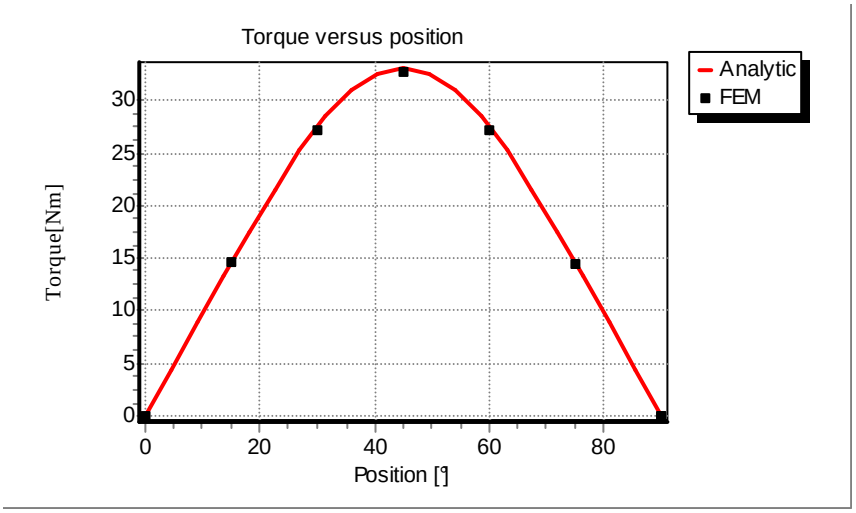

Figure 2.21 Parallel magnetisation for Furlani example with ten times permeability μ_r = 10 on source and μ_r = 1 on drive magnet.

This result verifies that relative permeability is included for the source magnet model since there is a good agreement between analytical calculated torque and FEM calculated torque. The relative permeability is used in (2.15) which is part of the free space field solution for the source magnet. The drive magnet model is represented by equivalent surface current density. This type of equivalent surface current density model representation is possible with $\mu_r = 1$ i.e. a solution in free space. Permanent magnetic material can have different permeability $\mu_r \neq 1$ and in this case the equivalent surface current density distribution will not be an equivalent representation of the drive magnet. Analytical methods are verified with FEM models and there is a good agreement when the permeability is low on the drive magnet rotor. But models show different results when the permeability is high on the drive magnet, so this is a limitation for this model.

2.8.7 Summary of verification and comparison

The torque expressions for the parallel magnetised and radial magnetised spur gear, seems to match the FEM calculations, when the relative permeability $\mu_r = 1$. However there will be a difference between the two calculation methods if the permeability $\mu_r > 1$. The hypothesis is that calculated B-field for source magnets is only a function of μ_r from source magnet, so drive magnet does not affect this field solution. However there is a dependency of $\mu_r > 1$ for drive and source magnets in the FEM model, so there will be a difference between the two models. Several papers write about surface currents [47], [48], [49], [50], [51], [52]. And a linear ($\mu_r = 1$ isotropic magnetisation, can be represented as a distribution of equivalent volume and surface current densities. Equivalent surface current densities are used in the torque expression and for that reason is this part of the calculation not consistent with the results obtained from the FEM calculations.

If the two models are supposed to show the same results, then there must be the exact same permeability properties for source and drive magnet in the analytical model and in the FEM model. The permeability in the FEM model is easy to change so the permeability is set to $\mu_r = 1$ on the drive magnet and $\mu_r = 2$ on the source magnet. These results should give an exact match. This configuration is verified in 2.8.5 with parallel magnetisation.

2.8.8 Comparison of the analytical model and the FEM model

Measured torque for a half period is compared with the analytical calculated torque Figure 2.22. The material used for the analytical calculated expression is data sheet values of the prototype material, and the separation distance for this analysis is 1 [mm] between the gear wheels

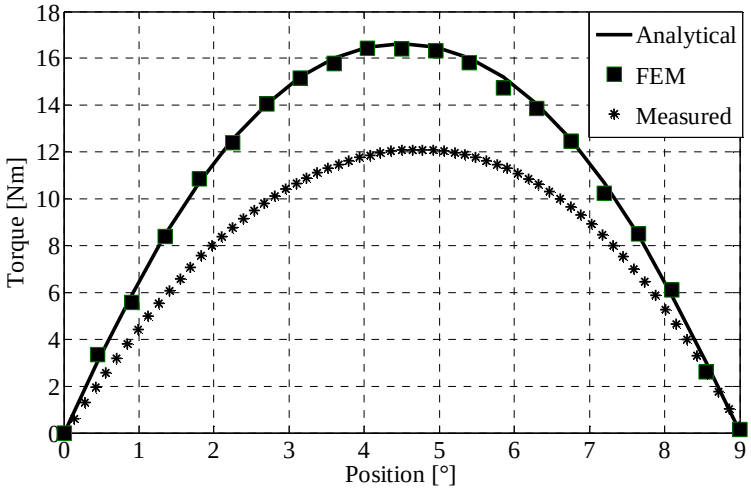

Figure 2.22 Measured torque compared with analytical calculated torque at different angles.

The shape of these curves is similar, but the magnitude is different. The percentage difference at peak torque is 38%. It is assumed that 3D effects can explain the relatively large difference between the results. The 3D effects will cause flux to leak at both ends of the rotors and these effects are not modelled in the analytical expressions. The end leakage flux will be increased if the air gap between the wheels is increased and if the leakage is increased there will be larger 3D effects. There is made an extra experiment to verify this assumption. The peak torque is measured at different separation distance starting at 1 [mm] and ending with 10 [mm]. And there is also made analytical torque calculations in that interval. The result from this analysis is shown in Figure 2.23.

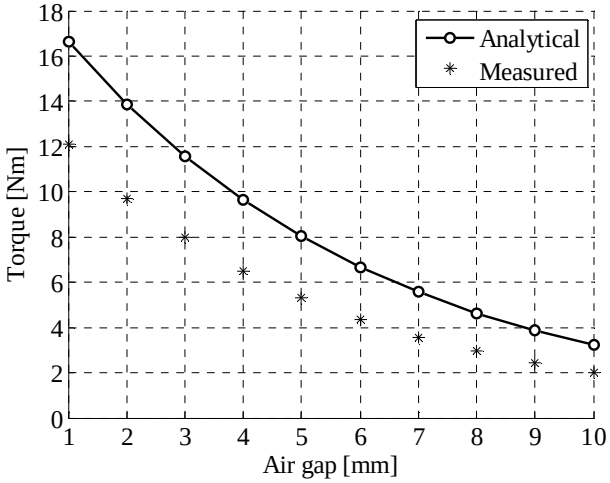

Figure 2.23 Measured peak torque compared with analytical calculated peak torque for different air gap distances.

Measured torques will decrease when the distance between the gear wheels is increased and the same will happen for analytical calculated torque. The percentage error between the analytical and measured results is shown in Figure 2.24.

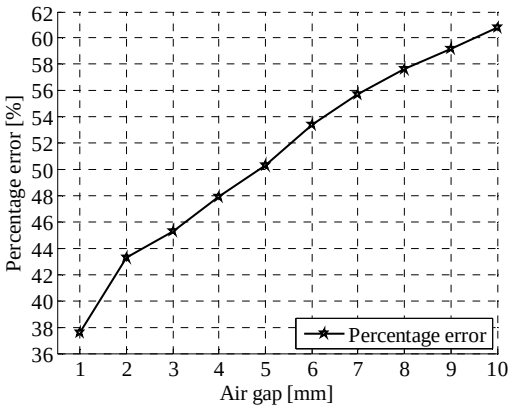

Figure 2.24 Percentage error between the analytical and measured results.

The percentage error between analytical and measured result is increasing when the distance between the gear wheels is increased. The 3D effects should also increase when the distance between the gearwheels are increased. On the basis of the 2D analytical calculated results and measured results, it is conclusion that 3D effects are one of the main causes of the differences between measured and calculated results. Also these effects are quite large.

2.8.9 Spur gear model comparisons

The results from the Analytical, 2D FEM, 3D FEM and a test model are compared. The torque transferring capability against drive magnet rotation are plotted in Figure 2.25.

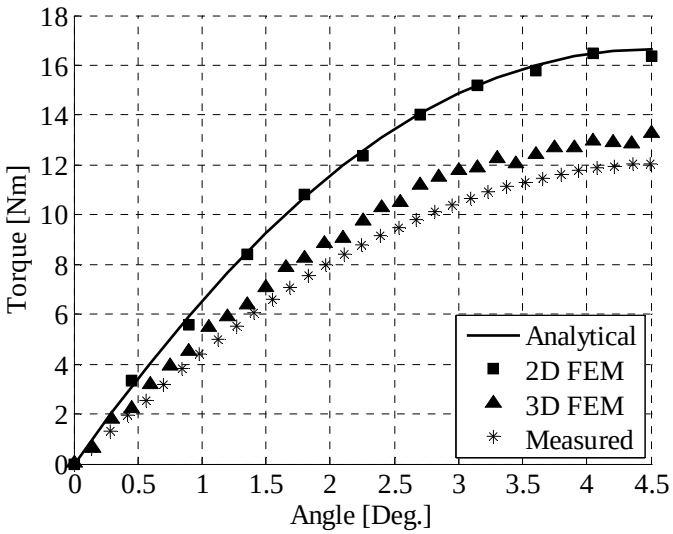

Figure 2.25 Measured torque compared with analytical calculated torque for different angle positions.

Torque from analytical calculation seems to follow the results from the 2D FEM analysis. These model results come from 2D models and are therefore not comparable with 3D models or experimental models because of a relative short axial distance which is chosen for the experimental test model.

The results from the 3D FEM model shows higher torque than measured from the experimental test. The small error between the measured and 3D calculated results can be caused by material variations, model dimension inaccuracies and measurement inaccuracies. However it can still be seen that there is a difference between the 2D and the 3D models which indicates that there are large 3D end effects for this gear with a small axial length.

2.9 Summary

An analytical expression for the torque of a parallel-magnetised spur gear is developed. The development of this expression takes its basis in a radial magnetised spur gear. Mathematical expressions from this theory are modified to be valid for parallel magnetised spur gear. Modifications involve redefining a solution matrix and solving this with new symbolic expressions, defining another magnetisation expression, defining new surface current expressions and torque expressions. The analytical expressions for radial and parallel-magnetised magnets are implemented in a software program, and there is developed a FEM model. The results from the FEM model and the analytical models show good agreement.

The measured peak torque is 12 [Nm], and the analytical calculated torque is 16.6 [Nm] at a separation distance of 1 [mm]. It is assumed that a 3D effect seems to cause the difference between the calculations. The analytical model is only a 2D model, so there will be end effects at the gear wheels ends, which is not included in the model. Measurements and calculations shows that the error between measured and calculated values will increase if the separation distance is made larger. It is the same case for the end effects. If the separation distance is increased, there will be larger end effects. It is therefore concluded that 3D end effects will cause difference between the analytical calculated torque and measured torque.

3D FEM calculations from the opera software program shows the gear has a maximum torque of 13.27 [Nm]. These calculation results are obtained with the Maxwell stress tensor. An extra 3D model in the program Comsol Multiphysics [57] is also modelled to verify the results. This model results in a calculated torque of 12.59 [Nm], which indicates that there might be some inaccuracy in these models as well which might converge if the models are meshed finer mesh or other modelling parameter is changed. However the timeframe for modelling these 3D models is not enlarged, so the obtained calculation results are accepted. The converged value of the 3D FEM calculation is close to 13 [Nm] and there will still be an 8% difference between the measured result and calculation results from the 3D programs.

The 3D FEM results and 2D FEM results shows that there is large 3D end effect for the given configuration. This will result in higher calculated torque than the real measured torque values. This is especially the case for the chosen prototype with a very short axial distance related to the outer dimension.

Chapter 3 Cycloidal magnetic gear

The magnetic cycloidal gear technology represented in this thesis is similar to the mechanical cycloidal gear technology. Magnets are used to transfer torque instead of mechanical teeth. An analytical model of the magnetic cycloidal gear is described and this analytical model is used for optimisation purpose. 2D FEM calculations and measured results are obtained from an experimental test model in order to compare results.

3.1 Analytical model of the magnetic cycloidal gear

A magnetic spur gear is analysed in the previous chapter. This spur gear is not so effective regarding torque density. One of the major problems for this gear configuration is that the magnetic material is not used very efficiently. Because a lot of magnets are ineffective while just a few of the magnets are carrying the entire load Figure 3.1a). This problem gives new ideas for developing a gear with a high expected torque density. The idea is originally from an inner magnetic spur gear Figure 3.1 b). The transferred torque from two magnetic gear wheels placed inside each other have better torque performance because more magnets are active, and the small gear does not take up volume. But there is a problem with that kind of inside gearing, because a high gearing relationship is not possible with that gearing type. But this problem can be solved by using the gearing principle from cycloidal gears where the inner part of the orbits in a circular path Figure 3.2.

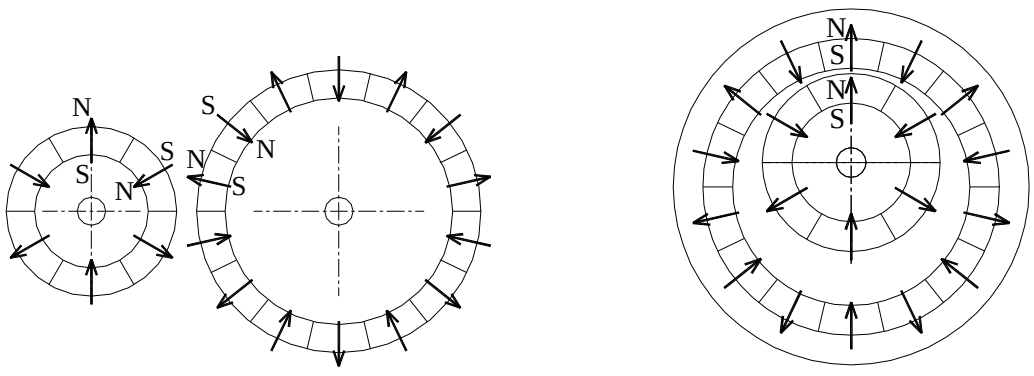

Figure 3.1 a) Magnetic spur gear. b) Inner spur gear with high magnetic interaction.

An example of a cycloidal gear movement principle is illustrated with two magnetic rotors. The inner rotor has fixed orientation. This rotor is moved along a circular path. 9 illustrations show how the inner rotor is moved and outer rotor is rotated. The outer rotor will follow a rotational motion because magnetic forces acting between the rotors. Gearing relationship depends on configuration and the number of poles on the inner rotor and outer rotor.

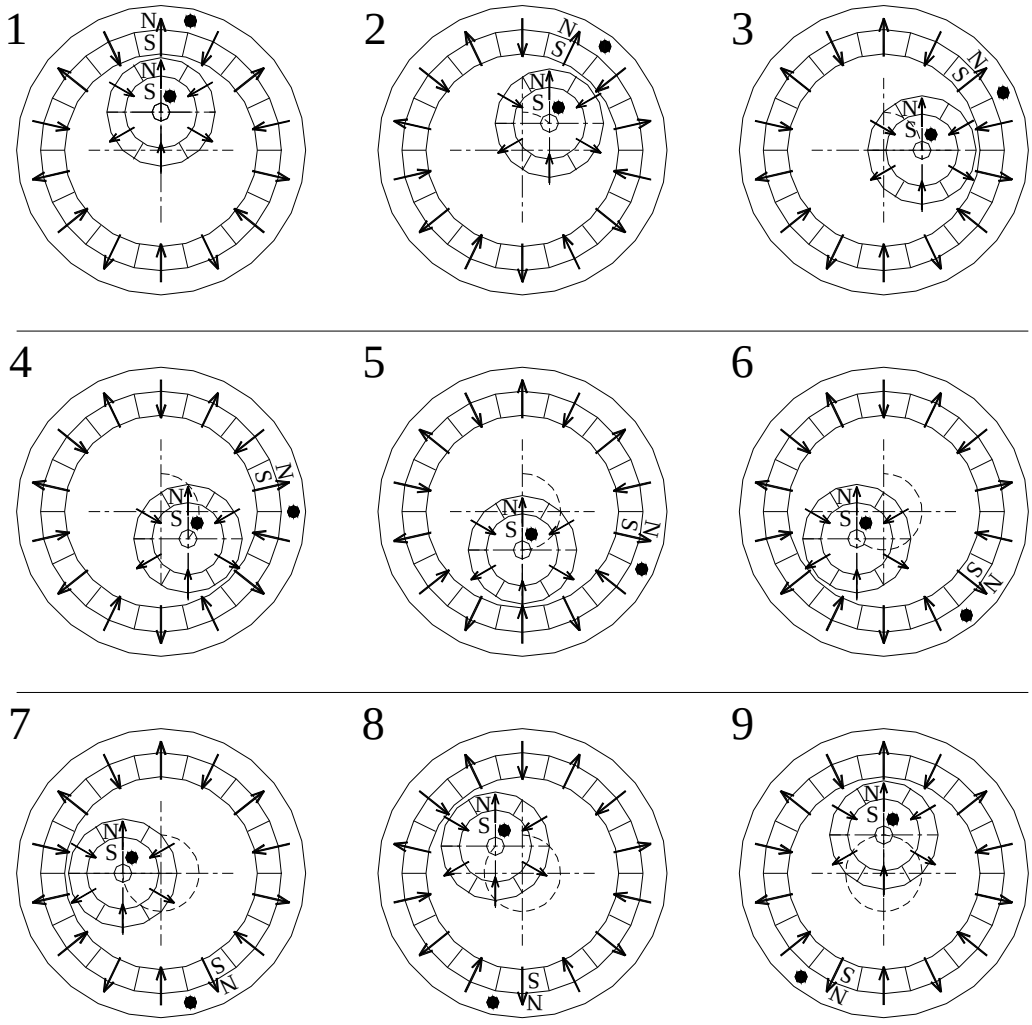

Figure 3.2 Rotor movement principle for a magnetic cycloidal gear.

3.1.1 Gear relationship for the cycloidal magnetic gear type

The mechanical cycloidal gear is a 2DOF system like a planetary gear. These gearing systems have two rotational inputs and a third rotation output or one input and two outputs. One of the two inputs can be held fixed regarding rotation. Such a system will act like a 1 DOF system where a certain input rotational speed on an input shaft corresponds to another rotational speed on an output shaft.

A magnetic version of the cycloidal gear configuration is also a 2DOF system. Illustration models of a cycloidal magnetic gear are show on Figure 3.3. The difference between a cycloidal mechanical and a magnetic cycloidal gear is the magnetic forces acting between two moving parts instead of direct contact forces on mechanical elements. 4 main components are part of this magnetic cycloidal gear. Cylindrical components/axles A, B and C are aligned along the same centre axis and some of these components can rotate around this axis. Component C is formed as a ring with magnets attached inside. These magnets are magnetically coupled to another inner movable cylindrical main component with magnets and the centre axis for this component is displaced relative to the other centre axis. An eccentric on shaft B ensures the displacement of the inner moving component. The inner component is exemplified with 3 holes where cylindrical columns from part A are inserted to ensure torque transfer to A. Magnets on inner moving component will interact with the magnets on “C”, however there will be a point where the two magnetic rings have an increased flux density, and that is where the air gap between the rotors are small. Three different cycloidal gear configuration types are illustrated, where different axles are fixed. A fixed shaft is visualised with an attached ground symbol, and moving parts are shown with arrows.

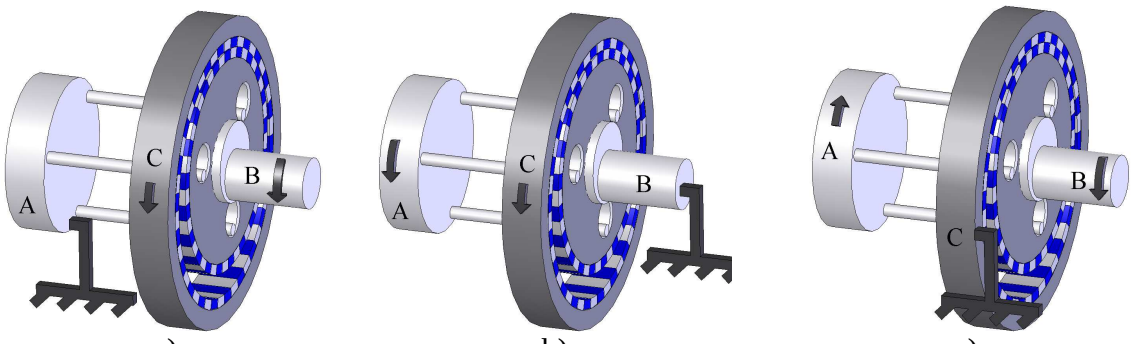

a) b) c)

Figure 3.3 Different type of configurations for a cycloidal gear.

The different configurations are named a), b) and c) type. Type a) configuration have the “A” shaft output fastened against rotation, b) type the “B” shaft fastened against rotation and c type the “C” shaft fastened against rotation. The three types are described in the following sub sections.

a) Type

Type a) configuration with the “A” shaft is fixed against rotation has the input shaft “B” and the output shaft “C”. The input shaft “B” has an eccentric. When the input shaft “B” rotates then it will change point of increased flux. A single rotation round of the shaft “B” will force the flux contact point between “C” and “A” to accomplish one round. The difference between pole numbers on shaft “C” and shaft “A” will be the number of poles that indexes the “C” shaft forward or backwards. Gear angular velocity equation for the a) type configuration can be written (3.74) . Gearing relationship is often specified as a positive number which indicates how many times the input shaft runs faster than the output shaft. Gearing relationship for the “A” type is (3.75). The torque on the output shaft is equal to the input shaft torque multiplied by gearing relationship (3.76). The resultant torque on shaft “A” can be calculated by (3.77).

$$\omega_C = \omega_B \cdot \frac{P_C - P_A}{P_C} \tag{3.74}$$

$$R_{ga)} = \frac{\omega_B}{\omega_C} = \frac{P_C}{P_C - P_A} \tag{3.75}$$

$$T_C = T_B \cdot \frac{P_C}{P_C - P_A} \tag{3.76}$$

$$T_A = -T_B + T_C = -T_B + T_B \cdot \frac{P_C}{P_C - P_A} = T_B \cdot \frac{P_A}{P_C - P_A} \tag{3.77}$$

b) Type – internal gear

Type b) configuration has “B” shaft fixed against rotation. The “C” shaft is the output shaft and the “A” shaft is the input shaft. The contact point between “A” and “B” will be fixed relative to a fixed “B” axle. The system will function similar to an internal gearing, with a gearing relationship equal to the two pole numbers divided with each other. This gearing relationship is (3.78) . Gearing relationship is shown in (3.79). The output torque and torque on the stationary shaft are shown in (3.80) and (3.81) respectively.

$$\omega_C = \omega_A \cdot \frac{P_A}{P_C} \tag{3.78}$$

$$R_{gb)} = \frac{\omega_A}{\omega_C} = \frac{P_C}{P_A} \tag{3.79}$$

$$T_C = T_A \cdot \frac{P_C}{P_A} \tag{3.80}$$

$$T_B = -T_A + T_C = -T_A + T_A \cdot \frac{P_C}{P_A} = T_A \cdot \frac{P_C - P_A}{P_A} \tag{3.81}$$

c) Type – cycloidal

Type c) configuration has the "C" shaft fixed against rotation and the "A" shaft can be the output shaft. The "B" shaft will therefore be the input shaft for the system. The contact point for this configuration will change if the input shaft "B" is rotated. When the input shaft has rotated one revolution then there will be a relative rotation of the output rotor "A". The difference between pole numbers on the "A" shaft and the "B" shaft are the number of poles shaft "A" is indexed with each time shaft "B" has rotated one round. An angular velocity relationship (3.82) can be expressed. Gearing relationship is shown in (3.83). The two torque expressions are shown in (3.84) and (3.85).

$$\omega_A = \omega_B \cdot \frac{P_A - P_C}{P_A} \tag{3.82}$$

$$R_{gc)} = \frac{\omega_B}{\omega_A} = \frac{P_A}{P_A - P_C} \tag{3.83}$$

$$T_A = T_B \cdot \frac{P_A}{P_A - P_C} \tag{3.84}$$

$$T_C = -T_B - T_A = T_B \cdot \frac{P_C}{P_C - P_A} \tag{3.85}$$

This type of configuration is named the cycloidal type because cycloidal gears are often made with this type of configuration. However type a) might also be called a cycloidal gear type.

Torque equations for different configurations are shown. These torque equations are used to calculate nominal torque between individual parts.

3.1.2 Spur gear expressions used to calculate torque on the cycloidal gear

The simplest way to calculate torque for a magnetic cycloidal gear is to modify the torque calculation equations from the magnetic spur gear. Magnetic spur gear has two rotors. A source rotor and one drive rotor Figure 3.4 a). The two rotors have different coordinate system centres. The source rotor is in a fixed coordinate system position and fixed angular rotation position. The drive rotor is also in a fixed coordinate system position and the torque is calculated for different rotor positions by rotating the drive magnet rotor coordinate system. These equations can be reused by changing the distance "d" between the two gear wheels to the cycloidal gear eccentricity distance.

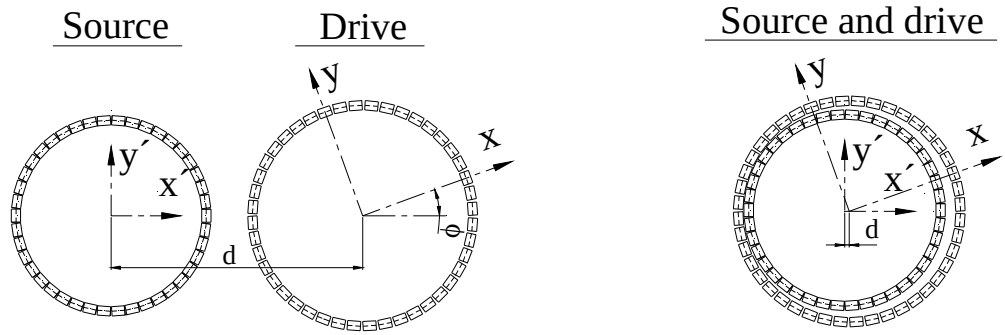

a) b)

Figure 3.4 a) Spur gear coordinate system and magnets b) Cycloidal gear coordinate system and magnets.

Source and drive magnet are placed inside each other and the torque is calculated at outer drive magnet. Such a system will be equivalent to an internal magnetic spur gear. Torque equations from the b) type – internal gear configurations is used to calculate the corresponding output torque of a c) type – gear configuration. Torque transformation is written in (3.86).

$$T_C = T_A \cdot \frac{P_C}{P_A} \Rightarrow \tag{3.86}$$

$$T_A = T_C \cdot \frac{P_A}{P_C} \Rightarrow$$

$$T_{cyc.} = T_{\text{int.}} \cdot \frac{P_A}{P_C}$$

Torque $T_{int.}$ for a internal gear calculation is known and this torque is transformed to the output shaft torque $T_{cyc.}$ for the c) type gear configuration.

Semi-optimisation of magnetic cycloidal gear is performed. Torque is calculated with analytical equations developed for the spur gear. These equations are therefore reused for the cycloidal gear torque calculations. Distance between the magnet wheels is set to cycloidal gear eccentricity. Input parameters are changed until a high torque density is

achieved. Since relative high torque density is obtainable it is decided to build a magnetic cycloidal gear prototype. Final parameters for the analytical calculations are shown in Table 11.

Symbol	**Dimensions for models**		
	Description	***Size***	***Units***
R_{2s}	Outer radius, source magnets	53.5	[mm]
R_{1s}	Inner radius, source magnets	48.5	[mm]
R_{2d}	Outer radius, drive magnets	61.5	[mm]
R_{1d}	Inner radius, drive magnets	56.5	[mm]
d	Distance between center points	2.5	[mm]
L	Length/height of the magnets	26	[mm]
B_r	Remanence flux	1.21	[T]
$H_c = M_s$	Coercivity	915000	[A/m]
i	Harmonic parameter, max value.	4	[-]
$N_r = N_t$	Torque integration parameter	10	[-]
μ_0	Permability for air regions	$4 \cdot \pi \cdot 10^{-7}$	[Tm/A]
$\mu = B_r/H_c$	Absolut permability, magnets	$13.22 \cdot 10^{-7}$	[Tm/A]
$\mu_r = \mu/\mu_0$	Relative permability, magnets	1.0523	[-]
N_p	Number of source magnets	42	[-]
N_{pole}	Number of drive magnets	44	[-]
φ_{max}	Max. torque calculation angle	4.09	[Deg.]

Table 11 Dimensions and physical parameters for the cycloidal gear model.

Rated torque for an internal magnetic gear configuration calculated with these parameters will result in 46[Nm] on outer rotor. This torque can be converted to a torque on a cycloidal gear configuration with (3.86), and corresponding torque for such a cycloidal gear will be 46·42/44 = 43.9 [Nm]. This will result in following torque density, if the analytical calculated torque is set as the maximum rated torque.

$$\rho_A = \frac{T_{\max}}{V_A} = \frac{T_{\max}}{\pi \cdot R_{2d}^{\,2} \cdot L} = \frac{43.9}{\pi \cdot \left(61.5 \cdot 10^{-3}\right)^2 \cdot 26 \cdot 10^{-3}} = 142.0 \left[kNm/m^3\right] \qquad (3.87)$$

These calculations will apply for two magnet rings with parallel magnetised magnets. However such magnets are difficult to manufacture so there is expected to be used rectangular magnets in the experimental prototype instead. These magnets are placed in stator and rotor yokes made of iron. Calculation method for the purposed design is a reuse of the previous analytical equations for the parallel magnetic spur gear and these equations will only represent permanent magnets and not iron yokes. But if the method of imaging is used, then it is possible to calculate torque using an approximated model. An approximated model of a magnet with iron yoke can therefore be modelled as a magnet ring with double height [58], [59], [19]. This means that 5 [mm] magnets in the analytical calculation should be equivalent to 2.5 [mm] magnets attached to an iron yoke.

3.2 Magnetic cycloidal gear optimisation

An experimental cycloidal gear test model is sized to fit rectangular shaped magnets [60] because these magnets do not have to be custom made for specific gear. Rectangular shaped magnets do not perform as arc shaped magnets however there is still used a magnetic arc shape model for the cycloidal gear calculations. But the arc is not that big so the error by using rectangular magnets is not huge. The parallel magnetisation expressions developed for the magnetic spur gear type are used. These expressions are first used in a semi optimisation process and later in a computerised optimisation process.

Semi optimisation

Rectangular magnet dimensions for the Magnetic cycloidal gear is chosen and also a gearing relationship. Cycloidal gear gearing relationship is chosen to be 1:21 and this is the same gearing relationship as SauerDanfoss A/S uses in one of their mechanical cycloidal gears. A mechanical cycloidal gear from SauerDanfoss A/S is used as inspiration for the magnetic gear design. Rectangular magnets size is chosen from a catalogue [60]. Fixed gearing relationship and the fixed magnet shape is sketched in a drawing in order to find appropriate radius dimensions for the magnetic cycloidal gear. Magnetic spur gear torque expressions are used in the semi optimisation of the magnetic cycloidal gear. Different eccentricity and radial dimensions are tried out with the expressions to find best nominal dimensions for the magnetic cycloidal gear. Result of the semi optimisation procedure gave the following design parameter results:

$R_{2s} = 53.5 \cdot 10^{-3}[m]$; $R_{1s} = 48.5 \cdot 10^{-3}[m]$; $R_{2d} = 61.5 \cdot 10^{-3}[m]$; $R_{1d} = 56.5 \cdot 10^{-3}[m]$;
$d = \quad 2.5 \cdot 10^{-3}[m]$

These parameters gave the best performance of semi optimisation procedure regarding the torque density, which is 142.0 [kNm/m^3].

Computerised optimisation process

The computerised optimisation is formulated as general optimisation problem [55] with a cost function (2.88), equality constrains (2.89), inequality constrains (2.90), and a number of constants, shown in Table 12. The cost function is set up as the torque density of magnetic spur gear with torque calculation from parallel magnetisation expressions developed in Chapter 2 and volume are set to the drive magnet wheel area times a constant length. The optimisation procedure routine is a minimisation routine, so the torque function $T(R_{2s}, R_{1s}, R_{2d}, R_{1d}, -d)$ is set up with a negative distance between the magnet wheels in torque calculation routine. It is also necessary to have an equality constraint for permanent magnet material limitation. Permanent magnet area constraint is setup to be the same area that can be calculated from the semi optimisation results variables. Inequality constrains are set for the minimisation routine. The outer radius must be greater than the inner radius in g_1 and g_2. Largest radius of the drive wheel radius has to be less than a certain value in g_3. The smallest radius for the inner gear wheel will have to be greater than a certain value in g_4. Eccentric distance does also have a limitation in g_5 and g_6.

$$f(x) = f(x_1, x_2 ..., x_n) \quad \Rightarrow \tag{2.88}$$

$$f(R_{2s}, R_{1s}, R_{2d}, R_{1d}, d) = \frac{T(R_{2s}, R_{1s}, R_{2d}, R_{1d}, -d)}{L\pi({R_{2d}}^2)} \cdot \frac{N_p}{N_{Pole}}$$

$$h_j(x) = (x_1, x_2, ...x_n) = 0 \quad \Rightarrow \tag{2.89}$$

$$h_1(R_{2s}, R_{1s}, R_{2d}, R_{1d}) = A_{Const} - \pi({R_{2s}}^2 - {R_{1s}}^2 + {R_{2d}}^2 - {R_{1d}}^2) = 0$$

$$h_2(R_{2s}, R_{1d}, d) = R_{1d} - d - g - R_{2s} = 0$$

$$g_i(x) = g_i(x_1, x_2, ...x_n) \le 0 \quad \Rightarrow \tag{2.90}$$

$$g_1(R_{2s}, R_{1s}) = R_{1s} - R_{2s} + 4 \cdot 10^{-3} \le 0$$

$$g_2(R_{2d}, R_{1d}) = R_{1d} - R_{2d} + 4 \cdot 10^{-3} \le 0$$

$$g_3(R_{2d}) = -61.5 \cdot 10^{-3} + R_{2d} \le 0$$

$$g_4(R_{1s}) = 48.5 \cdot 10^{-3} - R_{1s} \le 0$$

$$g_5(d) = -20 \cdot 10^{-3} + d \le 0$$

$$g_6(d) = 1 \cdot 10^{-3} - d \le 0$$

The following constants are used for the computerised optimisation procedure.

Symbol	**Optimisation constants**		
	Description	***Size***	***Units***
g	Air gap between magnet wheels	$0.5 \cdot 10^{-3}$	[m]
L	Length/height of the magnets	$26 \cdot 10^{-3}$	[m]
A_{Const}	Area of permanent magnets	$35 \cdot 10^{-4}$	[m^2]
B_r	Remanence flux	1.21	[T]
$H_c = M_s$	Coercivity	915000	[A/m]
i	Harmonic parameter, max value.	4	[-]
$N_r = N_t$	Torque integration parameter	10	[-]
μ_0	Permability for air regions	$4 \cdot \pi \cdot 10^{-7}$	[Tm/A]
$\mu = B_r/H_c$	Absolut permability, magnets	$13.22 \cdot 10^{-7}$	[Tm/A]
$\mu_r = \mu/\mu_0$	Relative permability, magnets	1.0523	[-]
N_p	Number of source magnets	42	[-]
N_{pole}	Number of drive magnets	44	[-]
ϕ	Angle for the maximum torque	4.09	[Deg.]

Table 12 Constants for the optimisation.

A constrained nonlinear minimisation routine is performed to find the optimal dimensions for the magnetic spur gear. The minimisation routine resulted in 142.5 [kNm/m^3] and following parameters:

$R_{2s} = 53.8 \cdot 10^{-3}[m]$; $R_{1s} = 48.5 \cdot 10^{-3}[m]$; $R_{2d} = 61.4 \cdot 10^{-3}[m]$; $R_{1d} = 56.7 \cdot 10^{-3}[m]$

$d = 2.4 \cdot 10^{-3}[m]$;

Comparison of semi and computerised optimisation

The semi optimised solution is very close to the computer optimised solution. The semi optimised solution is 142.0 [kNm/m^3] and the computer optimised solution is 142.5 [kNm/m^3]. The reason why the results are so close to each other is mainly caused by the limited freedom for the computerised model. The computerised model is locked by area limitation h_1 radius sizes must also be within limited values. This means that this computerised optimisation will be close to the semi optimisation solution for the current case.

The chosen gearing 1:21 is not necessarily the most optimal gearing relationship configuration. That is why other pole number configurations is calculated with the same constraints. Results from this optimisation are shown in Table 13.

Source poles	**Drive poles**	**Turn angle**	**Area constrain**	**Radius constrain**	**Radius constrain**	**Torque density**
N_p	N_{pole}	ϕ	A_{const}	R_{2d}	R_{1s}	ρ_A
[-]	[-]	[Deg]	[m^2]	[m]	[m]	[kNm/m^3]
42	44	4.09	$35\cdot10^{-4}$	$61.5\cdot10^{-3}$	$48.5\cdot10^{-3}$	142.5
52	54	2.22	$35\cdot10^{-4}$	$61.5\cdot10^{-3}$	$48.5\cdot10^{-3}$	157.6
62	64	2.81	$35\cdot10^{-4}$	$61.5\cdot10^{-3}$	$48.5\cdot10^{-3}$	172.4
70	72	2.5	$35\cdot10^{-4}$	$61.5\cdot10^{-3}$	$48.5\cdot10^{-3}$	173.8
72	74	2.43	$35\cdot10^{-4}$	$61.5\cdot10^{-3}$	$48.5\cdot10^{-3}$	173.9
74	76	2.37	$35\cdot10^{-4}$	$61.5\cdot10^{-3}$	$48.5\cdot10^{-3}$	173.9
76	78	2.31	$35\cdot10^{-4}$	$61.5\cdot10^{-3}$	$48.5\cdot10^{-3}$	173.8

Table 13 Optimisation results from pole number configuration change.

Result from optimisation with different pole configurations shows that a higher number of poles will be better for the given configuration. It is also found that the highest torque density is reached with a magnetic pole configuration of 72 and 74 for the given optimisation. This magnetic pole configuration will give a gearing relationship of 1:36. The very promising magnetic pole configuration has the following dimensional parameters:

$R_{2s} = 55.3\cdot10^{-3}[m]$; $R_{1s} = 49.6\cdot10^{-3}[m]$; $R_{2d} = 61.5\cdot10^{-3}[m]$; $R_{1d} = 57.3\cdot10^{-3}[m]$

$d = 1.5\cdot10^{-3}[m]$

There is obviously an optimal number of magnetic poles for the given dimensional configuration, and that is why it is interesting to see if there is optimal dimension parameters for a given magnetic pole number. Magnetic pole number is set to 42/44 and the outer drive wheel radius limitation is changed to less the 140[mm] and the inner radius of the source wheel is limited to minimum 15 [mm]. This optimisation will result in a torque density of 158.04 [kNm/m^3], and dimension parameters are:

$R_{2s} = 42.5\cdot10^{-3}[m]$; $R_{1s} = 34.6\cdot10^{-3}[m]$; $R_{2d} = 50.1\cdot10^{-3}[m]$; $R_{1d} = 45.0\cdot10^{-3}[m]$

$d = 1.9\cdot10^{-3}[m]$

Gear dimension sizes for the two gears are sketched on Figure 3.5 to get visual impression of an optimal computerised solution and a semi optimised solution.

It is to be noticed that the amount of magnetic material for the two gears are the same. Material costs for the two gears are expected to be the equal and higher torque is expected from the semi optimised gear but the outer dimension is smaller for the computer optimised gear shown on Figure 3.5 b) and this the main purpose for this optimisation although the permanent magnet material is not best utilised.

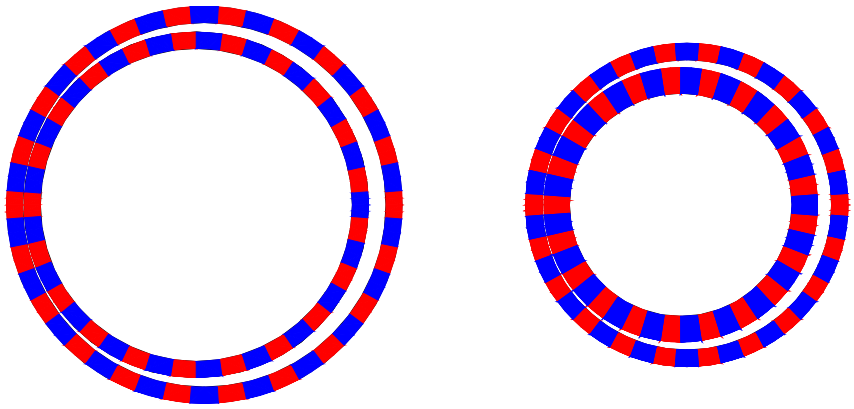

a) b)

Figure 3.5 a) Illustration sketch of the semi optimised gear with a torque density of 142.0 [kNm/m^3]. b) Illustration sketch of the computerised optimisation which results in a torque density of 158 [kNm/m^3].

The influence of adding different amount of magnetic material to the rotors is also investigated in this analysis. This analysis is performed with the 42 and 44 pole configuration and wide boundary on radius constraints. The result of this analysis is shown in Table 14. A tendency shows that the optimal torque density is increased if more magnetic material is put into the magnetic gear. But the torque density seems to saturate when a bigger amount of material is added to the optimisation procedure.

Source poles	**Drive poles**	**Turn angle**	**Area constrain**	**Radius constrain**	**Radius constrain**	**Torque density**
N_p	N_{pole}	ϕ	A_{const}	R_{2d}	R_{1s}	ρ_A
[-]	[-]	[Deg]	[m^2]	[m]	[m]	[kNm/m^3]
42	44	4.09	$30\cdot10^{-4}$	$140\cdot10^{-3}$	$15.0\cdot10^{-3}$	155.4
42	44	4.09	$60\cdot10^{-4}$	$140\cdot10^{-3}$	$15.0\cdot10^{-3}$	167.2
42	44	4.09	$90\cdot10^{-4}$	$140\cdot10^{-3}$	$15.0\cdot10^{-3}$	172.8
42	44	4.09	$120\cdot10^{-4}$	$140\cdot10^{-3}$	$15.0\cdot10^{-3}$	176.3
42	44	4.09	$150\cdot10^{-4}$	$140\cdot10^{-3}$	$15.0\cdot10^{-3}$	178.7
42	44	4.09	$180\cdot10^{-4}$	$140\cdot10^{-3}$	$15.0\cdot10^{-3}$	180.5
42	44	4.09	$210\cdot10^{-4}$	$140\cdot10^{-3}$	$15.0\cdot10^{-3}$	181.9
42	44	4.09	$240\cdot10^{-4}$	$140\cdot10^{-3}$	$15.0\cdot10^{-3}$	183.0

Table 14 Optimisation results from the increased area constrain.

The last optimisation resulted in a torque density of 183 [kNm/m^3] and the following dimensions are optimal:

$R_{2s} = 105.1 \cdot 10^{-3}[m]$; $R_{1s} = 81.0 \cdot 10^{-3}[m]$; $R_{2d} = 123.9 \cdot 10^{-3}[m]$; $R_{1d} = 110.4 \cdot 10^{-3}[m]$

$d = 4.8 \cdot 10^{-3}[m]$

Sub conclusion

The cycloidal magnetic gear is optimised with a computerised method and a semi optimisation method. The computer optimisation method resulted in a torque density at 142.5 [kNm/m^3] and it is possible to reach 142.0 [kNm/m^3] with the semi optimisation method. There is initially chosen a gearing relationship of 1:21 for the computer optimisation. This gearing relationship is changed by changing magnetic pole numbers for magnetic gear wheels and keep original area and radius constraints. The optimisation resulted in the highest torque density at gearing relationship 1:36. This gearing relationship resulted in a torque density of 173.9 [kNm/m^3] with the same optimisation constraints. These optimisations indicate that there are an optimum number of poles for a specific dimension configuration, so there must also be an optimal dimension for a given number of poles and a specified size of magnetic material. This hypothesis is tested in another optimisation where the limitations of inequality constrains is larger. The solution to this optimisation will give a result where the volume is utilised better than the computer optimised solution with limited inequality constrains and gearing relationship 1:21. The torque density optimisation with large limitations is optimised to 158 [kNm/m^3].

It will also be possible to use a bigger amount of magnetic material for the optimisation procedure to see if torque density will increase. This investigation is done in another optimisation procedure where the amount of magnetic material is changed from $30 \cdot 10^{-4}[m^2]$ to $240 \cdot 10^{-4}[m^2]$. The biggest torque density is 183[kNm/m^3] at biggest amount of magnetic material.

It can be concluded that larger amount of magnetic material will give a higher torque density and a higher gearing relationship will also give higher torque density but it saturates. The best optimisation result obtained in this analysis is 183 [kNm/m^3] for a magnetic cycloidal gear.

The optimisation models are a general tool to find optimal torque density for given design parameter limitations. This will help the magnetic gear designer to find optimal design solutions.

3.3 2D FEM calculations

A FEM model of a magnetic cycloidal gear is modelled to verify results from the analytical model. The 2D FEM model is modelled with the same dimensions as the analytical model consisting of two permanent magnetic rings. A screenshot from the program is shown in Figure 3.6. The two magnetic rings are placed inside each other similar to an internal gearing. Torque is calculated with Maxwell stress tensor method in the air gap between the two magnetic rings. The torque is calculated close to the outer ring and the centre point of the torque calculation is also the centre of the outer ring. The outer magnet ring is rotated and modelled in different angle positions. Torque is also calculated for different angle positions. Torque calculated from this configuration will be equivalent to an internal gearing torque calculation. This torque result is multiplied with a factor for transforming the calculated torque to a cycloidal gear configuration.

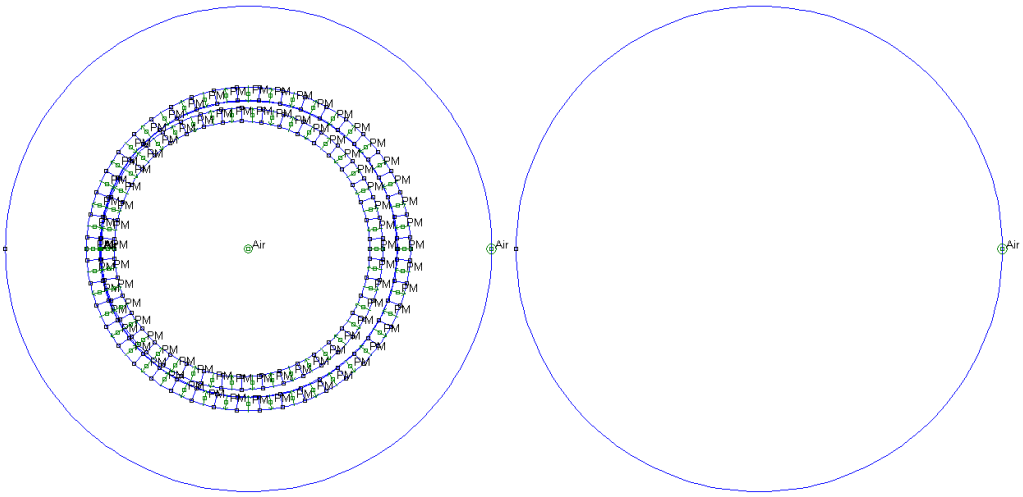

Figure 3.6 Screenshot from the FEM model.

Maximum torque calculated from 2D FEM model is 47.61[Nm]. This torque is multiplied by a factor for converting the result to a cycloidal gear configuration. Torque from a corresponding cycloidal gear will then be 47.51·42/44 = 45.35 [Nm]. The torque density of this configuration is calculated in (3.91).

$$\rho_A = \frac{T_{\max}}{\mathrm{V_A}} = \frac{T_{\max}}{\pi \cdot \mathrm{R_{2d}}^2 \cdot L} = \frac{45.35[Nm]}{\pi \cdot \left(61.5 \cdot 10^{-3}\right)^2 \cdot 26 \cdot 10^{-3}[m^3]} = 146.8[kNm/m^3] \quad (3.91)$$

This calculated density is close to result from the analytical model.

3.4 Experimental test model

A test model of the magnetic cycloidal gear is designed. A test model is made with rectangular shaped magnets. These magnets are placed on iron yokes Figure 3.7. The design outline is adapted to rectangular magnets chosen. The input shaft is placed at the centre of the gear box which has an eccentric and this is mechanically linked to inner iron yoke. Circular motion of the input shaft will force the inner yoke to move in orbit motion consisting of rotation and translation motion. Inner yoke magnets will perform a cycloidal motion. Strong magnetic flux paths between the inner and outer yokes will induce torque at the output shaft. This output shaft is connected to the inner yoke with three cylindrical columns with eccentrics. These eccentrics can compensate for misalignment between inner yoke and output shaft. These cylindrical columns will act like mechanical coupling to ensure torque transferred from the inner yoke to the output shaft.

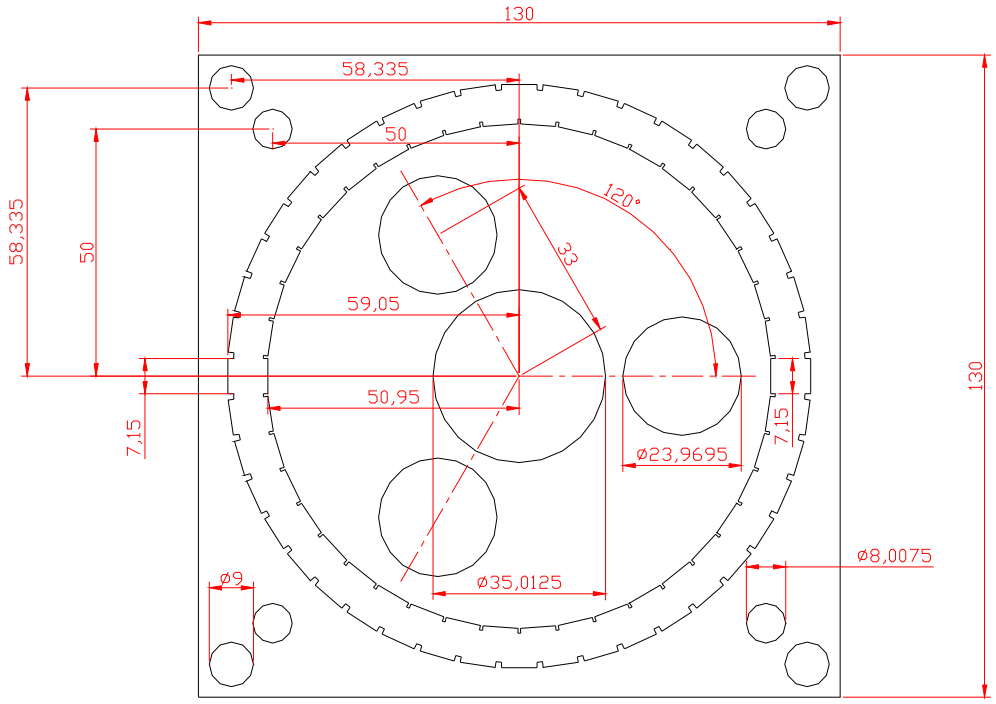

Figure 3.7 Outer and inner yoke for the cycloidal gear (plane view).

Two outer and inner yokes are manufactured and they are mounted with magnets, and placed as illustrated in Figure 3.8.

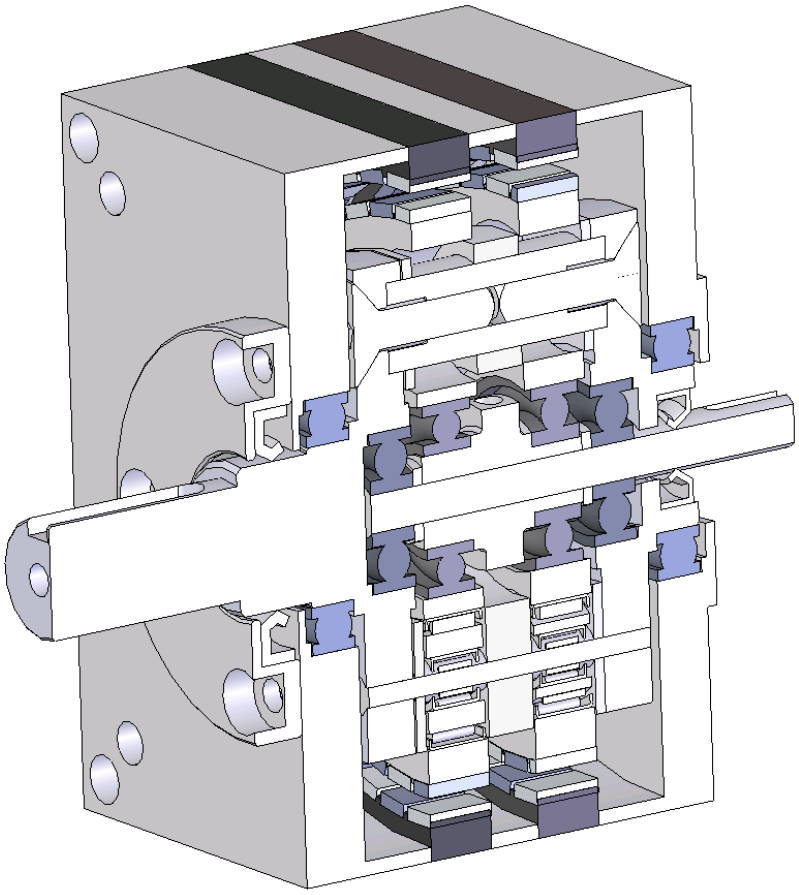

Figure 3.8 Cycloidal gear design (rendered view).

The rotor yokes are placed on the eccentric input shaft. The eccentricity is created by a central bushing. This central brushing has two eccentrics with 180 degree phase shift which will assist to outbalance the radial magnetic forces. 12 extra needle bearings are also included in design together with 6 support eccentrics. Their function is to ensure a parallel motion of the inner rotors relative to the output shaft reference. The purposed design will therefore have 18 bearings total.

The total magnetic gear volume can be smaller by choosing a round design and there might also be saved space by choosing smaller bearings. The space between the two iron yokes can also be made smaller to save volume. However 3D analysis is required to investigate the interference between magnetic components.

3.5 Measured results

The cycloidal gear is tested in two situations. One of the situations is a static torque test, where the maximum torque is measured on the output shaft. The maximum torque is measured to 33 [Nm]. The total torque density of the magnetic cycloidal gear is calculated in (3.92). Outer experimental cycloidal gear test model dimensions are used to calculate total volume.

$$\rho_T = \frac{T_{\max}}{\mathrm{V_T}} = \frac{T_{\max}}{W_T \cdot H_T \cdot L_T} = \frac{33[Nm]}{0.130 \cdot 0.130 \cdot 0.086[m^3]} = 22.7[kNm/m^3] \qquad (3.92)$$

The cycloidal gear is also dynamically tested in order to measure magnetic gear efficiency. This test is done in a test bench sketched in Figure 3.9. The test bench has two torque transducers an input drive to drive the magnetic gear and a load drive where different torque loads can be applied to the magnetic gear while running at a specified speed.

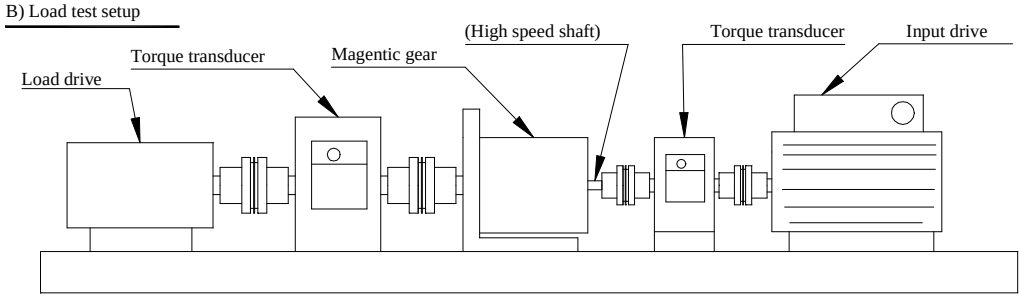

Figure 3.9 Sketch of dynamic test bench.

Torque and angular velocity is measured on magnetic gear output shaft and input shaft. The input and output power is calculated and efficiency is calculated by (3.93).

$$\eta = \frac{P_{out}}{P_{in}} \qquad (3.93)$$

Results from the dynamic cycloidal magnetic gear test are shown in Figure 3.10.

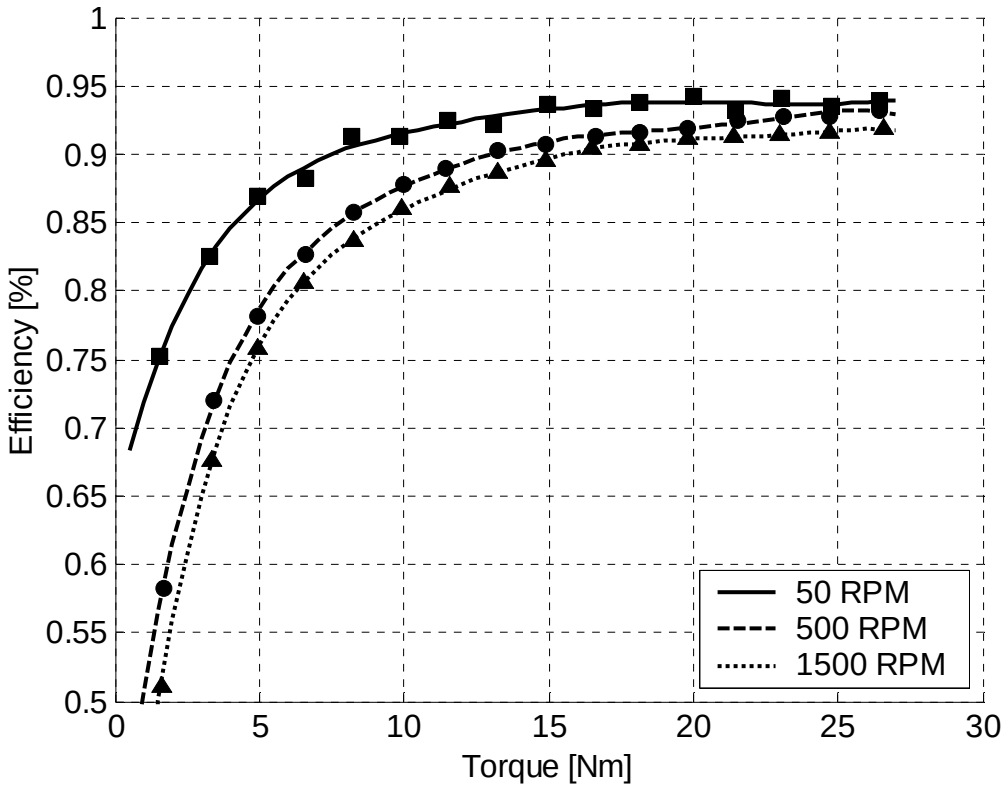

Figure 3.10 Measured efficiency results for the cycloidal magnetic gear.

Efficiencies are measured at 1500, 500 and 50 [RPM]. Highest efficiencies are generally obtained at low speed and high torque. The best gear efficiency measured at 50 [RPM] is 94 [%]. At 500 and 1500 [RPM] the efficiencies are 93[%] and 92 [%] respectively.

3.6 Verification and comparison of results

Torque results from analytical model and FEM model are compared with measured result from the prototype. These results are shown in Figure 3.11.

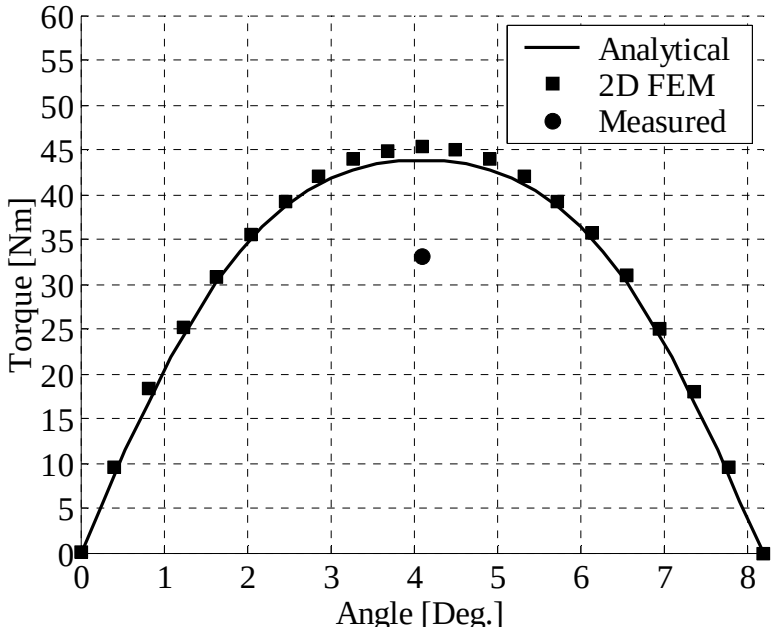

Figure 3.11 Torque versus rotation angle for analytical model and 2D FEM model. Measured maximum torque is also shown.

The analytical model and the 2D FEM model shows almost the same results; however there is a small difference between the two results, which is mainly caused by missing relative permeability of the drive magnet in the analytical model. Extra calculations with relative permeability set to one are also performed and these calculations give results that converge towards the same values for analytical model and 2D FEM model.

Maximum torque of the magnetic cycloidal gear is only measured a single operating point on the torque curve which results in 33 [Nm] on the output shaft. Measured result is much lower than the results from the 2D models. There are many factors that can cause this difference. A 3D end effect is one of the causes that will make large differences between calculated results and FEM results for the magnetic spur gear. The 3D end effects might also cause large differences for the cycloidal gear type, because each modelled yoke have a relative small axial length.

Model differences will also cause additional differences between the measured and the simulated results.

3.7 Summary

A magnetic cycloidal gear is mainly analysed regarding gearing relationship and torque density performance. Different gearing configurations of a cycloidal gear is analysed and gearing relationship for these different types is found. Torque relationships on the individual parts are also found. Analytical expressions for the magnetic spur gear torque are used to calculate torque of a magnetic cycloidal gear with an added modification for the current gear configuration design. Analytical expressions is used to semi optimise magnetic cycloidal gear experimental test model. Analytical expressions are also used in an optimisation process where a theoretical torque density will be 183 [kNm/m^3] for certain optimisation constrains. 2D FEM calculations are also performed for the semi optimised cycloidal gear design. These FEM calculations shows almost the same results as the analytical algorithms; however there is a small difference because of permeability influence on the analytical model. An experimental test model of a cycloidal gear is designed and manufactured partly to confirm theoretical results obtained from analytical model and FEM model, and partly to get experience with the design process for a magnetic cycloidal gear. The cycloidal gear experimental model will have a total torque density of approximately 22.7 [kNm/m^3]. This torque density is much lower than the predicted torque density from the analytical model and the FEM model. The reason why there are so big differences between predicted torque density and measured torque density is caused by many factors such as 3D end effect, the use of rectangular magnets instead of arc shaped magnets, modelling with an image current theory instead of magnetic material model. Another major factor is the use of axial machine length. The proposed prototype is only using 26 [mm] active length out of 86 [mm] total gear length. It is therefore obvious that a better use of this total length will increase the total torque density. A better utilisation of this length might be possible with only one eccentric rotor instead of two rotors. But this may give unbalance both mechanically and magnetically. The two rotor configuration is only chosen because this configuration will outbalance some of the added centripetal mass and magnetic forces; however these forces might also be possible to decrease with rotating counterbalance on the rotating shaft.

The experimental test model is tested dynamically to measure efficiency performance which is approximately 92 [%] for 1500 [RPM] input speed and 94 [%] at a input speed of 50 [RPM]. These efficiencies might also be further increased by choosing a single rotor configuration because this will decrease the number of bearings for the gear design.

Cycloidal magnetic gear will have an advantage where there is required a high gearing relationship, because this gear type shows increasing torque density performance with increasing gearing relationship. This is normally a problem for a traditional mechanical gear, because increased gearing relationship will normally result in decreased efficiency. However this is possibly not the case for this magnetic cycloidal gear type.

Chapter 4 Magnetic planetary gear

References from magnetic planetary gears and basic function principle are described. Design choice for iron segments and variation of transmitted torque is explained. Improved design theory is described regarding gearing relationship. 2D FEM analysis and optimisation is performed on an example gear and choice of iron segments duty cycle is also described.

4.1 History of magnetic planetary gear

One of the early patents [35] regarding planetary magnetic gears can be dated back to 1968. This patent describes magnetic transmissions and one of the gear technology's is similar to the one described in this chapter. Other patents [39], [38], [40] with comparable technology are published in 1972, 1996, 1997 respectively.

An important milestone paper [1] about planetary magnetic gears is published by K. Atallah and D. Howe in 2001. This paper is unique in the sence that they with help of FEA calculations predict a theoretical torque density that will exceed 100 [kNm/m^3]. However theoretical predicted torque from a 2D magneto static model will not be of same intensity as the measured torque value from a prototype. So the theoretical torque of 100 [kNm/m^3] corresponds to a less measured torque density. Theoretical and measured torques are investigated in a paper [65] which is published in 2003. It is possible to obtain an active torque density at 55 [kNm/m^3] from test measurements and 92 [kNm/m^3] from a 2D magneto static calculation. Another paper [61] from K. Atallah and D. Howe, published in 2004, the measured pull out torque is 60 [Nm] and this torque is approximately 30% lower than the predicted torque per unit stack length at a level of 1800 [Nm/m]. This information will result in a calculated active torque density at 78 [kNm/m^3] when stack length and outer diameter are 50 [mm] and 140 [mm] respectively. This planetary magnetic gear is with the highest torque density ever built. A paper [69] published in 2007 describes a 3D analysis of a gear similar to the planetary magnetic gear. It is found that an integral equations method is suitable together with a fast multipole method. Dimensions and measurement are not available in this paper so torque density is not possible to calculate for this gear.

Year	**Reference**	**Torque density 2D analysis**	**Torque density Measured**
2001	[1]	100 [kNm/m^3]	
2003	[65]	92 [kNm/m^3]	55 [kNm/m^3]
2004	[61]		78 [kNm/m^3]
2009	[68]		53 [kNm/m^3]

Table 15 Torque density values for stand alone planetary magnetic gears.

Papers [64] and [67] with integrated motor and planetary magnetic gear are proposed in 2007. Calculated theoretical active torque density for this device is 87 [kNm/m^3]. However prototype seems to be build to verify the calculation. Another paper [63] with integrated motor and planetary gear is presented in 2008. The overall active torque density is 60 [kNm/m^3] which is less than a stand alone planetary magnetic gear. Transient torque analysis of a planetary magnetic gear is analysed in a paper [66] from 2008. Another paper [68] from the same department is published in 2009 where a proposed planetary magnetic gear is designed with so called interior-magnet outer-rotor structure. This stand alone permanent magnetic gear has a measured torque density of 53 [kNm/m^3]. The percentage difference between calculated torque and measured torque is less than 5%. This accuracy is obtained by the use of a 3D-FEM calculation method. Another paper [70] with integrated motor and planetary magnetic gear is purposed in 2009. Expected active torque density from this drive is 130 [kNm/m^3] which is the highest predicted torque density among integrated motor planetary magnetic gear drives. This paper also includes an investigation of chosen dimensions for the planetary magnetic gear.

Year	Reference	Torque density 2D analysis	Torque density Measured
2007	[64],[67]	87 [kNm/m^3]	
2008	[63]		~ 60 [kNm/m^3]
2009	[70]	130 [kNm/m^3]	

Table 16 Integrated motor planetary magnetic gear torque density.

Analytical approach for calculating the magnetic field distribution in a planetary magnetic gear is presented in a paper [71] from 2009. 2D analytical expressions are compared with saturated and unsaturated FEM models. Unsaturated FEM model results show good agreement with the analytical model results. Calculated output torque, or an example are not presented in the paper, only magnetic flux density is shown.

Summary

Planetary magnetic gear principle can be dated back to 1968. A predicted torque density is 100 [kNm/m^3] which is investigated in research paper [1] from 2001. Best performance for a stand alone magnetic planetary gear [61] is 78 [kNm/m^3]. Integrated motor planetary magnetic gear drives are a research area which have had an increased interest ever since 2007. The drive with best performance is measured to a torque density at 60 [kNm/m^3]. Most promising drive is predicted to have a torque density of 130 [kNm/m^3].

4.2 Basic design theory

Magnetic planetary gear consists of two permanent magnet rotors and one rotor with iron segments Figure 4.1 a). The inner rotor is the high speed rotor and the outer rotor is the low speed rotor in this example. Flux paths in the iron parts are illustrated on Figure 4.1 b). This illustration is fixed in an instant where there is no load applied to the rotors. The iron segments are mechanically fixed and magnetic flux paths in these segments have the freedom to rotate as input shaft rotates. The main flux path directions in iron segments are illustrated with bold arrow in Figure 4.1 b). The individual main flux path directions in the iron segments will rotate counter clockwise as the inner rotor is driven clockwise and the outer rotor is driven counter clockwise. The nominal angular velocity of outer rotor is 5.5 times lower than the nominal velocity at inner rotor. This gear example is therefore a reduction gear with a gearing relationship of 5.5 when the input shaft is connected to the inner rotor and the output shaft connected to the outer rotor.

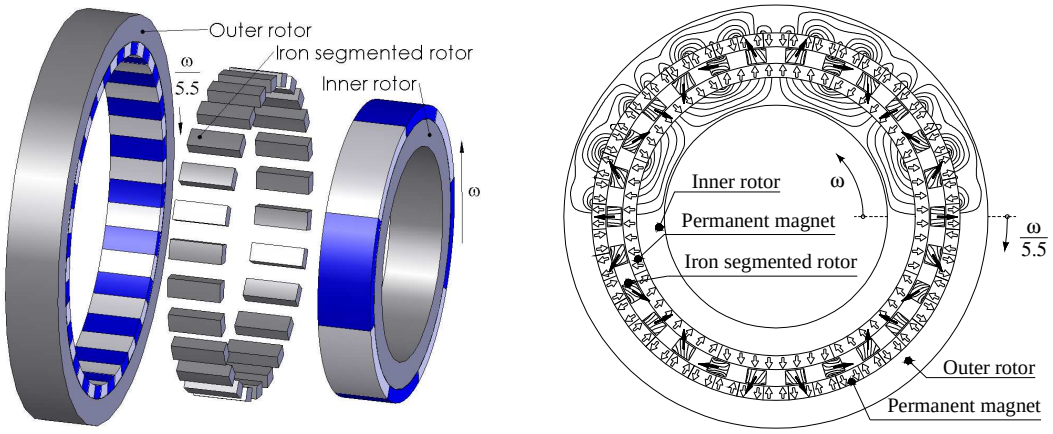

a) b)

Figure 4.1 a) Exploded view of the magnetic planetary gear b) Cross section of a planetary magnetic gear.

4.2.1 Choice of iron segments

The magnetic planetary gear configuration is previously analysed regarding pole number configuration and torque density [1][61]. The previously analysed gears have focus on space harmonics radial flux densities in the air gap which is adjacent to high speed rotor and adjacent to low speed rotor. The number of pole pairs in space harmonic flux density distribution is given by (4.94)[1][61].

$$p_{m,k} = \left| mp + kn_s \right| \tag{4.94}$$
$$m = 1,3,5,\ldots,\infty$$
$$k = 0,\pm 1,\pm 2,\pm 3,\ldots,\pm\infty$$

The analysis of the radial flux has shown that there is a certain relationship between pole numbers at high speed and low speed rotors and the number of iron segments which must fulfilled in order to have similar function principle as the described example in Figure 4.1. This certain pole relationship is characterized by the m=1 and k=-1 constants in (4.94). Pole constants are typed into (4.95) together with the number of PM pole pairs on the high speed rotor p = 4 and the number of iron segments n_s = 26 for an example shown in Figure 4.1, to clarify how the number of pole pairs in the space harmonic flux density distribution can be calculated.

$$p_{m,k} = \left| mp + kn_s \right| = \left| 1 \cdot 4 + (-1) \cdot 26 \right| = 22 \tag{4.95}$$

The calculation shows that 4 permanent magnet pole pair on high speed rotor will create a radial flux harmonic density content adjacent to the low speed rotor which corresponds to 22 pole pair. Radial flux distribution content is therefore transformed from 4 pole pair harmonics to 22 pole pair harmonics through 26 iron segments. Chosen pole pair at exactly 22 permanent magnets on low speed rotor will give synchronism between the previous described 22 pole pair harmonic flux density.

This is an explanation of how the 4 pole pair magnet gives harmonic flux density content at 22 poles in the air gap which is adjacent to low speed rotor. It is also possible to calculate the harmonic of a radial flux density which is coming from a 22 pole pair low speed rotor in an air gap adjacent to high speed rotor (4.96).

$$p_{m,k} = \left| mp + kn_s \right| = \left| 1 \cdot 22 + (-1) \cdot 26 \right| = 4 \tag{4.96}$$

The result of this calculation shows that 22 permanent magnet pole pairs on the low speed rotor will give a space harmonic flux density which is equal to 4 pole pairs in the air gap which is adjacent to high speed rotor.

A general equation (4.97) for choosing number of segments can be rewritten from (4.94) where pole relationship constants are set to m = 1 and k = -1 and pole pair space harmonic flux density distribution number $p_{m,k}$ is analysed for the number of pole pairs on low speed rotor and pole pair number p is set to number of pole pairs on high speed rotor.

$$p_l = \left|1 \cdot p_h + (-1) \cdot n_s\right| \Rightarrow \tag{4.97}$$

$$\begin{cases} n_s = p_h - p_l & for \quad p_h - n_s > 0 \\ n_s = p_h + p_l & for \quad p_h - n_s < 0 \end{cases}$$

The number of iron segments for all examples in [61] can be calculated by (4.97) because m = 1 and k = -1.

4.2.2 Variation of transmitted torque

Torque transmitted through a magnetic gear can have a torque ripple. This ripple depends on many parameters. Transmitted torque variation is previously analysed in [61] and there is shown that the pole number choice has influence on transmitted torque variation. This paper suggest a configuration with p_h = 4, p_l = 23 and n_s = 27 to minimise torque ripple. Such a configuration will have a lower torque variation than the p_h = 4, p_l = 22 and n_s = 26 configuration.

4.3 Improved design theory

4.3.1 Planetary magnetic gearing relationship

The planetary magnetic gear is two degree of freedom systems (DOF), where 2 inputs are needed to get one output. The 2 DOF gear is reduced to 1 DOF when one of the gear components are fixed. Figure 4.2 a), b) and c) illustrates 3 planetary gear types with one degree of freedom fixed. The 3 combinations of fixed degrees of freedom result in 3 different gearing. The example shown on Figure 4.2 have 22 pole pair on outer rotor, 4 pole pair on inner rotor and 26 iron segments. These pole combinations and fixed degree of freedom results in relative nominal angular velocities which are indicated on Figure 4.2.

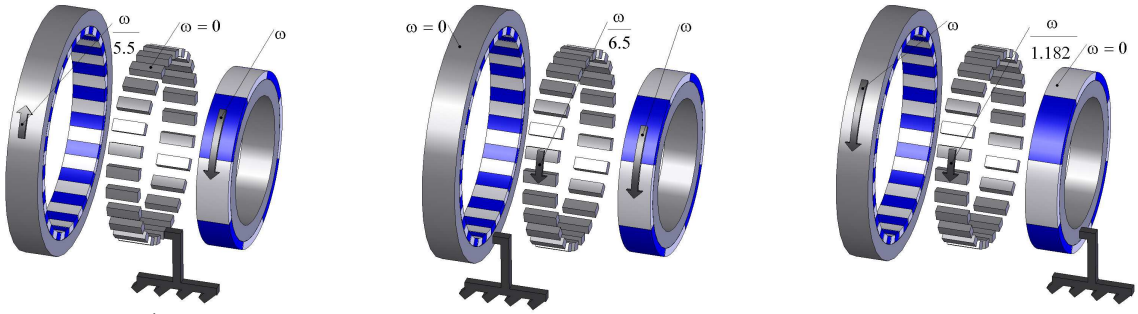

a) b) c)

Figure 4.2 Exploded view of the magnetic planetary gear in 3 different configurations: a) Iron segmented rotor fixed. b) Outer rotor fixed. c) Inner rotor fixed.

Iron segmented rotor fixed

Gearing relationship for the magnetic planetary gears is described in [61]. These equations are valid for the configuration with the iron segmented rotor fixed, which is shown on Figure 4.2 a).

$$G_{ra} = \frac{n_s - p}{p} \tag{4.98}$$

The example shown on Figure 4.2 a) have n_s = 26 iron segments and p = 4 pole pair on high speed rotor. This combination result in a gearing relationship of G_{ra} = 5.5. This gearing relationship equation expresses the absolute value of gearing relationship and does not take account for rotation direction shift. The nominal angular velocity can be calculated from (4.99). Where ω_l is angular velocity on low speed rotor and ω_h is angular velocity on high speed rotor. Angular velocity equation takes into account for rotational direction shift.

$$\omega_l = \frac{1}{-G_{ra}} \cdot \omega_h \tag{4.99}$$

The nominal torque relationship for this configuration can be calculated from a consideration of constant power, if the magnetic gear configuration is operating at a constant angular velocity and there is no loss. The total mechanical power of the system

must be equal to zero and nominal angular velocities are defined in (4.99) . When angular velocity of iron segmented rotor is zero will this result in (4.100).

$$P_l + P_i + P_h = 0 \tag{4.100}$$
$$T_l \cdot \omega_l + T_i \cdot \omega_i + T_h \cdot \omega_h = 0$$
$$T_l \cdot \frac{1}{-G_{ra}} \omega_h + 0 + T_h \cdot \omega_h = 0$$
$$T_l = G_{ra} \cdot T_h$$

Outer rotor fixed (low speed rotor)

Gearing relationship for a magnetic planetary gear with the outer rotor fixed is also described in [61].

$$G_{rb} = \frac{n_s}{p} = \frac{n_s}{p_h} \tag{4.101}$$

This gearing relationship from Figure 4.2 b) example result in a gearing at G_{rb} = 6.5. The nominal angular velocity relationship between inner rotor and iron segmented rotor can be formulated by (4.102).

$$\omega_i = \frac{1}{G_{rb}} \cdot \omega_h \tag{4.102}$$

Mechanical power consideration is again applied for calculating torque relationships in (4.103).

$$P_l + P_i + P_h = 0 \tag{4.103}$$
$$T_l \cdot \omega_l + T_i \cdot \omega_i + T_h \cdot \omega_h = 0$$
$$0 + T_i \cdot \frac{1}{G_{rb}} \omega_k + T_h \cdot \omega_h = 0$$
$$T_i = -G_{rb} \cdot T_h$$

Inner rotor fixed (high speed rotor fixed)

Gearing relationship for fixed inner rotor is not described in the paper [61]. This gearing relationship can be derived. Equation (4.100) and (4.103) are used to find the torque relationship between iron segmented rotor and low speed rotor in (4.104).

$$T_i = -G_{rb} \cdot T_h \tag{4.104}$$
$$T_i = \frac{-G_{rb}}{G_{ra}} \cdot T_l$$

There are used a constant power equation to calculate the angular velocity relationship between iron segmented rotor and low speed rotor in (4.105).

$$P_l + P_i + P_h = 0 \tag{4.105}$$

$$T_l \cdot \omega_l + T_i \cdot \omega_i + T_h \cdot \omega_h = 0$$

$$T_l \cdot \omega_l + \frac{-G_{rb}}{G_{ra}} \cdot T_l \cdot \omega_i + 0 = 0$$

$$\omega_i = \frac{G_{ra}}{G_{rb}} \cdot \omega_l$$

Gearing relationship G_{rc} for the configuration shown on Figure 4.2 c) can be calculated from either (4.104) or (4.105), which results in (4.106).

$$G_{rc} = \frac{\omega_l}{\omega_i} = \frac{G_{rb}}{G_{ra}} = \frac{\frac{n_s}{p_l}}{\frac{n_s - p_l}{p_l}} = \frac{n_s}{n_s - p_l} \tag{4.106}$$

Gearing relationship from Figure 4.2 c) example will result in a gearing at $G_{rc} = 26/(26-4) = 1.1818$.

A single torque vector diagram for the three gear configurations is drawn to illustrate action and reaction torque for magnetic gear components.

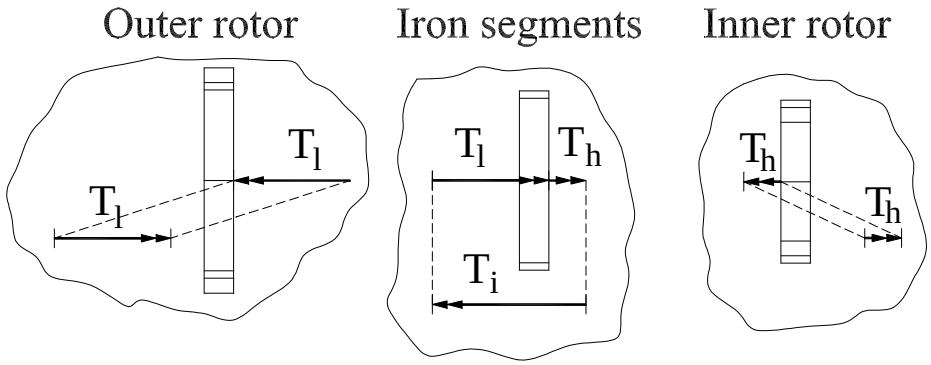

Figure 4.3 Torque vector diagrams of planetary magnetic gear.

Magnetic gear torque vectors for magnetic gear are consistent with the three torque relationship equations (4.100), (4.103) and (4.104) regarding torque directions.

The shown gearing relationship equations can be useful for magnetic planetary gears with pole relationship constants of k = -1 and m = 1. Gearing relationship in shown example [61] can be improved from a factor of 5.5 to 6.5 by the use of another configuration than the purposed. The torque density will therefore also be increased proportional to the gearing ratio.

4.4 2D FEM calculation

Previous analyses of planetary magnetic gear only cover simple influence from parametric dimension changes [61]. One of parametric change in [61] is iron segments radial thickness. Gear example with $p_h = 4$ pole pair on the low speed rotor and $p_l = 22$ pole pair on high speed rotor and 26 iron segments seems to be the best one of best performing planetary magnetic gears of its kind regarding torque per unit length. Optimal thickness for the current design in [61] is 5mm radial iron segment thickness. A model of a similar planetary magnetic gear is modelled in 2D FEM in order to have a point of reference for a parametric dimensional optimisation analysis. A sketch of planetary magnetic gear is shown on Figure 4.4 and dimensions and physical data are listed in Table 17. Notice that some of the dimensions are found from relative measurement from drawings in [61].

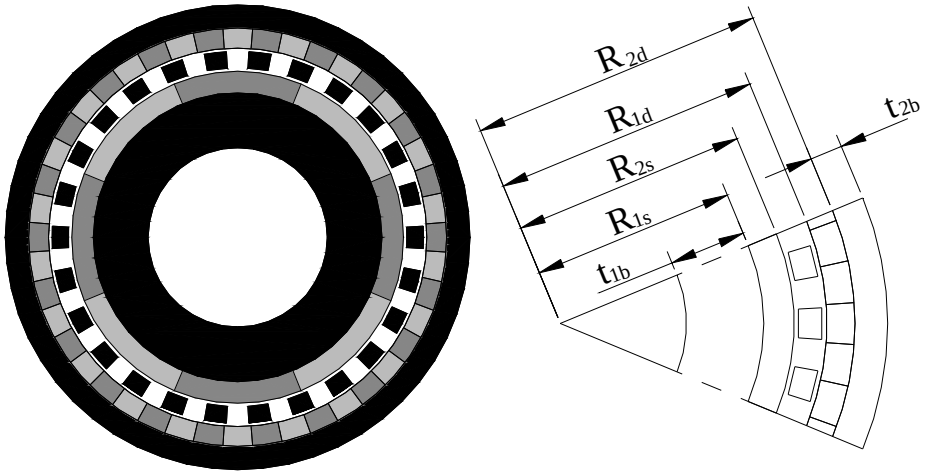

Figure 4.4 Sketch of a planetary magnetic gear similar to an example in [61].

Symbol	**Dimensions for models**		
	Description	***Size***	***Units***
t_{2b}	Thickness, outer back iron	7.0	[mm]
t_{1b}	Thickness, outer back iron	16.5	[mm]
R_{2s}	Outer radius, source magnets	50.0	[mm]
R_{1s}	Inner radius, source magnets	43.5	[mm]
R_{2d}	Outer radius, drive magnets	63.0	[mm]
R_{1d}	Inner radius, drive magnets	57.0	[mm]
g	Air gap	1.0	[mm]
L	Length/height of the magnets	50	[mm]
B_r	Remanence flux density	1.25	[T]
$H_c = M_s$	Coercivity	947350	[A/m]
$N_r = N_t$	Torque integration parameter	14	[-]
μ_0	Permability for air regions	$4 \cdot \pi \cdot 10^{-7}$	[Tm/A]

Symbol	Dimensions for models		
$\mu = B_r/H_c$	Absolut permability, magnets	$13.195 \cdot 10^{-7}$	[Tm/A]
$\mu_r = \mu/\mu_0$	Relative permability, magnets	1.05	[-]
N_p	Number of source magnets	8	[-]
N_{pole}	Number of drive magnets	44	[-]
N_{seg}	Number of iron segments	26	[-]
φ_{max}	Max. torque calculation angle	4.09	[Deg.]
	Silicon steel type (ANSI standard)	M-19	[-]

Table 17 Dimensions for similar model as [61].

A 2D nonlinear model of the planetary magnetic gear is modelled in the program FEMM. Maxwell stress tensor method is used to calculate the output torque from the outer rotor. The output torque is calculated to $T_{Maxwell}$ = 90.2 [Nm], which corresponds to a torque density of 117 [kNm/m^3] or a torque per unit length of 1804 [Nm/m]. A flux density visualization of the model is shown in Figure 4.5.

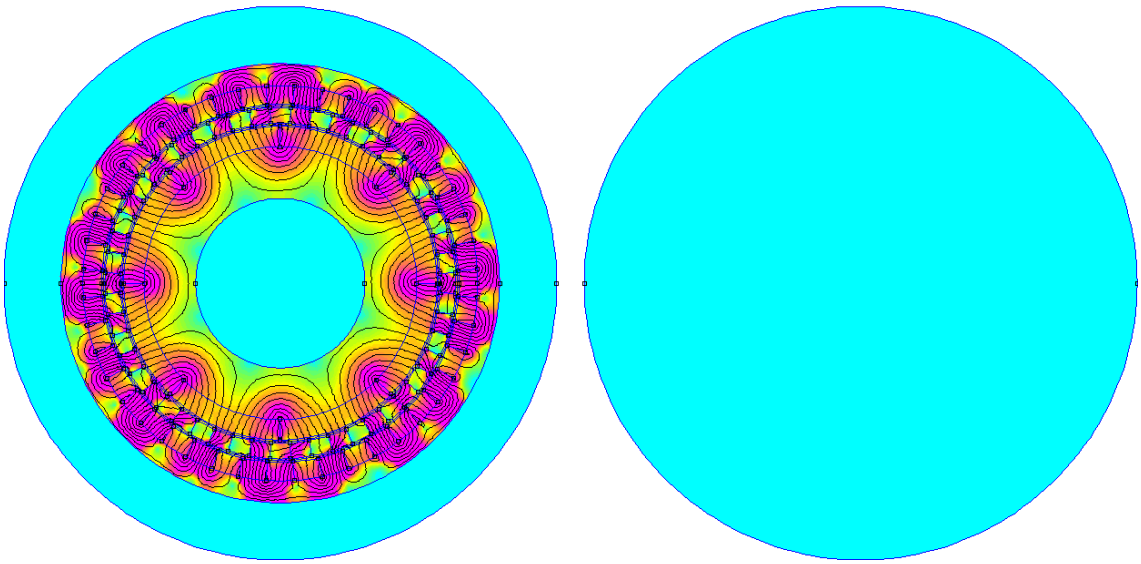

Figure 4.5 Flux density plot of the FEM model with torque calculated with Maxwell stress tensor.

The maximum obtainable torque stated in the [61] paper is about 1800 [Nm/m] for a 5 [mm] radial thickness of the iron segments. The results from this nonlinear analysis are therefore close to the results in [61].

4.5 Optimisation with FEM

An analysis of a planetary magnetic gear is made in order to be able to design an improved gear regarding torque density. So far, there is only made analysis where the radial thickness of the iron segments is changed and torque is calculated [61]. This analysis shows only one parametric change and since the planetary magnetic gear configuration can have several dimensions changes, there might be a better choice for the design. Dimensional design parameters are shown on Figure 4.6. Many design parameters can be changed, for example thickness of the magnets x_2 and x_4, thickness of the iron segments plus air gap x_3, thickness of the back iron x_1 and x_5. Optimisation with many variables is very time consuming that is why some design parameters is held constant for the optimisation namely the outer radius R_{out}, back iron thickness x_5 and the air gap thickness g.

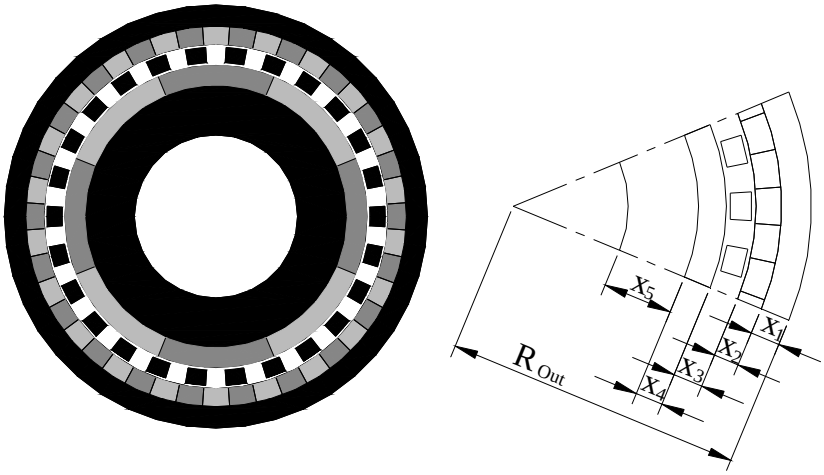

Figure 4.6 Sketch for a planetary magnetic gear with variable parameter dimensions.

The goal for the optimisation is to find dimensional relationship that result in a higher torque density than for initial dimensions. The problem is formulated as a general optimisation problem with object function (4.107), equality constrains (4.108) and inequality constrains (4.109). The optimisation algorithm is a large scale optimisation with approximation of hessian using finite differences.

$$f(x) = f(x_1, x_2 ..., x_n) \quad \Rightarrow \tag{4.107}$$

$$f(x_1, x_2, x_3, x_5) = \frac{T(x_1, x_2, x_3, x_4)}{L\pi(R_{Out}{}^2)}$$

$$h_j(x) = (x_1, x_2, ...x_n) = 0 \quad \Rightarrow \tag{4.108}$$

$$h_1(x_2, x_4) = x_2 + x_4 - 0.0125 = 0$$

$$g_i(x) = (x_1, x_2, ...x_n) = 0 \quad \Rightarrow \tag{4.109}$$

$$g_1(x_1) = -12 \cdot 10^{-3} + x_1 \le 0$$

$$g_2(x_1) = 1.5 \cdot 10^{-3} - x_1 \le 0$$

$$g_3(x_2) = -12 \cdot 10^{-3} + x_2 \le 0$$

$$g_4(x_2) = 1.5 \cdot 10^{-3} - x_2 \le 0$$

$$g_5(x_3) = -12 \cdot 10^{-3} + x_3 \le 0$$

$$g_6(x_3) = 3 \cdot 10^{-3} - x_3 \le 0$$

$$g_7(x_4) = -12 \cdot 10^{-3} + x_4 \le 0$$

$$g_8(x_4) = 1.5 \cdot 10^{-3} - x_4 \le 0$$

The object function is set to magnetic gear torque density, which is calculated for an angle position relative to the other two rotors, where the transferred torque to low speed rotor is at its maximum. An equality constraint is setup for keeping total magnet thickness constant. This limitation is set in order to find best possible thickness sharing of permanent magnet material on low and high speed rotors. Inequality functions are set to limit the optimisation solution space. Optimisation resulted in a torque density of 151 [kNm/m^3] and following dimensional thickness values:

$x_1 = 2.2 \cdot 10^{-3}$[m], $x_2 = 4.1 \cdot 10^{-3}$[m], $x_3 = 7.3 \cdot 10^{-3}$[m], $x_4 = 8.4 \cdot 10^{-3}$[m]

Torque increase is 29 % with a magnetic material increase of 7%. The amount of magnetic material has increased for the optimised solution because radii of the magnetic material are increased and the total magnet thickness is kept constant.

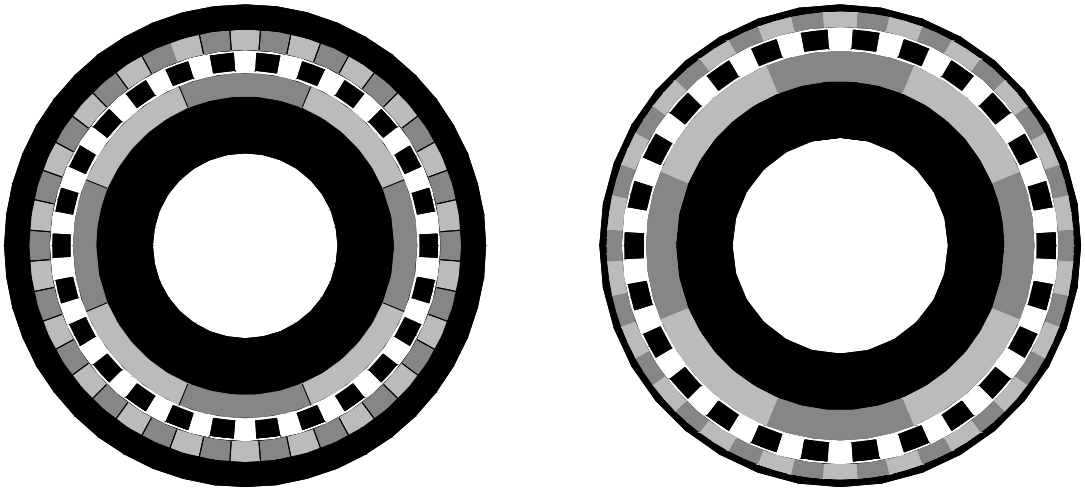

a) b)

Figure 4.7 a) Illustration of original gear b) Illustration of the optimised gear.

The result of this optimisation will be an optimal design for obtaining highest possible torque density within optimisation limitations. However this optimal design can be a local optimal design and not global optimum design. That is why the result must be considered as torque density improvement and not necessarily as absolute best obtainable torque performance. It is also possible to change the limitations of the optimisation in order to get better performance. Air gap thickness is one of the limitations that have a major influence on the torque density result and the total thickness of the permanent magnets has also influence. These limitations are primary chosen to be in the same size order as the initial design. The optimisation shows that more permanent magnet material thickness must be distributed on low speed rotor than high speed rotor. The thickness of the iron segments must be bigger than the low speed rotor magnets and smaller than the high speed magnets. Back iron thickness on the low speed rotor must be smaller than the low speed rotor magnets when high speed rotor back iron thickness is held constant.

Similar observed fact regarding magnet relationship thickness is also found in [70] where high speed rotor magnet thickness is thicker than low speed rotor magnets. Relationships for back iron yoke thickness is also analysed in [70] and it is found that high speed rotor yoke thickness does not have major influence on the torque performance. This discovery is not covered in the optimisation analysis since high speed rotor yoke thickness is held constant for the optimisation.

It is found that it is possible to improve theoretical torque density performance by changing dimensional design parameters. However other design parameters are also found important for the design and that is iron segmentation duty cycle which is described in the following section.

4.6 Parametrical change of segmentation duty cycle

The distribution between iron and air in the iron segmented rotor is also a variable parameter that can be changed. The relationship between iron and air can be described with a duty cycle factor d_c.

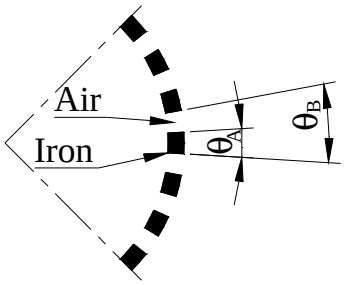

Figure 4.8 Sketch drawing of iron segmented rotor where angles for duty cycle factor are specified.

This duty cycle factor has also an influence on the torque transmission ability for the magnetic gear. The example modelled in the FEM analysis has initially a duty cycle of 0.5, i.e. 50% steel and 50% air. The duty cycle factor d_c can be calculated by (4.110).

$$d_c = \frac{\theta_A}{\theta_B} \tag{4.110}$$

This relationship is not optimal for the given example. The best duty cycle for the given example is around 0.54 duty cycle i.e. 54% iron and 46% air. The optimal duty cycle factor for the given example is plotted in Figure 4.9.

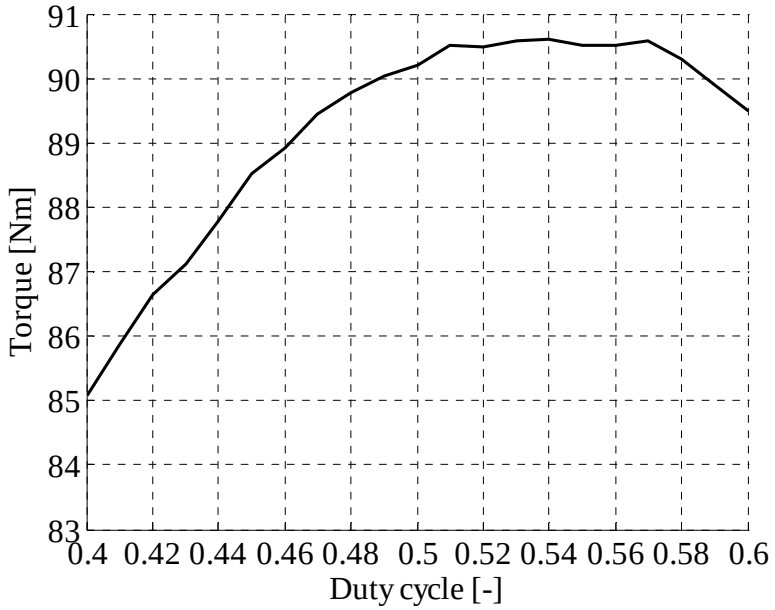

Figure 4.9 Torque versus duty cycle factor.

The best duty cycle factor for this configuration is investigated in an interval from 0.4 to 0.6 with steeps of 0.01. An iron segmentation duty cycle factor of 0.54 performs best. The best duty cycle factor is dependent of dimensions parameters and pole number configuration.

4.7 Summary

Analysis has shown that it is possible to increase the torque density of the planetary gear type even further than previous studies have show by changing configuration dimension. It is especially magnetic material distribution that has influence on the output torque. The best configuration is where most permanent material is placed on the high speed rotor. Back iron thickness on low speed rotor and iron segments must also have a specific size in order to obtain optimal torque density. An optimisation is performed to find the best material thickness distribution. The optimisation is limited regarding air gap thickness, outer dimensions, inner yoke for high speed magnets and total permanent magnet thickness. These limitations are set to values that are considered to be physical possible to implement in a prototype. The air gap thickness can be made smaller in order to get higher output torque, however this air gap must have a certain thickness to be sure that a prototype is possible to manufacture. Higher torque density can be expected with a narrow air gap. It is also possible to obtain higher torque density with larger outer diameter however this relationship is not covered in this analysis.

Iron segmentation duty cycle factor is also a changeable parameter. An initial investigation of a simple example has shown that torque is dependent on this parameter also and there is an optimal duty cycle factor for this specific example. This parameter is therefore also worth changing when designing planetary magnetic gears. Also the physical layout of the segment could be investigated and have segments like teeth in a machine. However this is left for further research.

Chapter 5 Conclusion

Patents about magnetic gears can be dated back to 1916 [37] where electro magnets were used, because permanent magnets at that time were very weak. Permanent magnets have become stronger since that time and that is one of the main reasons why magnetic gear research has become in focus. Many magnetic gear types are described in patents and only few papers are written about magnetic gears. Facts about torque performance for different gear technologies are not stated in patents as they are in scientific papers, which make it difficult to estimate the performance between each technology. This thesis focuses on 3 technologies which are expected to be most common for future machinery.

5.1 Thesis summary

The thesis starts with an introduction to mechanical power conversion, which is the fundamental reason to use a gear in a machine. A simple magnetic gear is described and performance characteristic are defined for the magnetic gear. State of the art analysis summaries are also briefly described.

The state of the art analyses are considered to be essential to be able to contribute with new research. Torque density characteristic for the magnetic gear technology is weak compared to the traditional mechanical gear technology. This torque density characteristic is considered to be and important parameter to improve in order to compete with the traditional mechanical gear technology. Scientific papers from the state of the art analysis has shown that theoretical calculation models and physical test modes is an accepted way to improve the magnetic gear technology. Following statements are therefore fundamental for magnetic gear research.

Problem statement

1. Determine state of the art for magnetic gear technologies, and also technologies from traditional mechanical gears.
2. Develop analytical and numerical calculation models of permanent magnetic gears. The purpose of the calculation models is to be able to estimate torque in an early stage for magnetic gear design process.
3. Develop two experimental magnetic gear models. The purpose with the test models is to compare the theoretical results with experimental test models and to gain practical experience.

Solutions to problem statements are summarised in the following sections.

5.1.1 Performance from existing mechanical gears

State of the art analysis of existing mechanical gears is introduced to review mechanical gear types and find a rough estimate for expected performance level in terms of total torque density and efficiency. The expected total torque density performance level is dependent on gear type, gearing and input speed. Investigated harmonic drive gears can reach a total torque density up to 300 [Nm/l], however these gears have a low efficiency sometimes down to 50%. Mechanical planetary gears can have a high total torque density up to 265 [Nm/l] and a high efficiency up to 98% at 500[RPM] and a gearing relationship at 5. Another planetary gear is rated down to 37 [Nm/l], which indicates that the torque density variation is high among the mechanical gears. A cautious rule of thumb for torque densities in mechanical gears will be 15 [Nm/l] to 190 [Nm/l] for planetary and cycloidal gear types in the gearing interval of 20 to 90. Spur gears can be expected to reach torque densities up to 83 [Nm/l]. The large variation in torque density for the mechanical gears makes it difficult to compare with magnetic gear types. Comparison between magnetic torque density and mechanical torque density can therefore best be performed for a specific case where several mechanical gear alternatives are compared with a specific magnetic gear.

5.1.2 Existing analysed magnetic gears and gears from patents

A search for the magnetic gears in various publications resulted in many different magnetic gear technologies. Most relevant search results from the literature are from scientific paper, because it is possible to quantify torque performance. One of the most promising technologies is the magnetic version of a planetary gear [1]. FEM models are used in [1] to analyse this type of gear technology. This technology has a high torque density. This is the reason why focus is directed toward this technology in chapter 4 and in section 5.1.5 Magnetic planetary gear. A variant of the planetary gear type is found in [75]. This type is modelled with FEA. The radial magnetised gear is another known magnetic gear technology. This type of gear is analysed analytically in [18], [19]. Another analytical model of a magnetic spur gear is modelled with some mathematical assumptions in [24]. Finite element analysis is used to model a radial magnetised spur gear in [21] and [22]. Axially magnetised versions of spur gears are analysed using a semi-analytical calculation and numerical methods in [26] and [28] respectively. A perpendicular axis gear is also modelled with FEM methods in [33]. A magnetic version of a harmonic gear is proposed in [72] and torque density is predicted to 110 [kNm/m^3]. A torque calculation method is not described in detail for this scientific paper. Practical implementation of the proposed gear type has similarities to the magnetic cycloidal gear described in chapter 3 and 5.1.4 Magnetic cycloidal gear. Other gear technologies are found in patents. Not all of these technologies are modelled in theory and it is therefore not possible to quantify torque performance.

5.1.3 Magnetic spur gear

Radial magnetised spur gear is analysed in [18] and [19]. Appropriate analytical calculation methods are not found in the literature for parallel magnetised gears even so parallel magnetised magnets are cheaper to manufacture than radial magnetised magnets. A parallel magnetisation model is developed for a parallel magnetised gear on

the basis of radial magnetisation theory. This includes new magnetisation functions and solutions. Other equivalent current models for permanent magnets and torque integration procedures are also introduced. The parallel magnetisation model and the radial magnetisation model are programmed in to a parameterised software program, where dimensions and physical properties can be defined by the user. User of this program can estimate torque performance before prototype design. A part of the program is able to start a FEM calculation routine where the analytical model and a FEM model are compared. Experience from this thesis has shown that torque calculation procedures are the key to design magnetic gears with better performance. However calculation must be verified with experimental test models and this is done for a magnetic spur gear with parallel magnetisation which is designed with a gearing relationship of 1:4. The experimental test model is measured to a maximum torque of 12.0 [Nm], while theoretical analytical 2D results showed 16.6 [Nm]. The theoretical analytical calculate result corresponds to an active torque density of 24.4 [kNm/m^3], while measured torque density performance from the same gear only is 17.6 [kNm/m^3]. There are found matching mechanical spur gars with gearing relationship of approximately 1:5 with a total torque density of 16 to 24 [kNm/m^3]. It can therefore be concluded that the magnetic spur gear has a poor active torque density compared to the existing traditional mechanical gear technology. Active torque density of the magnetic spur gear is almost comparable with the total torque density of a corresponding mechanical gear. The designer of magnetic spur gears must therefore be aware that it is important to optimise torque density and total torque density.

5.1.4 Magnetic cycloidal gear

The magnetic cycloidal gear is a new magnetic gear technology and this gear type is not found among scientific papers although this gearing principle seems to be promising in terms of torque density performance. This gear technology has a clear and obvious benefit in making use of better magnetic interaction between rotor elements compared to the magnetic spur gear principle. Magnetic rotors are also placed inside each other, which will give a better space utilisation. It is also possible to configure the magnetic cycloidal gear in different configurations. Gearing relationship equations and torque equations is defined for the different configurations. The analytical parallel magnetisation expressions from the spur gear are used to calculate torque of a cycloidal magnetic gear. A magnetic cycloidal gear test model is designed and tested. This cycloidal gear is semi optimised to a analytical calculated torque density of 142.0 [kNm/m^3]. A FEM model is also used to verify this calculation which resulted in 146.8 [kNm/m^3]. Maximum test gear torque is 33 [Nm], which result in an active torque density of 33 / (π x 0.0615^2 x 0.026) = 106.8 [kNm/m^3]. The relationship between analytical calculated torque density and active torque density is 106.8 /142.0 = 0.75. The measured total torque density for this gear will be 33 / (0.13 x 0.13 x 0.086) = 22.7 [kNm/m^3]. Corresponding mechanical gears with the same gearing relationship are found with a total torque density of 15 to 173 [kNm/m^3]. It is concluded that the designed test model have difficulties to reach the same level of performance as the traditional mechanical gears. Optimisation procedure is used to optimise torque density performance of the magnetic cycloidal gear. Improved torque density results at 173.9 [kNm/m^3] can be obtained with another pole number configuration and the same dimensional constrains, which will change gearing relationship to 1:36. The optimisation shows that there are an optimal number of magnetic poles for given

dimensions. Another optimisation procedure is set up with other dimension limits and with a 42 – 44 pole configuration. Optimisation resulted in a torque density of 158 [kNm/m^3]. This optimisation showed that dimensions of the given pole configuration is possible to scale down in order to reach better torque density performance. More magnetic material can also increase the torque density performance. This is discovered by increasing the area limitation in another optimisation procedure, where the best result is 183 [kNm/m^3] with larger volume and specific torque. Better torque density is expected if area limitation is increased more. A high reached torque density level makes this gear technology perform well compared to other magnetic gear technologies. However it is important to utilise the high obtainable torque density level together with a gear design where a great part of gear length utilises this high torque density unlike the cycloidal gear test model where the only 26 [mm] out of 86 [mm] total length is utilised. Available predicted active torque density intensity is for now 183 [kNm/m^3] for the cycloidal gear. It is impossible to predict an active torque density without building a test model with the decided design dimensions. A prediction for the active torque density will however be around 0.75x183 = 137 [kNm/m^3]. A total measured torque density for such a gear will most likely be around 137x22.7 / (106.8) = 29 [kNm/m^3] or higher depending on how well the design is utilised. The magnetic cycloidal gear efficiency is measured to 94% at 50 [RPM] and 92% at 1500 [RPM] on the input shaft. Efficiency of the test model is a little lower than efficiency from example gears found for corresponding mechanical gear types where the efficiency is 95 %. Test model is designed with 18 bearings which can have created extra friction compared to the mechanical gear. Mechanical cycloidal gear and the magnetic cycloidal gear include a torque transferring device where torque is transferred through parts with oscillating motion. It is assumed that the torque transferring device is responsible for a major part of the friction in the magnetic cycloidal gear, since this device consist of many rotating mechanical parts.

5.1.5 Magnetic planetary gear

The planetary magnetic gear technology is previously described in scientific papers [1][61]. Performance of this gear type is promising because a torque density up to 100 [kNm/m^3] is predicted. 78 [kNm/m^3] is measured which makes this gear the most torque dense stand alone planetary magnetic gear. The two scientific papers describe principles of operation with a focus on space harmonics in air gap, variation of torque and torque performance. Less attention is focused on possible configuration types. However an explanation of another improved configuration is shown in this thesis and this example shows an increased gearing relationship from 5.5 to 6.5. The torque performance will also be improved by a configuration change and that is why the configuration type is an important issue. A computer optimisation method to search for optimal solutions regarding torque density is not used in scientific papers about planetary magnetic gears. This approach is used where the torque density is calculated from a 2D FEM model. Initial dimensions for the 2D model are similar to the design used in [1] and [61]. Results from the optimisation shows a 29% torque density increase with only 7% more permanent magnet material used. A part of the gear design includes iron segments. These segments are placed in a circular pattern and with a certain air gap between them. The relationship between air thickness and segment thickness can be changed in order to reach better torque performance. This discovery is found by changing the relationship between air gaps and iron segments for a magnetic gear modelled with FEM. The example shows that the best relationship between air gap and iron segments is dependent of dimension parameters and pole configuration. The discovery is important to consider for obtaining an optimal magnetic gear design. Integrated motor with planetary gear drive is becoming more common among scientific papers since 2007. Torque density performance from this drive type is predicted to attain 130 [kNm/m^3] in a scientific paper [70]. This performance is high compared to prediction of 100 [kNm/m^3] for previous described stand alone planetary magnetic gears. Inside cylindrical space located in the planetary magnetic gear centre part is not utilized in the stand alone magnetic gear. However this is utilized in [70] which make the planetary magnetic gear especially suitable for motor incorporation in centre part.

5.1.6 Conclusion

It is the author's opinion that results from this thesis cover the problem statement. Relevant references for determining state of the art technology foundation within magnetic gears and mechanical gears are analysed. This thesis will improve the existing technology by improved analysis methods for analytical calculated magnetic field solutions combined with numerical integration in order to quantify and semi optimise magnetic gear torque transferring capabilities. The proposed analytical methods are programmed in a software program which is verified with traditional FEM methods. Prototype of a traditional magnetic spur gear is designed and later analysed with the proposed calculation methods. A new developed cycloidal magnetic gear prototype is also designed and later analysed with modified purposed analysis method. Analysis results from the new cycloidal magnetic gear technology are better than the existing magnetic gear technologies. A conventional magnetic planetary gear is also analysed with FEM methods and torque density is improved by use of optimisation tools.

Torque density lack can in some cases be the limitation for that the magnetic gear can not replace a traditional mechanical gear. This is believed to be the main disadvantage for magnetic gears in general. Boundary for obtained torque density is moved with the results of this thesis and this will increase possibility of using magnetic gears. Most important advantage of using magnetic gear technology is that it is considered to have mechanical wear free property for internal mechanical parts. Magnetic gears are therefore expected to be incorporated in machinery where this advantage is weighted high.

Magnetic gear	Analytical (Active)	2D FEM (Active)	3D FEM (Active)	Measured (Active)	Measured (Total)	Unit
Spur gear Test model	16.6	16.7	13	12	-	[Nm]
	24.4	24.5	19.1	17.6	-	[kNm/m^3]
Spur gear Optimised	11.6					[Nm]
	34.6					[kNm/m^3]
Cycloidal gear Test model	43.9	45.4		33	33	[Nm]
	142.0	146.8		106.7	22.7	[kNm/m^3]
Cycloidal gear Optimised						[Nm]
		183.0				[kNm/m^3]
Planetary gear Optimised						[Nm]
		151				[kNm/m^3]

Table 18 Torque and torque density for analysed gears.

5.1.7 Future work

Working with magnetic gears will generate ideas for future possible research work to be done within the subject of magnetic gears. Future expected research are described in the following.

- Dynamic models
- Losses and loss distribution
- Promising gear types
- Better magnetisation pattern
- Linear magnetic gears
- Devices with medium separation or other unique advantages
- Technology reliability tests

Dynamic models of a magnetic planetary gear are analysed in [66]. More research is expected in this field in order to ensure that magnetic gears performs according to expected specifications. Dynamic model simulation or dynamic test is necessary if the gear is supposed to run with variation loads and if gear slip effect is not accepted. Such dynamic models are useful to determine a suitable torque reduction factor k_{red} which will be used in equation (1.3) to reduce T_{max} to the nominal torque.

Losses and loss distributions has not been covered by this thesis. This is also an important theme to investigate in order to predict magnetic gear efficiency which is a competitive factor. Loss distribution theory from existing electromagnetic systems is expected be useful for calculating magnetic losses. Bearing losses will also have influence on the magnetic gear efficiency and these losses can be estimated from general bearing loss theory. Efficiency measurements are helpful for verification of loss models. However this will often require high accuracy measurement equipment because magnetic gears have a high efficiency in general. Calorimeters can be used if more accurate loss measurement must be performed.

The magnetic cycloidal gear and the planetary magnetic gear are the most promising gear types at current time. Magnetic cycolidal gear is one of most promising gear types in regards to torque density. Advantage for this gear type is to obtain high gearing relationship in a single gearing stage. One of the disadvantages for this gear type is the high number of mechanical parts in the present design. New simplified designs types with less mechanical parts is expected within magnetic cycloidal gear technology. Planetary magnetic gear is especially suitable for motor integration [70]. More research is expected within these integrated drive types because a high total torque density is reachable.

Improved magnetisation patterns are also expected for the future magnetic gears. Magnetisation pattern like halbach array is one of the known magnetisation patterns which have a focusing effect. Strong flux fields can be obtained by using this pattern.

A linear magnetic gear is patented in [38] and other references can be found. However this linear gear type is only mentioned briefly in this thesis. Linear magnetic gear types are also expected to go through a evolution like the magnetic gear because magnets is

becoming stronger and better simulation tools are also becoming better for analysis studies.

Application devices such as integrated magnetic coupling with water pump are state of the art within pump applications. The unique about this device type is that magnets have the ability to separate mediums from each other. It is expected that other mechanical devices will be integrated with magnetic gears where medium separation ability is utilised or other unique advantages like torque limitation is utilised.

Optimisation methods are expected to be used in general for optimising magnetic devices in the future. An example is the analytical solution of magnetic fields in a planetary magnetic gear proposed in [71]. These solutions will be useful for future gear optimisation.

Magnetic gear technology is still considered to be a relatively new technology and not proven technology. That is probably the reason why companies hesitate with implement magnetic gear technology in their products. More field tests with permanent magnet gear equipment are expected in the future to prove the reliability of this new emerging technology.

Nomenclature list:

Symbol	Description	Unit
$\hat{\boldsymbol{\varphi}}$	Angular tangential vector	[-]
$\hat{\mathbf{r}}$	Radial normal vector	[-]
η	Efficiency of the magnetic gear	[-]
μ	Absolute permeability	[Tm/A]
μ_0	Permeability for free space	[Tm/A]
μ_r	Relative permeability	[-]
φ	Angle used in source and drive coordinate systems	[Rad]
η	Integration variable used to integrate a radius	[m]
η	Efficiency	[-]
$\gamma^{(k)}$	Surface charge density	[T]
$\nabla\varphi_m{}^{(in)}$	Gradient of the magnet scalar potential	[A/m]
$\nabla\varphi_m{}^{(k)}$	Gradient of the in and outside air scalar potential	[A/m]
$\theta(q)$	Discrete angular integration variable	[Rad]
θ_A	Angle for iron segment	[Rad]
θ_B	Angle from one segment to the next segment	[Rad]
α'	Angular constant $\alpha' = \pi/2$ for the magnetisation	[Rad]
φ_1	Start angle for the surface integration	[Rad]
φ_2	End angle for the surface integration	[Rad]
ω_A	Angular velocity of part A	[Rad/s]
ω_B	Angular velocity of part B	[Rad/s]
ω_C	Angular velocity of part C	[Rad/s]
ω_h	Angular velocity of high speed rotor	[Rad/s]
ω_i	Angular velocity of iron segments	[Rad/s]
ω_l	Angular velocity of low speed rotor	[Rad/s]
φ_{edge}	Integration angle for the radial integration	[Rad]
ρ_m	Equivalent volume charge density	[T]
$\varphi_m{}^{(in)}$	Scalar potential of the magnet	[A/m]
$\varphi_m{}^{(in)}$	Scalar potential of the inside and outside air region	[A/m]

ρ_A	Active torque density	[Nm/l]
ρ_T	Torque density of the total used gear volume	[Nm/l]
ρ_T	Torque density of total gear box	[Nm/l]
$A_i^{(k)}$	Sinus Fourier coefficient for the volume charge dens.	[-]
$\mathbf{B}^{(in)}$	Flux density field vector for the magnet material	[T]
$\mathbf{B}^{(k)}$	Flux density field vector for in and outside air	[T]
$B_i^{(k)}$	Cosine Fourier coefficient for the surface charge dens.	[-]
B_r	Remanence flux density	[T]
C_i	Sinus Fourier coefficient for the volume charge dens.	[-]
d_c	Duty cycle factor for segment distribution	[-]
D	Distance between centre of the magnetic wheels	[m]
D_i	Cosine Fourier coefficient for the surface charge dens.	[-]
f()	Optimisation object function	[*]
g	Air gap thickness	[m]
$g_i()$	General inequality constrain optimisation function	[*]
G_{ra}	Gearing relationship – configuration a)	[-]
G_{rb}	Gearing relationship – configuration b)	[-]
G_{rc}	Gearing relationship – configuration c)	[-]
$\mathbf{H}^{(in)}$	Magnetic field vector for the magnet material	[A/m]
$\mathbf{H}^{(k)}$	Magnetic field vector for in and outside air	[A/m]
$h_j()$	General equality constrain optimisation function	[*]
H_T	Total height of gear box	[m]
I	Counter for Fourier coefficients	[-]
$\mathbf{j_m}$	Surface current density	[A/m]
k	Constant used in [1],[61]	[-]
k_t	Temperature coefficient	[-]
k_t	Torsion spring coefficient	[Nm/Deg.]
k_{red}	Torque reduction factor	[-]
L	Length/ depth of the active magnet	[m]
L_T	Total length of gear box	[m]
m	Constant used in [1],[61]	[-]
m_{PM}	Mass of the permanent magnet material	[kg]
M_φ	Tangential component of the magnetisation vector field	[A/m]

$M_{\varphi i}$	Tangential Fourier coefficients for the magnetisation	[-]
M_d	Magnetisation of drive magnet	[Am]
M_r	Radial component of the magnetisation vector field	[A/m]
M_{ri}	Radial Fourier coefficients for the magnetisation	[-]
$\mathbf{M_s}$	Magnetisation vector field	[A/m]
M_s	Magnetisation of source magnet	[A/m]
n_1	Speed of the input shaft	[RPM]
n_s	Number of segments	[-]
N_p	Number of poles, for drive and source magnet	[-]
N_{pole2}	Number of poles on second gear wheel	[-]
N_{pole2}	Number of poles on first gear wheel	[-]
N_{poleD}	Number of poles for the drive magnet	[-]
N_{poleS}	Number of poles for the source magnet	[-]
$N_r = N_t$	Integration parameter for the number of integrations	[-]
p	Pole pairs	[-]
p_h	Pole pairs for high speed rotor	[-]
p_l	Pole pairs for low speed rotor	[-]
P	Counter for pole number in the torque integration	[-]
P_A	Number of magnetic poles of part A	[-]
P_C	Number of magnetic poles of part C	[-]
P_i	Solutions constant for the cosine terms of the matrix	[-]
P_{in}	Input power of the magnetic gear	[W]
P_{in}	Power input	[W]
$P_{m,k}$	Number of pole pairs in space harmonic flux	[-]
P_{Out}	Output power of the magnetic gear	[W]
P_{out}	Power output	[W]
Q_i	Solutions constant for the cosine terms of the matrix	[-]
R	Radius variable for both coordinate systems	[m]
R(q)	Discrete radius integration variable	[m]
R´	Radius in the source magnet coordinate system	[m]
R_1	Inner radius of the magnet	[m]
R_{1d}	Inner radius of the drive magnet	[m]
R_{1s}	Inner radius of the source magnet	[m]

R_2	Outer radius of the magnet	[m]
R_{2d}	Outer radius of the drive magnet	[m]
R_{2s}	Outer radius of the source magnet	[m]
R_g	Gearing relationship	[-]
$R_{ga)}$	Nominal gearing relationship of configuration a)	[-]
$R_{gb)}$	Nominal gearing relationship of configuration b)	[-]
$R_{gc)}$	Nominal gearing relationship of configuration c)	[-]
R_k	Boundary radius for magnetic material	[m]
R_{Out}	Outer radius for planetary gear	[m]
$S_r(q)$	Simpson's integration number	[-]
T	Calculated torque from the integrations	[Nm]
T :	Permanent magnet temperature	[° C]
T()	Torque function for parallel magnetisation	[Nm]
T_{2N}	Maximum torque rated at input shaft speed	[Nm]
T_{2NX}	Maximum torque rated at another input shaft speed	[Nm]
T_A	Nominal torque on part A	[Nm]
T_B	Nominal torque on part B	[Nm]
T_C	Nominal torque on part C	[Nm]
T_{coeff} :	Temperature coefficient	[%T/K]
$T_{cyc.}$	Nominal torque from a cycloidal gear	[Nm]
T_{Dens}	Torque density	[Nm/l]
$T_{int.}$	Nominal torque from a internal spur gear	[Nm]
T_{Mass}	Calculated stall torque per permanent magnet mass	[Nm/kg]
T_{max}	Maximal torque of the magnetic gear	[Nm]
T_{max}	Maximal torque performance	[Nm]
T_{Nom}	Nominal torque performance	[Nm]
T_r	Torque contribution from the radial integrations	[Nm]
T_{Stall}	Torque at stall position	[Nm]
T_{t1}	Torque contribution from the inner tangential integral.	[Nm]
T_{t2}	Torque contribution from the outer tangential integral.	[Nm]
$U_i^{(in)}$	Fourier coefficients for the magnet (cosines terms)	[-]
$U_i^{(k)}$	Fourier coefficients for the air region (cosines terms)	[-]
V	Volume of the two gear wheels	[m^3]

V_A	Volume of the active magnetic material	[m^3]
V_A	Volume of active magnet material	[m^3]
$V_i^{(in)}$	Fourier coefficients for the magnet (sinus terms)	[-]
$V_i^{(k)}$	Fourier coefficients for the air (sinus terms)	[-]
V_T	Outside volume of the magnetic gear	[m^3]
V_T	Total gear box volume	[m^3]
W_T	Total wide of gear box	[m]
x_1	Outer yoke thickness	[m]
x_2	Low speed magnet thickness	[m]
x_3	Segment thickness including air gaps	[m]
x_4	High speed magnet thickness	[m]
x_5	Inner yoke thickness	[m]
[*] represent different unity values. [-] represent a numerical number.		

Table 19 Nomenclature list.

5.1.8 References

The references list is sorted in chronological order.

1. **Atallah, K. and Howe, D.** *A novel high-performance magnetic gear.* Issue.4 Part.1, 2001, IEEE Transactions on Magnetics, Vol. 37, pp. 2844-2846.

2. Bonfiglioli riduttori C. *Brd. Klee A/S - Brd. Klee.* [Online] [Cited: 12 06, 2005.] (Varekatalog; Transmissionselementer; Gear; Tandhjulsgear;Hovedkatalog C-gear(5052 kb)). http://www.bdr-klee.dk.

3. **Matek, Wilhelm; Muhs, Dieter; Wittel, Herbert; Becker, Manfred.** *Roloff/Matek Maschinenelemente.* Braunschweig/Weisbaden : Friedr. Vieweg & Sohn Verlagsgesellschaft mbH, 1994.

4. Sew eurodrive. *SEW-EURODRIVE.* [Online] 2004. [Cited: 12 06, 2005.] (Dokumentation; Getriebe; Servo-Getriebemotoren (R-,F-, K- und S-Getriebe) part 1-17; Teil 12; 6.989 kB). http://www.sew-eurodrive.de/deutsch/pdf/11248718_G12.pdf.

5. Helical Speed Reducers. *RD : Helical gearboxe series RD.* [Online] [Cited: 12 06, 2005.] (Products; Helical speed reducers; Series RD; Catalogue RD – it gb de; CMRD_Ed01_2005_it_gb_de.zip). http://www.varvel.com/html/page_2_frd.html.

6. **Norton, Robert L.** *Design of machinery.* Singapore : WCB/McGrw-Hill, 1999.

7. **Bühler.** Data sheet PLS 90 HP standard flange. [Online] 04 26, 2002. [Cited: 12 26, 2005.] (Products; PLS; Downloads; PLS HP; PLS 90 HP). http://www.neugartusa.com/Massblatt_PLS_HP_90_e.pdf.

8. SP+ Die Neue Generation. *WITTENSTEIN alpha.* [Online] [Cited: 12 07, 2005.] (Produkte; SP+;PDF Download). http://www.alphagetriebe.de/pdf/sp_plus_catalogus0805.pdf.

9. ServoFit Precision Planetary Gearhead. [Online] 2003. [Cited: 12 07, 2005.] (ServoFit Planetary Gearheads-SPG; Brochures & Catalogs; SPG-ServoFitPrecision Planetary Gearhead). http://www.stober.com/pdf/SPG.pdf.

10. Precision Series. [Online] 2002. (Fine Cyclo®; Catalogue). http://www.sumitomodriveeurope.com/_text/meta/files/products_66_Catalogue.pdf.

11. Cyclo drive. [Online] [Cited: 12 07, 2005.] http://home.paran.com/otislg/data/cyclo6000_e.pdf.

12. Shimpo Gyromax. [Online] [Cited: 12 07, 2005.] (Download Center; Products; GYROMAX® Speed Reducer; Download GYROMAX® Catalog; Entire Catalog (48 pages)). http://www.shimpodrives.com/pdf/gyromaxcatalog2002.pdf.

13. Products Gearheads. [Online] 2003. [Cited: 12 08, 2005.] (Products; Gearheads; RGH Robotic Gearhead). http://www.harmonic-drive.com/products/gearheads/rgh.htm.

14. RT: Worm gearboxes. *Series RT.* [Online] [Cited: 12 07, 2005.] http://www.varvel.com/html/page_2_frt.html.

15. The 200 Series Flexaline. *Website: grovegear.com.* [Online] [Cited: 12 09, 2005.] (Our Products; O.E. Series; Catalog; Download PDF; DOWNLOAD ENTIRE CATALOG AS .PDF FILE(11MB)). http://www.grovegear.com/catalog/groveseries200catalog.pdf.

16. Winsmith D-90 Typede. [Online] 2003. [Cited: 12 09, 2005.] (Worm Gearing; D-90 TYPE DE; Catalog). http://www.winsmith.com/products/DE_PDF/D90%20TYPE%20DE%20I.pdf.

17. Get into gear. [Online] 06 20, 1997. [Cited: 12 09, 2005.] http://www.baysidemotion.com/web/technical.nsf/0/8b025fe4f18414cf85256a4c00708dc1/$FILE/MarkR.pdf.

18. **Furlani, E. P.** *Analytical analysis of magnetically coupled multipole cylinders.* Issue.1, 2000, Journal of Physics D: Applied Physics, Vol. 33, pp. 28-33.

19. **Furlani, E. P.** *Permanent Magnet And Electormechanical devices.* s.l. : Academic Press, 2001.

20. **Rode, John E.** *Magnetic gear and gear train configuration. 5,569,967* Fonda, NY, 10 29, 1996. US patent.

21. **Yao, Y.D.; Huang, D.R.; Lee, C.M.; Wang, S.J.; Chiang, D.Y.; Ying, T.F.** *Magnetic coupling studies between radial magnetic gears.* Issue.5, 1997, IEEE Transactions on Magnetics, Vol. 33, pp. 4236-4238.

22. **Yao, Y.D.; Huang, D.R.; Hsieh, C.C.; Chiang, D.Y.; Wang, S.J.** *Simulation study of the magnetic coupling between radial magnetic gears.* Issue.2, 1997, IEEE Transactions on Magnetics, Vol. 33, pp. 2203-2206.

23. **Nagrial, M.H. and Rizk, J.** *Design and performance of a magnetic gear.* 2005, Magnetics Conference, 2000. INTERMAG 2000 Digest of Technical Papers. 2000 , pp. 644- 644.

24. **Ikuta, K.; Makita, S.; Arimoto, S.** *Non-contact magnetic gear for micro transmission mechanism.* 1991, Micro Electro Mechanical Systems, 1991, MEMS '91, Proceedings. An Investigation of Micro Structures, Sensors, Actuators, Machines and Robots. IEEE, pp. 125-130.

25. **Faus, H. T.** *Magnet Geearing. 2,243,555* US Patent, 05 27, 1941.

26. **Charpentier, J. F. and Lemarquand, G.** *Mechanical Behavior of Axially Magnetized Permanent-Magnet Gears.* Issue: 3, 2001, Magnetics, IEEE Transactions on, Vol. 37, pp. 1110-1117.

27. **Tsurumoto, K. and Kikuchi, S.** *A new magnetic gear using permanent magnet.* Issue: 5, 1987, Magnetics, IEEE Transactions on, Vol. Volume: 23, pp. 3622- 3624.

28. **Okano, M.; Tsurumoto, K.; Togo, S.; Tamada, N.; Fuchino, S.** *Characteristics of the magnetic gear using a bulk high-Tc superconductor.* Issue: 1, 2002, Applied Superconductivity, IEEE Transactions on, Vol. 12, pp. 979- 983.

29. **Yao, Y. D.; Huang, D. R.; Hsieh, C. C.; Chiang, D. Y.; Wang, S. J.; Ying, T. F.** *The radial magnetic coupling studies of perpendicular magnetic gears.* Issue: 5, 1996, Magnetics, IEEE Transactions on, Vol. 32, pp. 5061-5063.

30. **Kikuchi, S and Tsurumoto, K.** *Design and Charateristics of a New Magnetic Worm Gear Using Permanent Magnet.* Issue: 6, 1993, Magnetics, IEEE Transactions on, Vol. 29, pp. 2923-2925.

31. **Baermann, M.** *Magnetic Worm Drive. 3,814,962* US Patent, 11 22, 1972.

32. **Kikuchi, K and Tsurumoto, K.** *Trial construction of a new magnetic skew gear using permanent magnet.* Issue: 6 Part 1-2, 1994, Magnetics, IEEE Transactions on, Vol. 30, pp. 4767-4769.

33. **Kyung, H. H.; Young, J. O.; Jung, P. H.** *Design and characteristic analysis of non-contact magnet gear for conveyor by using permanent magnet.* 2002, Industry Applications Conference, 2002. 37th IAS Annual Meeting. Conference Record of the, Vol. 3, pp. 1922-1927.

34. **Henderson, J. Kirston and Bushman, Boyd B.** *Variable ratio angled magnetic drive. 6,411,001* US Patent, 7 25, 2002.

35. **Martin Jr., Thomas B.** *Magnetic Transmission. 3,378,710* US patent, 4 16, 1968.

36. **Schüssler, Gerd and Lindner, Jürgen.** *Magnetic parallel shaft drive for contactless transmission of torque - uses wheels with magnets at circumference at least two of which are rotationally located on shafts. DE4223826* DE Patent, 01 27, 1994.

37. **Neuland, A. H.** *Apparatus for Transmitting Power. 1,171,351* US Patent, 02 08, 1916.

38. **Robinson, Alan Keith.** *IMPROVEMENTS RELATING TO MAGNETIC COUPLING SYSTEMS. WO9622630* International Patent, 07 25, 1996.

39. **Laing, N.** *Magnetic Transmission. 3,645,650* US Patent, 02 29, 1972.

40. **Ackermann, Bernd and Honds, Leo.** *Magnetic drive arrangement comprising a plurality of magnetically cooperating parts which are movable relative to one another. 5,633,555* US Patent, 05 27, 1997.

41. **Ackermann, Bernd.** *Magnetic drive arrangement. 5,994,809* US Patent, 11 30, 1999.

42. **Meisberger, Artur.** *Magnetic gear and centrifuge having a magnetic gear. 6,440,055* US Patent, 09 18, 2000.

43. **Reese, G. A.** *Magnet gear arrangement. 3,301,091* US Patent, 01 31, 1967.

44. **Zhu, Z. Q.; Howe, D.; Chan, C. C.** *Improved Analytical Model for Predicting the Magnetic Field Distribution in Brushless Permanent-Magnet Machines.* Issue: 1, 2002, Vol. 38, pp. 229-238.

45. **Ree, J. D. L. and Boules, Nady.** *Induced voltage harmonic reduction of pm cylindrical machines.* Issue: 3, 05 1992, Industry Applications, IEEE Transactions on, Vol. Volume: 28, pp. 619-624.

46. **Hanselman, Duane C.** *Brushless permanent magnet motor design.* s.l. : The Writers´ Collective, 2003. ISBN: 1-932133-63-1.

47. **Reichert, K.** *The Calculation of Magnetic Circuits with Permanent Magnets by Digital Computers.* Issue: 2, 1970, Magnetics, IEEE Transactions on, Vol. 6, pp. 283- 288.

48. **Fouad, F. A.; Nehl, T. W.; Demerdash, N. A.** *Permanent magnet modeling for use in vector potential finite element field analysis in electrical machinery.* Issue: 6, 1981, Magnetics, IEEE Transactions on, Vol. 17, pp. 3002- 3004.

49. **Kabashima, T. Kawahara, A. Goto, T.** *Force calculation using magnetizing currents.* Issue: 1, 1988, Magnetics, IEEE Transactions on, Vol. 24, pp. 451-454.

50. **Ciric, I.R.** *Surface source models and formulas for the magnetic field of polygonal cross section conductors.* 1988, Magnetics, IEEE Transactions on, pp. 3132-3134.

51. **Rasmussen, K.F. Davies, J.H. Miller, T.J.E. McGelp, M.I. Olaru, M.** *Analytical and numerical computation of air-gap magnetic fields in brushless motors with surface permanent magnets.* Issue: 6, 2000, Industry Applications, IEEE Transactions on, Vol. 36, pp. 1547- 1554.

52. **Andreev, A.; Ngarmnil, J.; Nandhasri, K.** *Universal method for the calculation of magnetic microelectronic components.* 2000, Semiconductor Electronics, 2000. Proceedings. ICSE 2000. IEEE International Conference on, pp. 187-191.

53. **Meeker, D.** Finite Element Method Magnetics (FEMM). *Finite Element Method Magnetics: HomePage.* [Online] http://femm.foster-miller.net.

54. *Borland Software Solutions for Change Management.* [Online] http://www.borland.com/.

55. **Arora, Jasbir S.** *Introduction to optimum design.* s.l. : McGraw-Hill, Inc, 1989.

56. Opera 3D. *VECTOR FIELDS - Software for Electromagnetic.* [Online] http://www.vectorfields.com.

57. COMSOL 3.2. *COMSOL : Multiphysics Modeling and Simulation.* [Online] http://www.comsol.com/.

58. **Youmssi, A.; Rezzoug, A.; Gudefin, E. J.; Sargos, F. M.** *Equivalence between the method of magnetic images and the variable separation method in the study of some slotless surface permanent magnet synchronous machines.* Issue: 2, 1999, The European Physical Journal - Applied Physics, Vol. 8, pp. 163-170.

59. **Binns, K. J.; Lawrenson, P. J.; Trowbridge, C. W.** *The Analytical and Numerical Solution of Electrical and Magnetic Fields.* s.l. : Wiley, 1992.

60. Datablad. [Online] 08 1999. [Cited: 01 04, 2006.] (dansk;Produkter;Datablade;Datablade permanente magneter). http://www.sintex.com/media/datablad_sintrede_mg.pdf.

61. **Atallah, K.; Calverley, S.; Clark, R.; Rens, J.; Howe, D.** *Design, analysis and realisation of a high-performance magnetic gear.* Issue: 2, 2004, Electric Power Applications, IEE Proceedings -, Vol. 151, pp. 135- 143.

62. *Demagnetization Curve Test Report.*

63. **Attallah, K.; Claverley, S.; Clark, R.; Rens, J.; Howe, D.** *A New PM Machine Topology for Low-Speed, High-Torque Drives.* 2008, Proceedings of the 2008 International Conference on Electrical Machines.

64. **Chau, K. T.; Zhang, D.; Jiang, J. Z.; Liu, C.; Zhang, Y.** *Design of a Magnetic-Geared Outer-Rotor Permanent-Magnet Brushless Motor for Electric Vehicles.* Issue: 6, 2007, Magnetics, IEEE Transactions on, Vol. 43, pp. 2504-2506.

65. **Rasmussen, P. O.; Andersen, T. O.; Joergensen, F. T.; Nielsen, O.** *Development of a high performance magnetic gear.* 2003, Industry Applications Conference, 2003. 38th IAS Annual Meeting. Conference Record of the, Vol. 3, pp. 1696- 1702 .

66. **Chau, K. T.; Zhang, D.; Jiang, J. Z.; Jian, L.** *Transient analysis of coaxial magnetic gears using finite element comodeling.* Issue: 7, Journal of Applied Physics, Vol. 103.

67. **Jian, K. T.; Chau, K. T.; Zhang, D.; Jiang, J. Z.; Wang, Z.** *A Magnetic-Geared Outer-Rotor Permanent-Magnet Brushless Machine for Wind Power Generation.* 2007, Industry Applications Conference, 2007. 42nd IAS Annual Meeting. Conference Record of the 2007 IEEE, pp. 573-580.

68. **Liu, X.; Chau, K. T.; Jiang, J. Z.; Yu, C.** *Design and analysis of interior-magnet outer-rotor concentric magnetic gears.* 2009, Jurnal of applied physics 105, Vol. 105.

69. **Hafla, W., Buchau, A. and Rucker, W. M.** *Efficient design analysis of a novel magnetic gear on a high performance computer.* Issue : 3, 2007, COMPEL: The International Journal for Computation and Mathematics in Electrical and Electronic Engineering, Vol. 26.

70. **Rasmussen, P.O.; Mortensen, H.H.; Matzen, T.N.; Jahns, T.M.; Toliyat, H.A.** *Motor integrated permanent magnet gear with a wide torque-speed range.* 2009, Energy Conversion Congress and Exposition, 2009. ECCE. IEEE, pp. 1510 - 1518.

71. **Jian, L.; Chau, K. T.** *ANALYTICAL CALCULATION OF MAGNETIC FIELD DISTRIBUTION IN COAXIAL MAGNETIC GEARS.* PIER 92, 2009, Progress In Electromagnetics Research, pp. 1-16.

72. **Rens, J.; Clark, R.; Calverley, S.; Atallah, K.; Howe, D.** *Design, Analysis and Realization of a Novel Magnetic Harmonic Gear.* 2008, Electrical Machines, 2008. ICEM 2008. 18th International Conference on, pp. 1-4.

73. **Mezani, S.; Atallah, K.; Howe, D.** *A high-performance axial-field magnetic gear*. 2006, J. Appl. Phys. 99.

74. **Schüssler, G. and Lindner, J.** *Exzentergetriebe mit magnetisher Drehmomentübertragung. DE 44 28 441* DE Patent, 08 11, 1994.

75. **Cheng, C. H.; Mi, C. T.; Dorrell, D. G.; Bor, J. L.** *Development of a Magnetic Planetary Gearbox.* Issue: 3, 2008, Magnetics, IEEE Transactions on, Vol. 44.